# Durability Characterization of a High Performance Building Envelope with Vacuum Insulation Panels and Energy Recovery Ventilation

by

Christopher Campbell

A thesis submitted to the Faculty of Graduate and Postdoctoral Affairs in partial fulfillment of the requirements for the degree of

Master of Applied Science

in

Mechanical Engineering

Carleton University

Ottawa, Ontario

# Abstract

Vacuum insulation panels (VIPs) can help achieve thin, highly insulated building envelopes, but poor implementation and insufficient ventilation can lead to durability issues. This thesis describes a field study that was used to characterize the durability of a research house with a thin, VIP-integrated building envelope and an energy recovery ventilator (ERV). The study employed long term hygrothermal monitoring of the building envelope and various tests to evaluate the insulation performance, airtightness, and ventilation effectiveness. The impacts of VIPs and ventilation on durability were discussed, with emphasis on moisture buffering, drying potential, mold growth risk, and VIP aging. The house demonstrated exceptional insulation performance with no risk of visible mold growth during the study. The walls and floor showed acceptable conditions for VIP longevity, and the ERV showed a potential to sufficiently buffer indoor moisture loads. Recommendations were provided to improve the durability and efficiency of the house.

# Acknowledgements

I would like to thank my supervisors Cynthia Cruickshank and Scott Bucking for their incredible support and guidance throughout this project. I aspire to be half the leader that they have been for me.

I would like to thank my colleagues in the Solar Energy Systems Laboratory and the Northern Nomad team for their friendship, discussion, and advice throughout this research. My experience was made truly special by their camaraderie. Thank you to Brock Conley, Chris Baldwin, Calene Treichel, Jordan McNally, Tyler Ulmer, Kayla Lewry, Ben Beauchamp, Belal Daouk, Tait Seguin, Seungyeon Hong, Joshua Reinhart, and Colin Ward.

I would like to acknowledge the financial support provided by the Carleton University Centre for Advanced Building Envelope Research (CU-CABER).

I would finally like to thank my family for their unwavering faith and support, and my partner Isabella Huot for her patience, love, and support that inspires me every day.

# Table of Contents

# List of Tables

# List of Figures

# Nomenclature

| Symbol | Description | Units |
|---|---|---|
| $\varepsilon$ | Effectiveness | |
| $E$ | Arrhenius Fit Parameter | |
| $h$ | Relative Humidity | % |
| $K, K_1, K_2$ | Coefficients | |
| $\lambda$ | Thermal Conductivity | W/mK |
| $\lambda_{\text{evac}}$ | Thermal Conductivity of Evacuated VIP | W/mK |
| $\lambda_{\text{gas}}$ | Gaseous Thermal Conductivity | W/mK |
| $\lambda_{\text{w}}$ | Thermal Conductivity due to Water Content | W/mK |
| $m$ | Mass | g |
| $\dot{m}_{\text{air,exf}}$ | Mass Flow Rate of Exfiltration Air | kg/s |
| $\dot{m}_{\text{air,inf}}$ | Mass Flow Rate of Infiltration Air | kg/s |
| $M_{\text{ERV,exhaust}}$ | Moisture Transported via ERV Exhaust Air | g |
| $M_{\text{ERV,supply}}$ | Moisture Transported via ERV Supply Air | g |
| $\dot{m}_{\text{ERV,exhaust}}$ | Mass Flow Rate of Exhaust Air | kg/s |
| $\dot{m}_{\text{ERV,supply}}$ | Mass Flow Rate of Supply Air | kg/s |
| $M_{\text{exf}}$ | Moisture Transported via Air Exfiltration | g |
| $M_{\text{gen}}$ | Generated Moisture | g |
| $M_{\text{inf}}$ | Moisture Transported via Air Infiltration | g |
| $M_{\text{min}}$ | Minimum Air Mass Flow Rate | kg/s |
| $M_{\text{s}}$ | Supply Air Mass Flow Rate | kg/s |
| $\Delta M$ | Change in Total Moisture | g |
| $n$ | Number of Timesteps or Periods | |

| | | |
|---|---|---|
| $\dot{p}$ | Increase in Internal Pressure per year | Pa/a |
| $p_{\text{gas}}$ | Gas Pressure | Pa |
| $Q$ | Heat Flux | W/m$^2$ |
| $R$ | Gas Constant | J/mol·K |
| RSI | Thermal Resistance | m$^2$·K/W |
| t | time | seconds or years |
| T | Temperature | °C |
| $T_{\text{eff}}$ | Effective Temperature | °C |
| $T_{\text{ext}}$ | Exterior Surface Temperature | °C |
| $T_{\text{i}}$ | Temperature at Timestep $n$ | °C |
| $T_{\text{int}}$ | Interior Surface Temperature | °C |
| $\Delta$t | Duration | s |
| $\dot{u}$ | Increase in Moisture Content per year | mass%/a |
| $u_{eq}$ | Equilibrium Moisture Content (VIP) | mass% |
| $W$ | Coefficient | |
| $\overline{w}_{\text{exhaust}}$ | Mean Exhaust Air Humidity Ratio | g/kg$_{\text{dry air}}$ |
| $\overline{w}_{\text{outdoor}}$ | Mean Outdoor Air Humidity Ratio | g/kg$_{\text{dry air}}$ |
| $\overline{w}_{\text{supply}}$ | Mean Supply Air Humidity Ratio | g/kg$_{\text{dry air}}$ |
| $X_1$ | Supply Inlet Humidity Ratio or Temperature | g/kg$_{\text{dry air}}$ or °C |
| $X_2$ | Supply Outlet Humidity Ratio or Temperature | g/kg$_{\text{dry air}}$ or °C |
| $X_3$ | Exhaust Inlet Humidity Ratio or Temperature | g/kg$_{\text{dry air}}$ or °C |
| $X_{\text{w}}$ | Water Content | g/kg |

# Acronyms

| | |
|---|---|
| ACH | Air Changes per Hour |
| BIPV | Building Integrated Photovoltaics |
| CMHC | Canadian Mortgage and Housing Corporation |
| EA | Effective Area |
| EIFS | Exterior Insulation and Finishing System |
| ELA | Equivalent Leakage Area |
| EMC | Equilibrium Moisture Content |
| EPS | Expanded Polystyrene |
| ERV | Energy Recovery Ventilator |
| FSP | Fiber Saturation Point |
| GHG | Greenhouse Gas |
| HRV | Heat Recovery Ventilator |
| MC | Moisture Content |
| MGI | Mold Growth Index |
| NL | Normalized Leakage |
| OSB | Oriented Strand Board |
| RH | Relative Humidity |
| SVR | Surface to Volume Ratio |
| VIP | Vacuum Insulation Panel |

# Chapter 1: Introduction

The trend toward highly insulated, airtight buildings has drastically improved the energy efficiency of homes in Canada. From 1990 to 2016, space heating energy use intensity in the residential sector was reduced by 45% due to improved energy efficiency of enclosures and energy systems [1]. Further improvements are needed though, as residential buildings still account for 19% of Canada's total energy consumption, over half of which is used for space heating and cooling [2, 3]. Residential buildings also account for 12.7% of Canada's total greenhouse gas (GHG) emissions, largely due to the combustion of natural gas for space heating and hot water [4]. As per the Paris Agreement, Canada has pledged to reduce GHG emissions by 30% by 2030, and as part of this pledge, there is a plan for all provinces and territories to adopt a "net-zero energy ready" building code by 2030. This will undoubtedly call for highly insulated walls with an increase in code requirements for minimum thermal resistance, currently 3.9 RSI ($m^2 \cdot K/W$) or R-22 ($ft^2 \cdot °F \cdot h/BTU$) according to the Ontario Building Code (OBC). It is necessary then to develop highly insulated wall assemblies for widespread residential use.

Highly insulated wall assemblies that use typical insulation materials need to be very thick, and this can be infeasible and undesirable in many cases. Current code-compliant wall assemblies are around 240 mm (9.5 inches) thick and achieve 4.2 RSI (R-23.9) with 2x6 framing (140 mm thick), fiberglass cavity insulation and 38 mm of continuous extruded polystyrene (XPS) exterior foam boards. To increase insulation performance by 50%, around 65 mm of XPS may be added, increasing wall thickness by almost 30%. In situations where the available footprint to build a house is limited, such as close-packed suburban developments and tiny houses, these thicker walls consume valuable interior floor space. In terms of cost per floor area, 30% thicker walls in an

average sized house would reduce floor space by upwards of $10,000 in many cities. For a tiny house with only 200-300 square feet (18.5-37 square meters) in floor space, thicker walls would have a dramatic impact on the useability of the home. To avoid these drawbacks, more advanced insulation materials with better thermal performance can be used to build highly insulated walls that are thinner than what is possible with traditional methods.

## 1.1 Vacuum Insulation Panels

New insulation materials are being introduced to the residential buildings industry that offer higher performance in thinner packages; one of the most promising products being vacuum insulation panels (VIPs), pictured in Figure 1-1. VIPs are thin, flat panels made by encapsulating a block of fumed silica or fiberglass in an envelope of aluminum foil or a metallized polymer film, which is depressurized to around 2 mbar and sealed to maintain the internal vacuum [5]. A schematic of a typical VIP is shown in Figure 1-2, illustrating the porous core and sealed envelope. The vacuum reduces the thermal conductivity of the core material, achieving a center-of-panel effective thermal conductivity of around 0.004 W/mK which is roughly 10 times less than traditional insulation materials [6]. The exceptional thermal resistance of VIPs can help to build highly insulated wall assemblies that are much thinner than what could be achieved with traditional insulating materials. In houses where space is limited and walls cannot be made thick, VIPs may allow for levels of insulation performance that would otherwise be infeasible.

**Figure 1-1: A vacuum insulation panel**

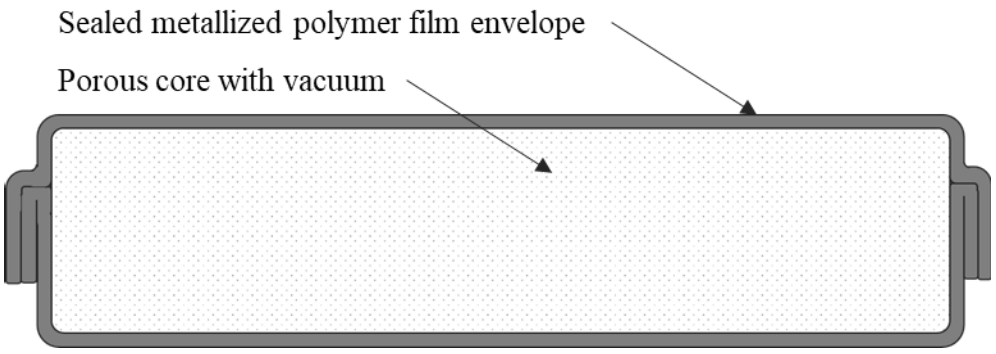


**Figure 1-2: A cross-section schematic of a typical VIP**

VIPs possess their own suite of problems, however. The outer foil of VIPs can be easily punctured so special care and training is required when installing them in buildings. They have also been shown to age over time by slowly absorbing gas and moisture through the foil casing

which reduces the thermal resistance of the panel, resulting in a limited service life. Exposure to elevated heat and humidity levels accelerates aging, so it may be beneficial to integrate VIPs into buildings in a way that minimizes unfavourable exposure for a prolonged service life. Aside from aging and punctures, another major challenge with VIPs is ensuring that they are integrated such that the building assembly is durable against moisture problems. The risk is that VIPs may block the diffusion of moisture within a building envelope which could inhibit the drying process of moist building materials and make it susceptible to excessive moisture accumulation. This can lead to a host of moisture problems such as mold or wood rot, so when moisture inevitably infiltrates the enclosure, it is important that VIPs are arranged in a way that allows the assembly to dry.

## 1.2 Moisture and Durability in Houses

Improving efficiency is certainly a major focus in new building envelopes, but maintaining durability is arguably more important, as it contributes to healthy and comfortable spaces for occupants and reduces environmental impact by requiring minimal repairs. The durability of a building envelope is largely related to moisture, which is the main cause of deterioration in building materials. Inadequate control of moisture in wall assemblies from sources like rain or humidity can lead to excessive accumulation that can cause problems such as rot, corrosion, mold, warping, and freeze-thaw damage [7]. Mold is particularly harmful as it can be difficult to detect in a house and can have minor to severe health effects on occupants such as coughing, wheezing, asthma development [8]. Building envelopes can avoid moisture problems by maintaining a balance of wetting, moisture storage, and drying, and wall assemblies achieve this with exterior rainscreen systems, interior vapour barriers, moisture storage capacity, and vapour-permeable materials to allow drying. However, as building assemblies trend toward higher levels of insulation

and airtightness, and new materials like VIPs enter the market, maintaining this balance becomes more complex.

Highly insulated and airtight wall assemblies pose challenges relating to indoor humidity, condensation, and drying. More insulation inboard of wall sheathing causes the sheathing to be colder in the winter, making it more susceptible to condensation and mold. High levels of airtightness tend to reduce the drying potential of a wall assembly, compounding the problem. Vapour-impermeable insulation materials like VIPs and closed cell polyurethane foam reduce drying potential and moisture buffering capacity compared to traditional batt insulation, increasing sensitivity to moisture. Engineered wood products like OSB that are less permeable than solid lumber or plywood also reduce drying potential and moisture buffering capacity. Furthermore, airtight buildings tend to exhibit higher indoor humidity in the heating season than less airtight homes, which has been linked to the prevalence of mold growth and related health effects. With all these challenges associated with insulation and airtightness, it is important to carefully study new building concepts for their wetting and drying characteristics.

## 1.3 Impact of Indoor RH and Ventilation on Occupant Health

Ventilation and indoor relative humidity (RH) play a major role in the prevalence of moisture problems in houses, especially those relating to occupant health. The effects of RH on occupant health were reviewed by Sterling et al. [8] and the findings are summarized in Figure 1-3.

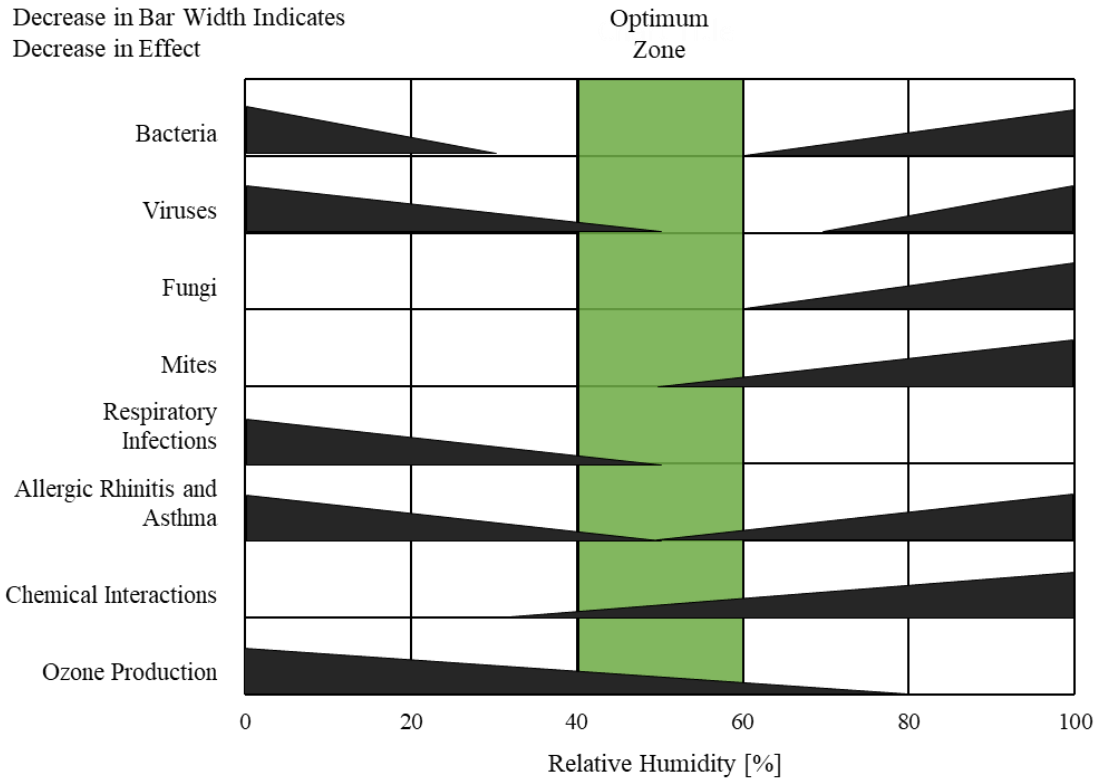


**Figure 1-3: Optimum zone of relative humidity for human health and the prevalence of different health effects, adapted from Sterling et al. [8]**

As illustrated in Figure 1-3, high indoor humidity has been linked with increased prevalence of microbial growth such as mold, bacteria, mites, and viruses. This is a result of condensation or high moisture content of materials such as drywall, framing, or sheathing, which facilitates microbial growth. Houses with inadequate ventilation, low moisture buffering capacity, excessive moisture infiltration, or inadequate drying, are more likely to cause these types of health problems in occupants. Allowing for air leakage or vapour permeability of the building envelope may avoid problems related to dampness, but these mechanisms are difficult to control and can cause excessively dry conditions. Excessive dryness below 40% RH can cause drying of skin and eyes, and irritation of mucus membranes, making occupants more susceptible to symptoms of allergic rhinitis, viruses, bacteria, respiratory infections, and asthma. Indoor humidity should be controlled

to stay around 40% and 60% RH for occupant health, which can be achieved through proper enclosure design and controlled ventilation.

## 1.4 Energy Recovery Ventilation

Newer houses often achieve proper ventilation using a heat recovery ventilator (HRV) or an energy recovery ventilator (ERV). HRVs provide exhaust, supply air flow, and transfer heat and between the supply and exhaust air streams through an exchanger core. An ERV works the same way except the core allows for an exchange of moisture as well, illustrated in Figure 1-4. This functionality preconditions the incoming fresh air, reducing the associated conditioning load. HRVs are usually preferred in colder climate applications because ERVs tend to accumulate frost in the core when outdoor air is below freezing. This is remedied with a defrost cycle that intermittently blocks the intake duct to warm the exchanger core.

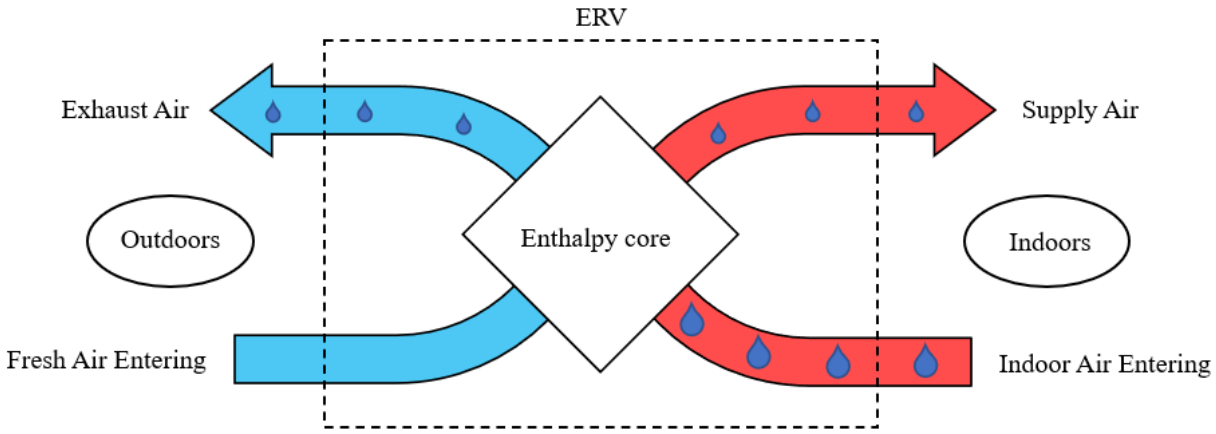


**Figure 1-4: Schematic of an ERV operating in the heating season with higher indoor humidity**

Characterizing the performance of ERVs is important for understanding their effects on indoor humidity, moisture problems, and occupant health. The amount of heat and moisture that an ERV is capable of transferring is referred to as sensible and latent effectiveness, respectively (see Equation (4.2) for calculating effectiveness). In commercially available ERVs, sensible

effectiveness is around 70-80% and latent effectiveness is around 50%. Effectiveness can vary with flow rate, temperature, and humidity, and so they can have substantial and varying effects on indoor humidity levels when used in different situations. Depending on the weather, effectiveness, flow rates, occupant activity, and building characteristics, ERVs could create favourable or detrimental indoor conditions compared to other types of ventilation or no ventilation at all. If an ERV could help improve VIP aging by buffering indoor humidity, then it would be a much less energy intensive method for doing so compared to using a dehumidifier. Therefore, ERV performance should be considered when evaluating the durability of a proposed building system that incorporates ERVs.

## 1.5 Motivation

The trend toward more energy efficient buildings calls for new insulation materials that meet higher performance requirements without creating excessively thick walls. VIPs may provide good insulation performance and allow for thinner wall assemblies, but their aging characteristics may be problematic and their impact on drying potential may introduce moisture problems like mold and wood rot. These issues are more prevalent when there are prolonged periods of high indoor humidity caused by moisture generation and inadequate ventilation. Since insulation is paired with airtightness, mechanical ventilation needs to be provided in energy efficient houses. ERVs offer energy efficient ventilation that can moderate indoor humidity, although the actual impact varies depending on the system, the house, and operating conditions. Therefore, it is worth characterizing a VIP-integrated house with an ERV to see if the interactions between the building envelope and the ventilation system result in a moisture balanced, thermally efficient house.

## 1.6 Background: Moisture in Wood Framed Houses

Moisture interactions in wood-framed houses is a complex subject with many important aspects. A brief review of wood-moisture relations and moisture in buildings is presented to provide a basic understanding of the processes that affect the durability of houses.

### 1.6.1 Wood-Moisture Relations

Wood is hygroscopic, meaning it absorbs water and allows movement of water through it in the form of vapour or liquid. Wood naturally contains some amount of water depending on species, how recently it was milled, and exposure to humid air or liquid water. Excessive moisture is the primary cause of the decay of wood products in houses, so careful control of moisture in wood is necessary for ensuring the longevity of houses. A common indicator of moisture in building materials is moisture content (MC) which describes the amount of water contained within a piece of wood. It is expressed as the weight of water stored within the wood as a percentage of the weight of oven dry wood, as described in Equation (1.1).

$$MC = \frac{m_{\text{water}}}{m_{\text{wood,dry}}}(100\%) \tag{1.1}$$

MC can range from 0% in the oven dried condition to over 200% in completely saturated or green wood. The MC of wood in buildings is typically less than 20% MC unless there is consistent exposure to liquid water or high ambient relative humidity.

Relative humidity (RH) can be described as the ratio of water vapour in air to the total vapour-storage capacity of the air. 100% RH is the saturation point of air, at which point condensation forms. The vapour-storage capacity of air increases with temperature, which is why condensation forms on colder surfaces. Moist air and wood interact by exchanging water vapour

via diffusion. Under steady-state conditions, the RH of air and the MC of wood reach an equilibrium. The relationship between equilibrium moisture content (EMC) and RH at room temperature is represented graphically by the sorption isotherm, pictured in Figure 1-5 for Sitka spruce [9].

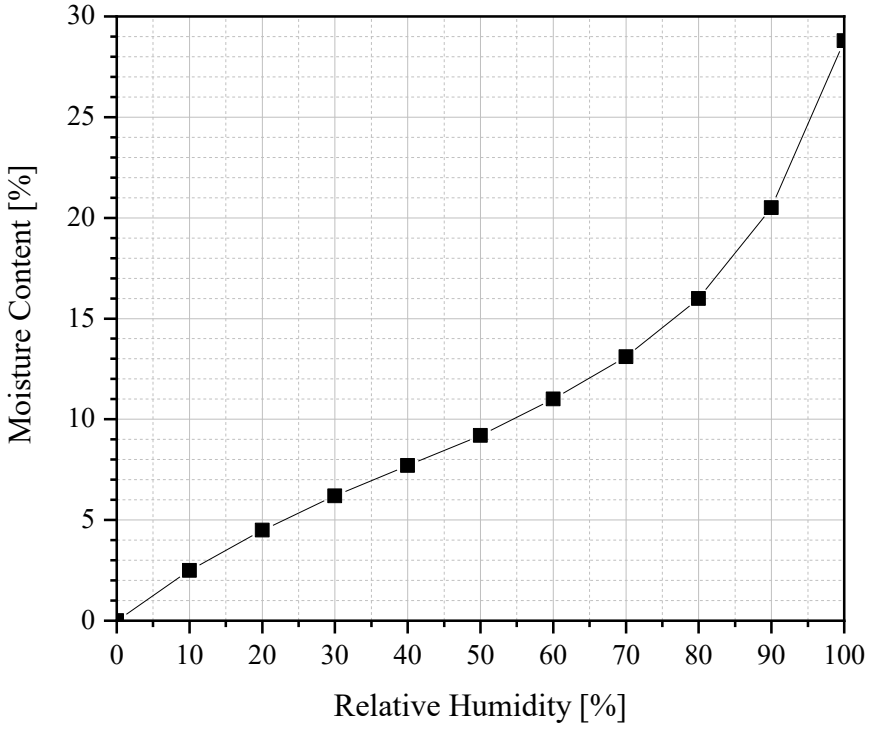


**Figure 1-5: Sorption isotherm for Sitka Spruce at 21.1°C, based on data from [9]**

The MC of wood at 100% RH, which for most species is around 25-30%, is termed the fiber saturation point (FSP). At MC near or above the FSP, there is liquid water stored in the wood which can allow for decay processes such as rot and mold growth to occur.

### 1.6.2 Moisture Sources, Transport, and Drying

Moisture sources include precipitation, melting snow, damp soil, pipe leaks, and water vapour. These sources can originate from outside or indoors and can be generated by occupant activity. Liquid water and water vapour can be transported through building assemblies in several ways:

- Water vapour moves from areas of high vapour concentration to low vapour concentration by diffusion through air and vapour-open materials like wood.
- Air leakage creates vapour convection through openings in the building envelope and can transport large quantities of water.
- Capillary suction transports liquid water from areas of high liquid concentration to areas of low concentration through small pores in moisture permeable building materials.
- Gravity transports water downward through large openings like cracks, holes, and air spaces.

Exterior roofing and cladding systems are designed with considerations for these transport methods, particularly gravity. Drip edges are often incorporated along a fascia, windowsills, and door arches. They are small, sloped overhanging trim features meant to direct rainwater away from the building. Shingles and flashing seams are installed such that the upper piece overlaps the lower piece, keeping water droplets from entering the seam.

Vapour permeability is the ability of a material to allow vapour transport through it; an important property when considering moisture transport in buildings. Vapour permeability is measured in units of perms ($gn \cdot h^{-1} \cdot ft^{-2} \cdot inHg^{-1}$) and can be used to classify materials into three general categories: vapour impermeable (less than 1 perm, referred to as vapour barriers), semi-vapour permeable (between 1 and 10 perms, also referred to as vapour retarders), and vapour permeable (greater than 10 perms, referred to as breathable or vapour-open) [10]. Vapour impermeable materials include polyethylene film, rubber membranes, closed-cell polyurethane foam ("sprayfoam"), aluminum foil, sheet metal, and oil-based paint. Semi-vapour permeable materials include plywood, OSB (oriented strand board), EPS (expanded polystyrene), certain

building papers, and latex paint. Materials that are vapour permeable include gypsum board, plaster, stucco, fiberglass insulation, cellulose insulation, lightweight asphalt impregnated building papers, and “housewrap” (air barrier building papers).

Hygroscopic materials such as wood or cellulose insulation are vapour permeable or semi-vapour permeable and can store water in safe concentrations without degrading. This property allows hygroscopic materials the ability to buffer excess moisture and dissipate it to avoid high levels of moisture content. An example of this is a wood-frame wall with cavity insulation where a penetration in the vapour barrier causes warm indoor air to leak into the wall and contact the cold OSB sheathing. Elevated MC in the sheathing is less likely to occur if the insulation and framing materials can absorb the water vapour from the air and store it safely until it can be dried. However, the moisture buffering capacity of materials is limited and they must be dried quickly enough to avoid excessive moisture content that may lead to mold growth and decay.

Wet materials can be dried if there is a sufficient driving force and pathways for moisture to exit the building assembly. Sun exposure, airflow, and low ambient RH can help dry building assemblies. Vapour-open materials are useful for allowing diffusion to help transport moisture toward the outdoors. Materials that are air and vapour permeable facilitate faster drying via convection through wall cavities; fiberglass batt insulation is an example of this. Plywood or OSB sheathing with a cellulose building paper form a semi-vapour permeable air barrier that blocks exterior liquid water and allows outward drying. An open chamber rainscreen, such as the example shown in Figure 1-6, is a simple exterior cladding system that is effective at blocking wind driven rain while permitting drying of the sheathing and other materials behind it. A rainscreen includes cladding that is fastened to vertical battens or strapping 13-19 mm thick (1/2-3/4 inches) that are

spaced apart and fastened to the sheathing through the exterior foam insulation and air barrier. This creates wide vertical air passages between the insulation and cladding from the top of the foundation all the way up to the soffit.

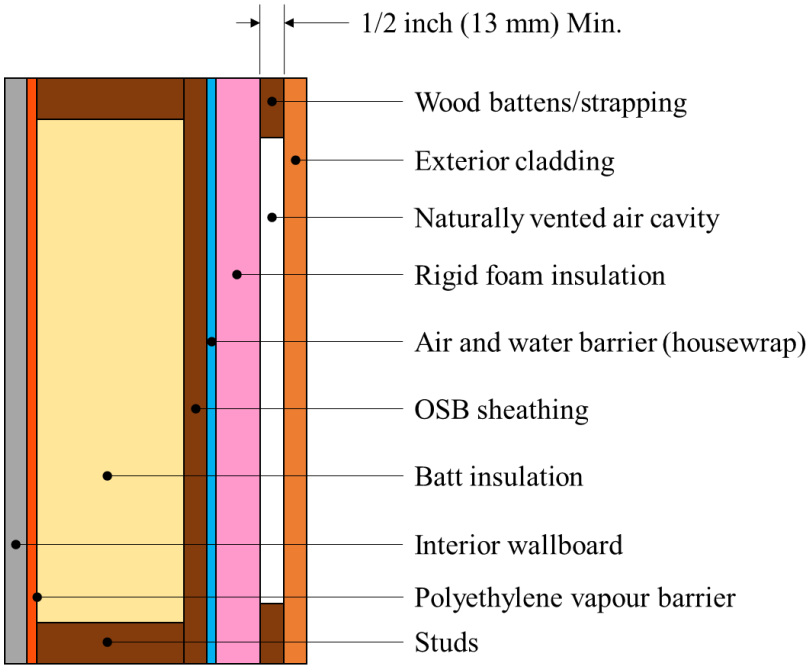


**Figure 1-6: Top-down cross-section view of a residential rainscreen wall**

In the pursuit of thin, airtight, highly insulated walls, it is important to maintain durability so that occupant health and long-term thermal performance are optimized. The risks of moisture problems such as mold growth and VIP aging can be minimized by characterizing proposed building systems to determine appropriate building envelope designs and ventilation strategies. This study aims to contribute by characterizing the hygrothermal performance of a house with VIP-integrated walls and an ERV. Existing research in this area was reviewed to assess the current state of knowledge and identify methods that can be used for this work.

# Chapter 2: Literature Review

This section explores the relevant work related to characterizing a wood frame VIP-integrated building with an ERV, with a focus on durability. The section starts with a review of studies related to the hygrothermal performance of buildings with VIPs. Studies on VIP aging in buildings were reviewed next, followed by a review of criteria for mold growth. This is followed by reviews of hygrothermal characterization methodologies and work relating to indoor humidity and ERVs. Gaps in the existing research were identified, which help define the objective and scope of this work, presented last.

## 2.1 Hygrothermal Studies of Buildings with VIPs

VIPs have demonstrated exceptional thermal performance in buildings, both in retrofit applications and new construction. In 2011, the Canadian Mortgage and Housing Corporation (CMHC) opened the Harmony House in Burnaby, British Columbia: a net-zero energy house that employed VIPs in the walls [11]. With 15 mm thick VIPs, 50 mm isocyanurate foam board, and 75 mm spray foam insulation, the walls achieved an overall thermal resistance of 6.78 RSI (R-38.5) with a total thickness of 180 mm. This is nearly twice the performance required by local building codes, yet the overall thickness is like traditional walls that may not even meet code compliance. This demonstrated the potential for thin, highly insulated building envelopes for new build applications.

Retrofit applications of VIPs have shown similar success. A study by Sveipe et al. [12] implemented 30 mm thick VIPs mounted externally on a timber frame wall with mineral wool cavity insulation to represent a retrofit of typical Norwegian houses from the 1980's. The assembly achieved 7.0 RSI (R-40) and exceeded the highest local energy standards while adding minimal

thickness to the wall assembly. This minimizes the work required during retrofits to adapt the roof overhangs, doors, and windows, making VIPs appealing for such applications.

With respect to hygrothermal investigations of building envelopes with VIPs, retrofit applications are more common in the literature than new-build applications. Johansson et al. [13] used large-scale lab experiments to characterize an historical brick wall in Sweden with an interior VIP retrofit, with a focus on how VIPs would affect drying potential and the risk of deterioration. A brick wall with a 20 mm thick layer of VIPs on the inside surface was assembled in a climate chamber and instrumented with temperature and RH sensors in parts of the brick wall, and MC and temperature sensors in the ends of wood beams that were embedded in the wall. The wall was exposed to a two-day wetting period with daily 30-minute periods of simulated wind driven rain and a constant temperature gradient, followed by a 30-day drying period. The VIPs were then removed, and the experiment was repeated. Since moisture loads were external and outward drying potential was high for both experiments, the interior VIPs only caused a slight reduction in drying ability. The biggest factors that affected moisture levels were the wind driven rain loads and the material properties of the masonry. These results are limited to mild temperatures, since the outdoor temperature in the study was 10°C. Condensation problems are more likely to occur at much colder temperatures, which is an area of concern regarding VIPs.

In VIP-retrofits with very high air leakage and vapour permeance, condensation at VIP surfaces may not be a problem. Johansson et al. [14] demonstrated this using field measurements of temperature and RH in VIP-retrofitted wood and brick walls on a historic multi-unit building in Sweden. The assembly layers from outside to inside were as follows:

- 22 mm wood cladding boards
- 28 mm air space

- 30 mm fiberglass wool boards
- 20 mm VIPs
- 0.2 mm polyethylene film
- 320 mm brick (lower floors) / three 80 mm layers of wood planks (upper floors)

The assembly had very poor airtightness, measuring around 2.65 l/s·m$^2$ at 50 Pa for the brick wall and around 4.0 l/s·m$^2$ at 50 Pa for the wood wall. This caused significant movement of air and vapour through the wall which is known to assist with drying the wall assembly. The existing wall structure of brick and wood had no interior vapour barrier, so inward diffusion of vapour was permitted. These features provided a high drying ability even with exterior VIPs, and during the 2.5-year monitoring period, the VIP retrofit did not increase the MC of the existing wall assembly. New building envelopes are much more airtight and vapour impermeable, so the likelihood of condensation due to VIPs in new construction may be higher. It is noted that the outdoor climate for this study, Gothenburg, was not as cold as many locations in Canada, as the coldest outdoor temperature was -12.7°C and the outdoor air was below 0°C for just a few weeks each year. Colder weather would be likely to increase the risk of condensation.

A hygrothermal retrofit study conducted by Sveipe et al. [12] found that VIPs can cause condensation in walls in cold climates in the absence of a vapour control layer. The study employed numerical models and climate chamber experiments to analyze the risk of condensation on VIP surfaces in retrofits of Norwegian houses. A sample wall was built with wood framing and 100 mm thick mineral wool cavity insulation, with four divided areas of the wall to study four different cases: exterior 30 mm VIP, exterior 20 mm VIPs, interior 30 mm VIPs, and a reference wall with no VIPs. Even though the typical houses would have vapour barriers, the wall samples did not use vapour barriers due to time restraints of the study so the assemblies were highly susceptible to

vapour penetration. The study observed condensation on the warm side of the exterior-mounted VIPs when outdoor air conditions were -18°C and 60% RH, and indoor air was 20°C and 60% RH. Under the same conditions, the un-retrofitted reference wall and the interior VIP wall did not experience condensation. The study concluded that under such outdoor conditions and indoor temperature, the maximum acceptable indoor humidity is 40% RH. This result reinforces the concern of moisture accumulation due to VIPs in walls in cold climate applications where indoor vapour can penetrate the assembly.

## 2.2 VIP Aging

The increase in effective thermal conductivity in VIPs over time, referred to as aging, is a major area of research in the realm of VIPs in buildings. The service life of VIPs is often defined as the time required for the center-of-panel thermal conductivity to double [5]. New VIPs usually have a center-of-panel thermal conductivity of around 0.004 W/mK, making their end of service life arise when they have reached 0.008 W/mK. Although this is still well below the conductivity of other insulation materials, the high cost of VIPs necessitates reliable thermal performance. Many studies have used VIP aging as the primary criteria for characterizing building envelope assemblies.

It is generally established that aging is caused by two mechanisms: increasing internal gas pressure and increasing moisture content inside the panel [5, 6, 15]. The International Energy Agency Annex 39 [6] released in 2005 presented a comprehensive collection of VIP aging studies completed by several institutions to characterize these mechanisms and define a model for effective thermal conductivity. The annex presented experimental work by Simmler and Brunner [5], Schwab et al. [16], and the NRC that all established the following conclusions. Internal

pressure increases as air slowly permeates through the VIP envelope (either aluminum foil or metalized-polymer film) from the outside, driven by the pressure differential. This process slows down over time as internal pressure rises to create a smaller pressure differential. The moisture content within a VIP increases as water vapour permeates through the envelope, driven by the differential vapour pressure, which decreases over time as the core approaches saturation. The thermal conductivity of the fumed silica or fiberglass core increases approximately linearly with moisture content [15] and internal pressure [16]. Under constant boundary conditions, the change rates of pressure and moisture content have each shown an exponential dependence on both ambient temperature and vapour pressure [6]. Cyclic temperature and humidity have shown to have a greater effect on pressure and moisture content than constant conditions. To analyze VIP aging in buildings, the temperature and humidity at VIP surfaces under real conditions need to be analyzed.

### 2.2.1 Constant Condition VIP Aging Model

Schwab et al. [16] established an empirical model that predicts the effective thermal conductivity, $\lambda$, of a VIP as a function of internal gas pressure and water content under constant ambient conditions. It assumes independent effects of moisture content and pressure, taking the general form of Equation (2.1):

$$\lambda(p_{\mathrm{gas}}, X_{\mathrm{w}}) = \lambda_{\mathrm{evac}} + \lambda_{\mathrm{gas}}(p_{\mathrm{gas}}) + \lambda_{\mathrm{w}}(X_{\mathrm{w}}) \tag{2.1}$$

where $\lambda_{\mathrm{evac}}$ is the conductivity of a fully evacuated dry panel, $\lambda_{\mathrm{gas}}$ is the gaseous conductivity at pressure $p_{\mathrm{gas}}$, and $\lambda_{\mathrm{w}}$ is the thermal conductivity caused by the water content, $X_{\mathrm{w}}$. The model by Schwab et al. also includes expressions for these terms which are based on results from laboratory experiments. These expressions may be substituted into Equation (2.1) so that temperature and

relative humidity values are the independent time-series variables. The constant condition model has been used in studies based on temperature and relative humidity values generated by different methods with varying degrees of complexity and accuracy. These methods were reviewed to determine how a VIP aging study can best be incorporated into this work.

### 2.2.2 Model Input Methods

Annex 39 discussed three methods for applying the constant condition model to estimate VIP aging rates under measured or simulated dynamic conditions: time averaging, weighted averaging, and time integration.

The simplest method is to assume a constant RH and use the average temperatures on each side of a VIP over one year and apply those values directly to the aging model. The assumption of constant high humidity is reasonable for most vapor-tight cavities containing hygroscopic materials [6]. This method ignores the non-linear dependence of gas and vapour transmission rates on temperature and vapour pressure, so it is likely to underestimate aging rate in dynamic conditions. Although it is not particularly accurate, the simplicity of this method allows for quick comparisons between different VIP assemblies.

An improvement to the time average method can be achieved using a weighted average method that accounts for the non-linearity of gas and vapour transmission rates with respect to temperature and humidity. Simmler and Brunner [5] determined that the non-linear dependence of pressure increase on temperature is consistent with an Arrhenius-like behavior at a constant high relative humidity. Instead of average temperature, effective temperature, $T_{\text{eff}}$, can be calculated using Equation (2.2):

$$T_{\text{eff}} = \frac{-E}{R \ln\left[\frac{1}{n}\sum exp\left(\frac{-E}{RT_{\text{i}}}\right)\right]} \tag{2.2}$$

$$E = 5.00 \times 10^4 \text{ J/mol} \qquad R = 8.3145 \text{ J/mol} \cdot \text{K}$$

where $E$ is the Arrhenius fit parameter derived in [5], $R$ is the gas constant, $n$ is the total number of timesteps, and $T_{\text{i}}$ is the hourly temperature.

Due to the nature of the Arrhenius relation, $T_{\text{eff}}$ is always higher than the average temperature over a fluctuating period, so this method gives a more pessimistic service life estimate than the time average method. Simmler and Brunner [5] used this technique to estimate the service life of VIPs in a flat roof construction in Switzerland based on hourly VIP surface temperatures from a building simulation. A constant 80% RH at the VIP surfaces was assumed and $T_{\text{eff}}$ was calculated for each side. On the conditioned side of the VIP, temperature was constant, so average and effective temperatures were both 21.5°C. The exterior side fluctuated between -18°C and 44°C with an average temperature of 11.9°C and effective temperature of 16.0°C. This 4.1°C difference led to a significant increase in aging rate and helped to capture the exponential effect of temperature on aging. The weighted average temperature could be readily calculated from experimental or simulated temperature data for different VIP arrangements using a rearranged version of Equation (2.2), which can allow for an easy comparison of conditions between the different arrangements with theoretically more accuracy than the time average method.

The time integration method captures changing exposure conditions via a transient model that applies the constant condition aging model to short timesteps, typically 15 minutes, over the course of a year. This method assumes the constant condition model applies instantaneously to

changing conditions, whereas experimental results show a lag of up to several days between changed conditions and vapour permeation rate, meaning the result is still a somewhat crude estimate [6]. A transient model is obviously much more time consuming to apply than the previously mentioned methods and requires the direct use of the model for any type of aging analysis.

### 2.2.3 VIP Aging Field Studies

Field monitoring work has demonstrated that VIPs in roof assemblies may be exposed to high levels of temperature and humidity that can be detrimental to service life of the VIPs. A study by Brunner and Simmler [17] monitored the moisture conditions at the surfaces of VIPs installed in a flat roof assembly. The assembly contained some initial moisture due to some rainfall upon installation. Despite efforts to dry the assembly before sealing the exterior water barrier layer, the bottom surface of the VIPs was saturated for the entire year of monitoring. The top face of the VIPs frequently experienced temperatures above 50°C and average humidity between 50% and 80% RH. Based on the aging model, the estimated increase in thermal conductivity under these unfavourable conditions was 0.0023 W/mK +/-15% over 25 years: an increase of approximately 50% from the initial thermal conductivity. The study concluded that the rate of aging would have been reduced if exposure temperatures were reduced, namely with the use of more thermal mass to absorb solar heat energy with lower temperature increases. When installing VIPs in water-tight roof assemblies, efforts should be made to minimize initial moisture content in the assembly and protect the VIPs from high temperatures.

Some work has been done to compare the suitability of different VIP integration techniques in walls. A study by ZAE-Bayern [18] monitored temperature and relative humidity in four

different types of VIP-integrated assemblies exposed to real climatic conditions for one year in Germany. The conditions were compared with each other based on average temperature, relative humidity, and vapour pressure. A model was used to estimate the increase rates of internal pressure and moisture content inside the VIPs based on experimental data. Assembly 1 was a balustrade panel made with 20 mm thick VIPs sandwiched between an aluminum sheet and a glass pane, forming an air and vapour-tight envelope around the VIPs. Assembly 2 was an exterior insulation composite system with 15 mm VIPs sandwiched between 10 cm polystyrene sheets installed on a thick concrete wall and finished with plaster. Assembly 3 was another exterior insulation system with a 13 mm VIP encased between two 10 mm corrugated boards and two 3 mm wood sheets, installed on a concrete wall. Assembly 4 was an interior insulation system, but there was little data presented on it, so it is left out from this review. Assembly 3 had the VIP removed and reinstalled throughout the test to measure the pressure and moisture content, providing some validation for model estimates.

When the measured and calculated water contents were compared, it was found that the model was reasonably accurate at estimating the rate of pressure increase, and it slightly overestimated the rate of water transmission into the panel. This suggests that the current state of the art in VIP aging models are rather effective. Comparing the different assemblies, Assembly 1 had the best aging properties due to the effective vapour seal of the assembly. Assembly 2 had the worst aging properties since the plaster finish was porous and allowed for the highest vapour pressures at the VIP surfaces compared to the other assemblies. Assembly 3 was more effective at blocking wind driven rain than the plaster faced assembly, which helped reduce the rate of water transmission into the VIPs. The study found that the levels of temperature and RH that the VIPs were exposed to were influenced by the mass of the assembly, with the concrete walls helping to

buffer temperature increases due to sun exposure. Shading from other buildings was also a factor during the winter months.

The existing literature regarding VIPs in buildings have provided some details about the hygrothermal properties of different wall and roof assemblies and how they affect VIP aging and moisture accumulation risks. However, research has been mostly focused on VIP aging and not the risks of moisture accumulation and problems such as mold growth. The few studies that did assess moisture accumulation were in the context of retrofits, which cannot necessarily be applied to newer, airtight, highly insulated building envelopes. More literature was reviewed to learn about how to evaluate the risks of moisture problems such as mold growth and decay, discussed in Section 2.3. Additionally, hygrothermal studies related to high performance building assemblies were reviewed and discussed in Section 2.4.

## 2.3 Conditions for Mold and Decay in Buildings

Visible mold growth is considered by some researchers to be an effective and conservative indicator for moisture durability problems in building envelopes [19]. If visible mold can be prevented, other moisture problems are likely to be prevented as well. When characterizing a building envelope, studies typically measure three metrics: temperature, RH, and MC. These measurements can then be analyze based on thresholds or models to determine the risk of mold growth.

One widely used tool for estimating mold growth risk is the VTT model, first presented in 1999 by Hukka & Viitanen [20] for pine and spruce sapwoods, and then improved in 2007 [21] for better accuracy and to apply to other building materials. The VTT model is available in a software add-on to WUFI (Wärme Und Feuchte Instationär, or “dynamic heat and moisture”)

hygrothermal simulation software [22] and it accepts input files containing hourly temperature and RH data at a material surface. Other inputs include material sensitivity and level of exposure to occupants. The model generates a mold growth index (MGI) that ranges in value between zero and six that symbolizes the risk of mold growth based on what a visual inspection would find. The MGI is described in Table 2-1.

**Table 2-1: Description of mold growth indices [20]**

| Index | Description of mold growth | Risk |
|---|---|---|
| 0 | No growth | Low |
| 1 | Some microscopic growth | Low |
| 2 | Moderate microscopic growth, over 10% coverage | Low |
| 3 | Some visible growth | Moderate |
| 4 | Visually detected coverage over 10% | High |
| 5 | Visually detected coverage over 50% | High |
| 6 | Visually detected 100% coverage | High |

Figure 2-1 illustrates the approximate limits of favorable conditions for microscopic mold growth used as part of the VTT model [20]. Outside of these limits, mold growth is halted, and within the limits, MGI increases or decreases based on temperature and RH. The MGI has been used as a performance indicator in experimental and simulation-based methodologies, discussed further in Sections 2.4.1 and 2.4.2.

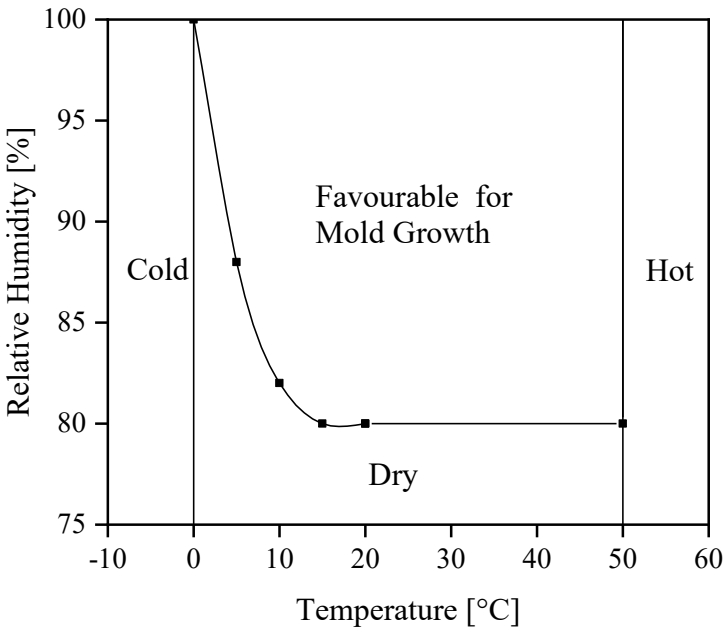


**Figure 2-1: Limits for microscopic mold growth according to Hukka & Viitanen [20]**

When temperature and RH data is not available to the completeness required by the VTT model, a mold risk analysis may be completed based on thresholds or ranges of temperature, RH and MC that permit visible mold growth. Many sources claim that 80% surface RH is sufficient to support mold growth [23], but there is often no associated distinction between visible and invisible growth. More recent studies have determined that 80% RH will support microscopic growth but will not lead to visible growth. The accepted humidity threshold for visible mold growth is 85% RH [24]. Above 85% RH, the mold growth rate increases with a higher RH. Hukka and Viitanen [20] concluded that the extreme temperature limits for mold growth are 0-50°C, outside of which mold growth is halted. However, Tsongas and Riordan [24] state that 40°C is the upper limit for mold growth. Since growth depends also on species and material susceptibility, the upper limit can be treated as a range between 40-50°C instead of an absolute limit. Hukka and Viitanen also state that most species of mold will exhibit slowed growth below 15°C. Trechsel et al. [23] conclude

that the most suitable conditions for rapid mold growth are 18-30°C. MC is less commonly used for evaluating mold growth risk than RH, but since MC and RH are closely linked, MC thresholds may apply. According to a review by Tsongas & Riordan [24], surface mold can be avoided by keeping the MC below 18%, and persistent MC above 15% is an early warning sign of possible future mold problems.

Prevalence of visible mold growth is strongly dependent on the duration of favourable conditions. Tsongas & Riordan concluded that for most susceptible materials, surface RH must exceed a 30-day average of 85% RH for visible mold growth to become apparent. At higher RH levels, visible mold may become widespread in just a few days or weeks. Periods of dryness, freezing temperatures, or excessive heat have been shown to halt mold growth. If temperature and surface RH of building materials are generally below 85% RH, except for short periods of a few hours or days, mold will not become a problem [25].

Material type is a contributing factor to mold growth risk since some materials are more susceptible than others. OSB is a particular material of interest in this study as it is commonly for sheathing in new construction. Some work has been done to assess the mold susceptibility of OSB. According to Laks et al. [26] and Ye et al. [27], the mold susceptibility of OSB panels vary based on wood species, but they are generally slightly less susceptible to mold than solid softwood lumber. Viitanen et al. [22] also suggest that wood-based boards like OSB are slightly less susceptible to mold growth than spruce lumber, with OSB classed as “sensitive” to mold growth and plain spruce as “very sensitive.” Thus, the threshold of 85% RH for visible mold growth is considered applicable to OSB.

Wood rot can be a problem in buildings, but the levels of moisture required are higher than that for mold, so it is less prevalent. Wood rot generally will not occur in wood with MC much below the FSP (around 28-30%) [9]. Ideal MC for the growth of wood rot fungi is slightly above the FSP, usually around 35 to 50% [28]. A publication by ASTM [23] states that for wood rot to develop, the FSP of wood must be exceeded for weeks or months. For many decades, the rule for avoiding degradation of wood products in buildings with some factor of safety has been to keep the moisture content below 20% [29, 9, 30]. The moisture levels and time required for wood rot is greater than that for mold, so when studying the durability of a building envelope, mold growth risk can be evaluated first. If there is no risk of mold growth, there is generally no risk of wood rot either.

## 2.4 Building Characterization Studies

Many studies have been done to characterize the hygrothermal performance of building enclosures, using various methodologies and performance indicators. Some studies were reviewed to determine the effectiveness, benefits, and drawbacks of each type of methodology and performance indicator, and how they may relate to a thin, VIP-integrated envelope with an ERV.

### 2.4.1 Field Monitoring

Field monitoring is a common method for characterizing building envelopes. Studies monitor conditions within test assemblies or actual buildings exposed to real indoor and outdoor conditions using sensors installed in the assembly to collect moisture content, relative humidity, and temperature data. Results are analyzed with a focus on wetting, moisture storage, drying, and risk of moisture problems using the criteria discussed in Section 2.3, including RH thresholds and mold growth index. Researchers appreciate the validity of field studies since they closely represent

real world scenarios. Conclusions from field studies are typically limited to the context of the specific study, so model simulations are often used to provide expanded results for different exposure conditions or longer time periods.

Simulated loads or deficiencies are sometimes used to observe the response of a proposed building envelope to worst-case scenarios that may be difficult to observe naturally. This was done by Ge et al. [31] where the objective was to investigate potential durability issues in highly insulated walls when air leakage was present. The hygrothermal conditions of six different highly insulated wall assemblies were monitored over nine months with exposure to different levels of simulated air leakage. The results clearly indicated the prevalence of elevated moisture content in the wall sheathing in response to air leakage. Another study by McClung et al. [32] evaluated the drying characteristics of wall assemblies by pre-soaking the timber to 30% MC before assembly, simulating a worst-case build scenario. The assemblies were able to dry adequately, providing confidence in the design. Some studies simply control the indoor conditions with a humidifier, dehumidifier, or other equipment to observe the hygrothermal response of a proposed building envelope to different humidity levels [33]. Depending on the study, simulating certain moisture loads can be a useful technique.

When characterizing buildings with field measurements, conditions can only be observed where sensors are located. Installing sensors in every part of a building is usually infeasible, so it is important to have an initial estimate of where the critical locations are so that a reasonable number of sensors can be used. Suitable locations to install sensors are in areas with a higher risk of moisture problems or locations that are typical of the building envelope. Studies typically place sensors in high-risk areas like wall sheathing, windowsills, and framing joints [12, 31, 33].

Some field monitoring studies use wall samples and test huts, and others use whole buildings. Monitoring of complete buildings has been done with heritage houses such as the study by Said et al. [34] which monitored a museum in Ottawa to identify causes for poor indoor climate and moisture problems. Alternatively, a whole building study may be used to study a newer building envelope, such as in Simonson et al. [33] which monitored a house in Finland with an airtight, vapour-permeable enclosure. The study was able to determine the risk of moisture problems in such an envelope under real operating conditions.

The type of sensors used can be impactful to the results of a field study. The lab experiment by Johansson et al. [13] compared the suitability of RH sensors and wood MC sensors for monitoring moisture levels on the surface of wood beams when exposed to increasing ambient RH. MC measurements were converted to RH using a sorption isotherm and the results were compared to the measured RH. The MC and RH sensors showed consistent results long-term, over a few weeks, but the MC sensors had a more delayed response to moisture conditions. This was because the RH sensors respond directly to ambient humidity, while the wood needed to absorb the moisture before it would be measured by the MC sensor. This suggests that for measuring RH for short term testing, RH sensors are more suitable than converting MC with sorption isotherms. For long term testing, either option is suitable.

Aside from monitoring conditions in the building envelope, several other techniques are often incorporated into field studies to characterize air leakage, heat loss pathways, insulation performance. Airtightness plays a major role in the temperatures and humidity in buildings, and a blower door test is an effective method for characterizing the airtightness as part of a durability study [35]. Studies such as Simonson et al. [33] have employed blower door tests to help determine

the effect of airtightness on moisture levels in the building envelope. Infrared thermography is another test method that has been shown to identify air leakage pathways, moisture problems, and thermal bridges in buildings envelopes [36]. The R-value or RSI-value of a wall can be measured in a field study to confirm the thermal performance of a proposed wall system, which is an important detail when considering high performance walls.

### 2.4.2 Model Simulations

Model simulations have the benefit of characterizing buildings without needing to build and test real assemblies. Many software tools exist for generating models, each with specific intended applications, benefits, and drawbacks. 1-D or 2-D hygrothermal models such as WUFI or Delfin are commonly used for predicting moisture levels and the MGI in a building envelope [32] [33]. 2-D heat flow models can be developed using software such as THERM by Lawrence Berkeley National Labs, which can be used to simulate heat conduction in a wall assembly and estimate RSI-values.

One significant simulation-based characterization study was completed by Pallin et al. [19], which determined the impacts of air leakage and internal moisture generation MGI in high performance wall assemblies. The study used WUFI and the VTT mold growth index to model two highly insulated wall assemblies with different combinations of climates, material properties, air leakage rates, and internal moisture generation schedules, resulting in 6000 different simulations. The walls were 2x6 stud walls with cavity batt insulation and exterior XPS, with a total R-value of R-31.25. One wall had no vapour barrier and the other used a 1 perm interior vapour barrier. The study found that simulations with higher internal moisture generation and higher airtightness rates resulted in higher risks of mold growth, especially in cold climates. This

was a result of indoor air leaking outward through the wall assemblies and creating elevated surface RH on the inside face of the sheathing. Furthermore, the wall with a vapour barrier exhibited more time with a high mold risk than the wall with no vapour barrier, suggesting that a vapour-open wall may be more resistant to mold growth. This is potentially due to the tendency for a vapour barrier to increase indoor RH instead of allowing the building envelope to buffer moisture. It is important then to ensure indoor humidity is moderated in buildings with high airtightness and vapour barriers so that mold risk is minimized. Often, simulation results are not trusted to the same extent as experimental results, but by simulating such a vast number of scenarios, this study gave reasonably sound conclusions.

## 2.5 ERVs

ERVs were introduced in the residential sector as a ventilation solution that minimizes energy costs associated with heating or cooling fresh air by recovering enthalpy from exhaust air. This section investigates previous work on evaluating ERV performance with a focus on the effects on indoor humidity.

ERV effectiveness is an important input for energy models or hygrothermal models and can vary under different operating conditions. Some studies have been done to try and improve the accuracy of effectiveness values for such models. Boardman and Glass [37] measured the in-situ performance of an ERV installed at a test house in Madison, Wisconsin to determine the correlations between latent effectiveness, average temperature, and the average relative humidity of indoor and outdoor air. Temperature and relative humidity probes were installed at the inlets and outlets of the ERV, and measurements were collected every minute for a full year. Analysis of the data showed that latent effectiveness increased with increasing average relative humidity of

indoor and outdoor air and decreased with increasing average temperature. A finite difference model was created using physical properties of the ERV core and the results were consistent with measured trends.

Min and Su [38] completed a theoretical study to determine the effects of outdoor air temperature on sensible and latent effectiveness of an ERV. A numerical model was generated to describe the heat and moisture transfer between two airstreams in a membrane-based crossflow enthalpy exchanger. The results indicated that latent effectiveness increases with increasing outdoor relative humidity and decreases with increasing outdoor temperature. The effect of relative humidity is greater in warmer weather, while the effect of temperature is greater in colder weather. Sensible effectiveness showed little sensitivity to weather, only decreasing slightly with increasing outdoor relative humidity.

The two studies above show close agreement with each other so it can be accepted that latent effectiveness depends on exposure conditions. The above studies acknowledge that the results pertain primarily to the specific products that were examined and that general trends could be applied to other ERVs, but exact characteristics vary and should be considered on a case-by-case basis.

## 2.6 Research Gaps

The review indicated that significant work has been done regarding VIP aging characteristics in buildings. However, comparatively few studies focused on the risk of moisture problems like mold due to VIPs. Highly insulated building envelopes such as those incorporating VIPs may be susceptible to mold growth under certain conditions, making this a valid area for further research. The studies that did analyze hygrothermal performance of VIP walls were in the context of retrofit

applications which are rather different from new construction cases regarding materials, air leakage and moisture diffusion properties. This leaves a deficit in the existing knowledge regarding hygrothermal performance of newly built VIP integrated walls. The VIP aging studies completed by Brunner and Simmler or ZAE-Bayern applied to newly built VIP integrated assemblies, but their results were not interpreted for risks of moisture problems other than VIP aging. Their results could conceivably be interpreted to estimate mold growth risks, but the set of assembly archetypes (flat roof, balustrade, plaster faced exterior, and wood panel) are not exhaustive and are not representative of walls in Canada. Considering how many variables affect the risk of moisture problems, there is a significant amount of work required to develop a full understanding of the potential problems with new VIP walls. Airtightness, vapour permeability, climate, indoor humidity, and ERV operation all show potential for impacting the prevalence of mold growth and VIP aging. A study of a particular building envelope that can incorporate some of these effects would contribute to the existing literature.

## 2.7 Objective

The objective of this work was to characterize the hygrothermal performance of a thin, VIP-integrated building envelope in a Canadian climate by in-situ testing of a research house. The tests evaluated key characteristics such as insulation performance, airtightness, ERV performance, and wetting and drying of the building envelope. The suitability of VIPs in the walls, roof, and floor was characterized based on mold growth risk and VIP aging characteristics. The impact of ERV operation on indoor humidity was examined to predict the effects on durability. The study includes recommended improvements for the next iteration of the house.

## 2.8 Scope

The scope of this work was defined based on the research outcomes of interest, the landscape of existing work in this field, and available resources. Characterizing the research house inherently includes many different aspects that can easily lead to scope creep, so some scope limitations were implemented to ensure the quality of work was maintained. The study primarily focused on experimental characterization and collecting useful data for validating future simulation studies. Long-term and short-term tests were included to examine different characteristics. Long-term moisture monitoring was included in the work to observe seasonal changes and to collect sufficient data for analyzing mold growth risk and VIP aging. Short-term moisture monitoring with humidification was used to observe the relationships between the ERV, moisture loads, and indoor humidity. Testing of wall RSI values, air leakage, and ERV effectiveness were included as they all contributed to the characterization of the house and may be used for model validation later. The VIP aging analysis was kept simple, with comparisons between different VIP arrangements and approximate service life estimates. A more detailed analysis may be considered for the basis of a future study. Some simple complimentary model simulations were included, but more detailed simulations were suggested for future work, including long-term hygrothermal modelling with different wall assemblies, ventilation schedules, or climates. Destructive techniques were not used so that the finish of the house could be preserved for other activities. Lab testing of wall assemblies was considered but determined to be infeasible based on resource requirements.

# Chapter 3: Northern Nomad

This section describes the Northern Nomad house that is characterized during this study. Background information is briefly discussed, followed by construction details and mechanical equipment. Points of interest are discussed, including surface to volume ratio, battery box leakage, and the building integrated photovoltaics (BIPV) in the roof.

## 3.1 Introduction and Background

The Northern Nomad shown in Figure 3-1 to Figure 3-3, is a tiny house with net-zero energy and water capabilities and that was instrumented for researching its hygrothermal performance. The house was developed by students at Carleton University from the Faculty of Engineering and Design and was completed in 2018. The house is located on the Carleton University campus and was designed for Ottawa's cold climate, therefore requiring high insulation performance and airtightness to achieve net zero energy. The house is built on a v-nose dual axle trailer frame and as per the Ontario Highway Traffic Act [39], the width of the house was limited to 2.6 m to be towed on public roads. This constraint made it desirable to minimize wall thickness to maintain as much useable interior space as possible, which was the motivation for using VIPs in the envelope. VIPs were installed in the roof, south wall, and floor, but were excluded from the north wall since the door and window arrangement left little space for VIPs to fit.

**Figure 3-1: The Northern Nomad research house viewed from the north side**

**Figure 3-2: South side of the house**

**Figure 3-3: Interior of the house**

## 3.2 Size and Form Factor

The house is significantly smaller than traditional houses, resulting in specific ventilation and conditioning demands. With a floor area of 19 $m^2$ (203 square feet), the Nomad is approximately eight times smaller than the average single-family dwelling in Canada [40] [41]. The interior volume is also about eight times smaller than an average house, at 45 $m^3$. This reduces the amounts of air volume required to be conditioned, so a small air source heat pump satisfies conditioning requirements. The small volume of indoor air makes the indoor environment easily affected by heat and moisture generation from occupant activity, as there is little capacity for the air to buffer moisture, heat, and pollutants like carbon dioxide. Since the house was intended to be relatively airtight, mechanical ventilation was implemented.

A two-speed energy recovery ventilator (ERV) was installed to meet the ventilation demand, with supply/exhaust flow rates of 18.8/14.2 L/s (40/30 CFM) on the high setting and 9.4 L/s (20 CFM) on the low setting. The published sensible effectiveness of the ERV is 66%, but no latent

effectiveness was provided [42]. The ERV features two stages of defrost cycles, where it uses an actuated intake damper to intermittently close the supply inlet duct and operate in an exhaust-only mode to avoid frost formation in the core. When the supply inlet air is between 0°C and -7°C, the intake damper closes for 30 minutes, then opens for one hour. The cycle repeats if the inlet air is in this temperature range. Below -7°C, the intake damper closes for 10 minutes, opens for 60 minutes, and then opens for 10 minutes again. The cycle repeats if the temperature stays in this range. The performance of this unit with respect to efficiency and impact on indoor humidity are points of interest.

A feature of significance with the Nomad is the high surface to volume ratio (SVR). SVR indicates how much surface area is available for heat to be transferred through the enclosure for a given volume of air. Air infiltration and heat transfer through enclosure elements generally increase with a higher SVR, resulting in reduced energy efficiency [43]. A typical single-family home has an SVR around 0.8 – 1.0 $m^{-1}$, and the recommendation by passive house is 0.7 $m^{-1}$ or less [44, 45]. The total enclosure area of the Nomad is 96 $m^2$ and the volume is 45 $m^3$, giving an SVR of 2.1 $m^{-1}$. When evaluating the airtightness of the Nomad, it was important to consider this SVR. Reporting and comparing airtightness using air changes per hour would give an inflated result that does not represent the quality of the enclosure, but more so represents the high SVR. Normalized air leakage, in $L/s \cdot m^2$, was more suitable for evaluating the quality of the air barrier system of the Northern Nomad, but it would not represent the total proportional impact of air infiltration on heating and cooling demands. Therefore, both units of airtightness were examined. This unfavorable SVR emphasizes the need for efficient design and build quality in the house to minimize air infiltration and other forms of heat transfer through the enclosure.

## 3.3 Construction Details

The envelope of the house was constructed using typical methods for wood-framed houses in Ontario. Construction details are shown in Figure 3-4. The foundation of the house is a galvanized steel trailer which was built with rectangular steel tubes that form a perimeter frame with smaller lateral tubes strung between them. The lateral tubes sit 51 mm below the top surface of the perimeter tubes, allowing a space for sheets of 51 mm (2 inch) extruded polystyrene (XPS) insulation with the top surface flush with the top of the trailer. The floor frame was bolted down on top of the trailer and was built with 38 x 89 mm (2x4) joists spaced 610 mm on center. VIPs with a thickness of 10 mm were positioned between the floor joists on top of the XPS, and closed cell polyurethane spray foam insulation was applied over the VIPs, before the 13 mm (1/2 inch) plywood subfloor and 13 mm (1/2 inch) hardwood were installed. In the kitchen area, an additional floor structure was built over the subfloor to elevate the kitchen an additional 30 cm to provide a space for the water storage tanks and associated plumbing.

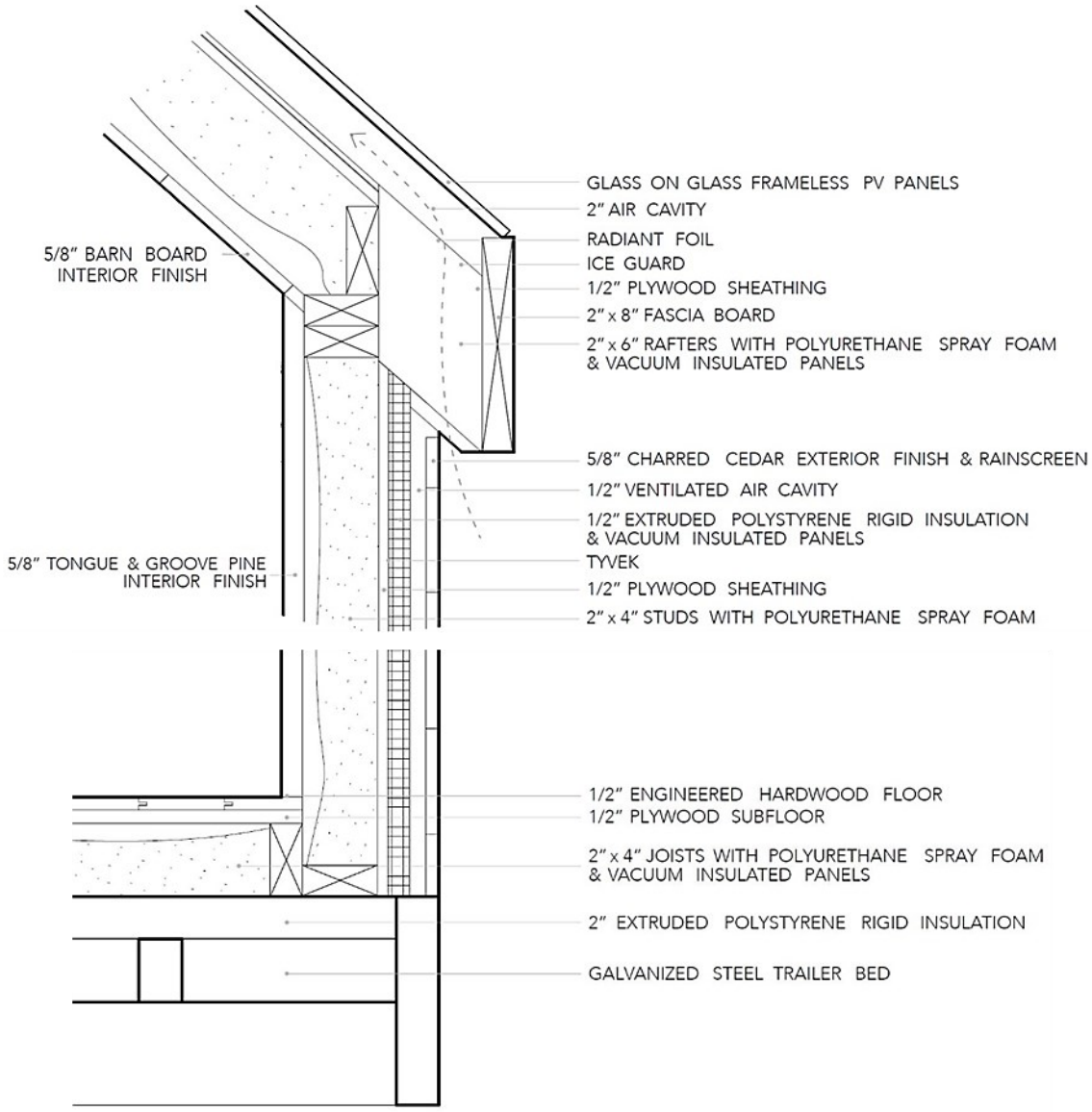


**Figure 3-4: Envelope detail (not to scale)**

The walls were built with 2x4 studs and are positioned outside the floor frame and bolted down to the trailer frame. Figure 3-5 shows the framed south wall and floor framing during construction. Painted 16 mm thick tongue-and-groove pine boards were nailed to the inside of the stud walls to create the interior finish over closed cell polyurethane foam applied inside the stud cavities. OSB sheathing (12 mm) was screwed to the outside of the studs and covered with a housewrap to form a vapour-permeable air barrier. XPS (25 mm) was applied to the outside of the

walls, except on the south-facing wall which received a layer of 10 mm VIPs and 13 mm of XPS, shown in Figure 3-6. Strips of 13 mm XPS were used between VIPs to provide some regions for fasteners to pass through for securing the 12 mm plywood furring strips and 16 mm charred cedar siding which formed an open chamber rainscreen. The total thickness of the walls is 170 mm (6.75 inches).

**Figure 3-5: floor and wall framing during construction**


**Figure 3-6: VIPs adhered to the air barrier of the south facing wall**

The gable roof features a 43-degree pitch on both sides which allowed the PV panels to form the exterior roof surface, with a dormer section on one side and the other being continuous. While the house can be towed and rotated to any orientation, it was designed such that the continuous roof faces due south, optimizing the solar panel orientation. The dormer is covered with black, metal roof finish, while the rest of the roof is completely covered with frameless photovoltaic panels; nine on the south side and five on the north side. The panels are supported by 50 mm square treated wood battens fastened to the 13 mm roof sheathing which is covered by a self-adhering ice guard membrane bonded to the OSB using a primer. The battens provide a 50 mm air gap behind the panels that is continuous from the soffits to the ridge, allowing natural airflow to regulate the temperature of the solar panels. Beneath the roof sheathing, 38 x 140 mm (2x6) rafters are spaced at alternating widths to accommodate VIPs in every second cavity, installed against the inside of the sheathing. Spray foam was applied inboard of the VIPs and the ceiling was finished with untreated barn boards.

## 3.4 Battery Box

One unique feature of the Nomad is the ventilated battery box at the west end of the house, pictured in Figure 3-7 with the lid removed. The box was built to satisfy electrical code requirements relating to the safe storage, charging, and discharging of lead-acid batteries. As such, it features a vent to outside that allows gases generated by the batteries to be exhausted in the event of an electrical malfunction. It also features conduit that routes wiring to outdoor equipment and a lid for accessing the batteries from inside. All these features introduced air leakage pathways through the building envelope that were difficult to seal. Expanding foam and foam tape were used, but there remains noticeable air infiltration along the edges of the battery box on cold days.

Although not ideal in a net-zero energy house, the battery box leakage presents an opportunity to observe the effects of infiltration on moisture conditions in the house during this study.

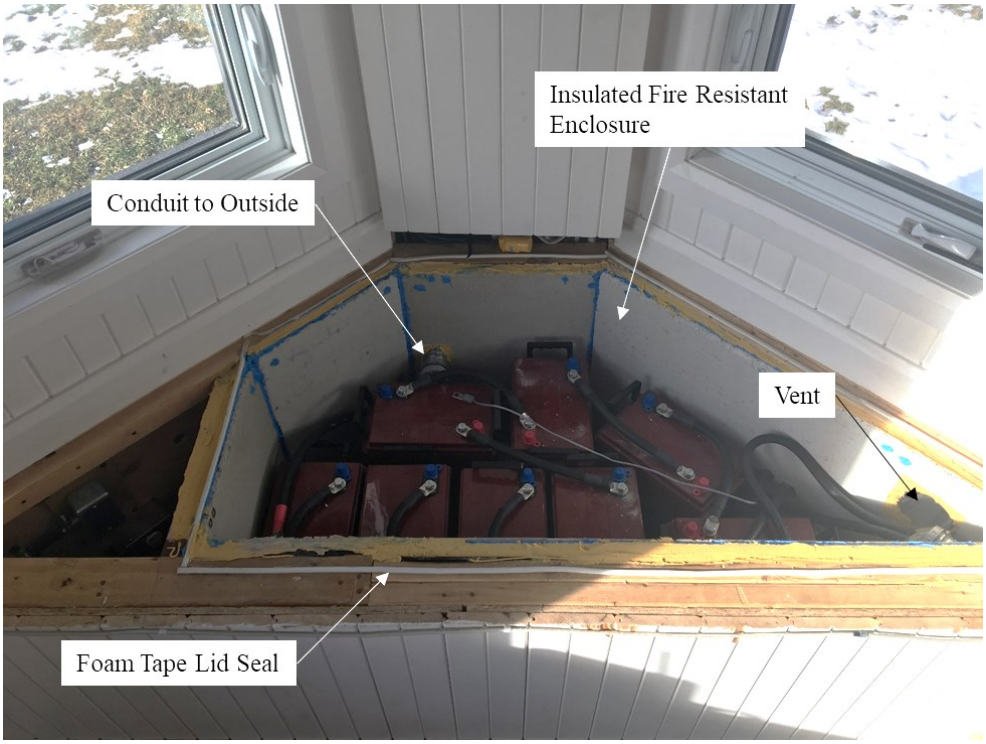


**Figure 3-7: The battery box with the lid removed**

## 3.5 Building Integrated Photovoltaics Roof

The BIPV system on the roof provides an aesthetic finish and material efficiency. The system was designed specifically for this house and, as such, the thermal characteristics of the roof are unknown. Solar panels require convective cooling to avoid overheating during periods of high solar insolation, which can damage the panels and reduce efficiency. Panel temperatures above 70°C should be avoided. Overheating could also be detrimental to the sheathing of the roof, as high thermal cycling is known to cause degradation over time. High roof temperatures also increase heat conduction through the roof into the space, increasing cooling loads in the summer. If there is moisture present in the roof sheathing where the VIPs are installed, the high roof

temperatures could be associated with high vapour pressure which would accelerate VIP aging and reduce service life. Conversely, the high temperature roof sheathing could help improve drying which could improve VIP service life. It is unknown whether the 5 cm air gap beneath the panels is deep enough to allow for sufficient natural convective cooling and what effects it will have on the durability of the roof assembly. Temperature in the roof air gap should be monitored to assess the risk of overheating. If required, a mechanical ventilation retrofit could be added to provide increased panel cooling.

## 3.6 Relevance of Case Study to Thesis

The Northern Nomad presents a unique high performance building system that employs a thin VIP-integrated envelope to maximize living space as well as an ERV to provide ventilation. Both the ERV and the VIPs contribute to the moisture characteristics of the house: the ERV adjusts the indoor humidity and temperature, and the VIPs reduce moisture transport through the envelope. The ways that these features interact with the rest of the building systems determine the durability of the house in a way that is not entirely understood yet. A few questions about the Northern Nomad include:

- What impact does the ERV have on indoor humidity and, in turn, mold growth potential and occupant comfort?
- Do the VIPs interrupt the drying potential of the enclosure and/or cause a buildup of moisture at their surfaces?
- Which of the VIP arrangements (roof, wall, floor) in the Northern Nomad are suitable for the VIPs with respect to their aging?
- Are the VIPs contributing to a high level of thermal performance in this design?

- Does the envelope of the house exhibit any other strengths or weaknesses?
- How can the house be improved in a future iteration with respect to durability, buildability, performance, and value?

This work aimed to answer these questions using the methodology described in Chapter 4:. These answers were interpreted according to the objective in Section 2.7 and, in doing so, a broader knowledge of the durability of thin-walled high performance buildings was developed.

# Chapter 4: Methodology

This chapter presents the research methods used to characterize the Northern Nomad and answer the research questions from Section 3.6. The work includes experimental methods with complimentary simulations, which was determined to be an effective characterization strategy based on a review of the literature, availability of test equipment, and the specific research goals. The characterization of the Northern Nomad was conceptually divided into six characteristics: insulation performance, air leakage, ERV performance, wetting and drying of building materials, mold growth risk, and VIP aging potential. Table 4-1 lists these characteristics and the methods used to evaluate each area of interest, which provides the approximate structure for this chapter.

**Table 4-1: Summary of the key characteristics and the associated methods that were used**

| Characteristics | Characterization Method |
|---|---|
| Insulation performance | -RSI measurements of walls with and without VIPs<br>-Heat flow models of walls<br>-Analyze the performance and space savings of VIP walls |
| Air Leakage | -Infrared thermography indoors and outdoors<br>-Blower door tests<br>-Compare airtightness with standards |
| ERV Performance | -Monitor psychrometric conditions and air speed in the ERV<br>-Calculate effectiveness, air flow rate, and moisture flow rate<br>-Analyze short-term impacts on indoor RH with simulated moisture loads<br>-Evaluate defrost cycle implications |
| Wetting and drying of building materials | -Monitor long-term temperature, moisture content, and relative humidity in different parts of the building envelope in real weather conditions<br>-Interpret building envelope data using known properties of the materials and envelope design |
| Mold growth risk | -Evaluate the building envelope data using criteria for mold growth<br>-Determine areas of high and low risk for mold and estimate future risks |
| VIP Aging Potential | -Estimate service life of VIPs in different arrangements with a simple temperature and humidity model and building envelope data<br>-Compare between walls, roof, and floor to determine most suitable VIP arrangements |

## 4.1 Insulation Performance

The first characterization objective was to verify the insulation performance achieved using VIPs compared to thicker wall assemblies with traditional insulation. This was done experimentally by measuring the RSI-values of the north and south facing walls of the house and by simulation using THERM to create 2D heat flow models of the walls.

### 4.1.1 RSI Measurements

The insulation performance of the north and south facing walls were measured using a kit that includes surface thermistors (±0.1°C) on the interior and exterior wall surfaces, indoor and outdoor air thermistors (±0.1°C) and a heat flux sensor (±3%) on the interior surface. Measurements were sampled at 10-minute intervals and collected over periods of several days in cold weather conditions. With this data, the mean RSI for the test period was calculated within the data acquisition software using a simple thermal resistance equation:

$$RSI = \frac{\sum(T_{\text{int}} - T_{\text{ext}})}{\sum Q} \tag{4.1}$$

where $T_{\text{int}}$ is the interior surface temperature in Celsius, $T_{\text{ext}}$ is the exterior surface temperature in Celsius, and $Q$ is the heat flux in W/m$^2$. Measurements were conducted on the north and south facing walls to compare the VIP-integrated wall with a wall without VIPs.

One of the goals of the RSI measurements was to achieve conformity with ISO 9869, a standard for regulating in-situ RSI measurements [46]. The main criteria for conformity are as follows:

- A minimum measurement period of 72 hours to reduce the impact of any single measurement or period of measurements

- The mean RSI obtained from the last two days of measurement should not differ by more than 5%
- The mean RSI obtained from the first and last days should not differ by more than 5%

Several other recommendations for achieving reliable results were also followed. Sensors were shaded to mitigate effects of solar radiation on the surface temperature and heat flux measurements. Studs were avoided when positioning sensors to observe more representative properties of the whole wall, as the thermal bridging at studs create localized areas of lower surface temperature. Finally, to minimize the residual error associated with sensor accuracy, the experiment was done with a minimum temperature differential of 20°C between indoors and outdoors. These were recommendations by experienced researchers in this area, and they helped to provide more accurate and reliable results.

### 4.1.2 Heat Flow Modelling

Heat flow modelling was done on the north and south wall assemblies using Therm software, a graphical finite element tool for simulating 2D steady state heat conduction through windows and wall assemblies. The wall components were drawn in a top-down view with a sample width of 406 mm (the on-center stud spacing), capturing one wall cavity and half of each of the bounding studs as shown in Figure 4-1. The XPS strips that divide VIPs were positioned halfway between studs to approximate the actual arrangement, whereas the other XPS strips and studs were at varying relative positions along the wall due to their different spacing. The VIPs are 500 mm wide and the XPS strips between them are 50 mm wide, so to represent the VIPs and XPS strips in the model, the widths were scaled down to 406 mm total width while maintaining proportions of 9% XPS and 91% VIP. This resulted in 36 mm XPS strips and 370 mm VIPs. Similarly, for the

100 mm wide plywood battens that occupy 17% of the wall area at 550 mm spacing O.C., a virtual width of 66 mm was used.

The default values in the LBNL material libraries were used for all the materials' conductivities, listed in Table 4-2, except the VIP material which was set as 0.004 W/mK as per the manufacturer's center of panel thermal conductivity. Indoor and outdoor surface temperatures were 20°C and 0°C, respectively. Default surface transfer coefficients of 5 $W/m^2K$ indoors and 8 $W/m^2K$ outdoors were used, representing estimated combined convective and radiant heat transfer at the interior and exterior surfaces. These estimated values are potential sources of error and were examined later by comparing with results from RSI-value testing and infrared thermography.

**Table 4-2: Thickness and conductivity of materials used for 2D heat flow model**

| Material | Thickness [mm] | Thermal Conductivity [W/mK] |
|---|---|---|
| Pine interior finish boards | 16 | 0.140 |
| 2x4 studs | 89 | 0.140 |
| Spray applied polyurethane foam insulation | 89 | 0.024 |
| OSB sheathing | 13 | 0.170 |
| Vacuum insulation panel | 10 | 0.004 |
| Air cavity | 3 | 1.239* |
| XPS strips between VIPs | 13 | 0.034 |
| XPS | 13 | 0.034 |
| Plywood strapping | 13 | 0.170 |
| Air cavity | 13 | 0.775* |
| Cedar cladding boards | 16 | 0.110 |

*Effective thermal conductivity

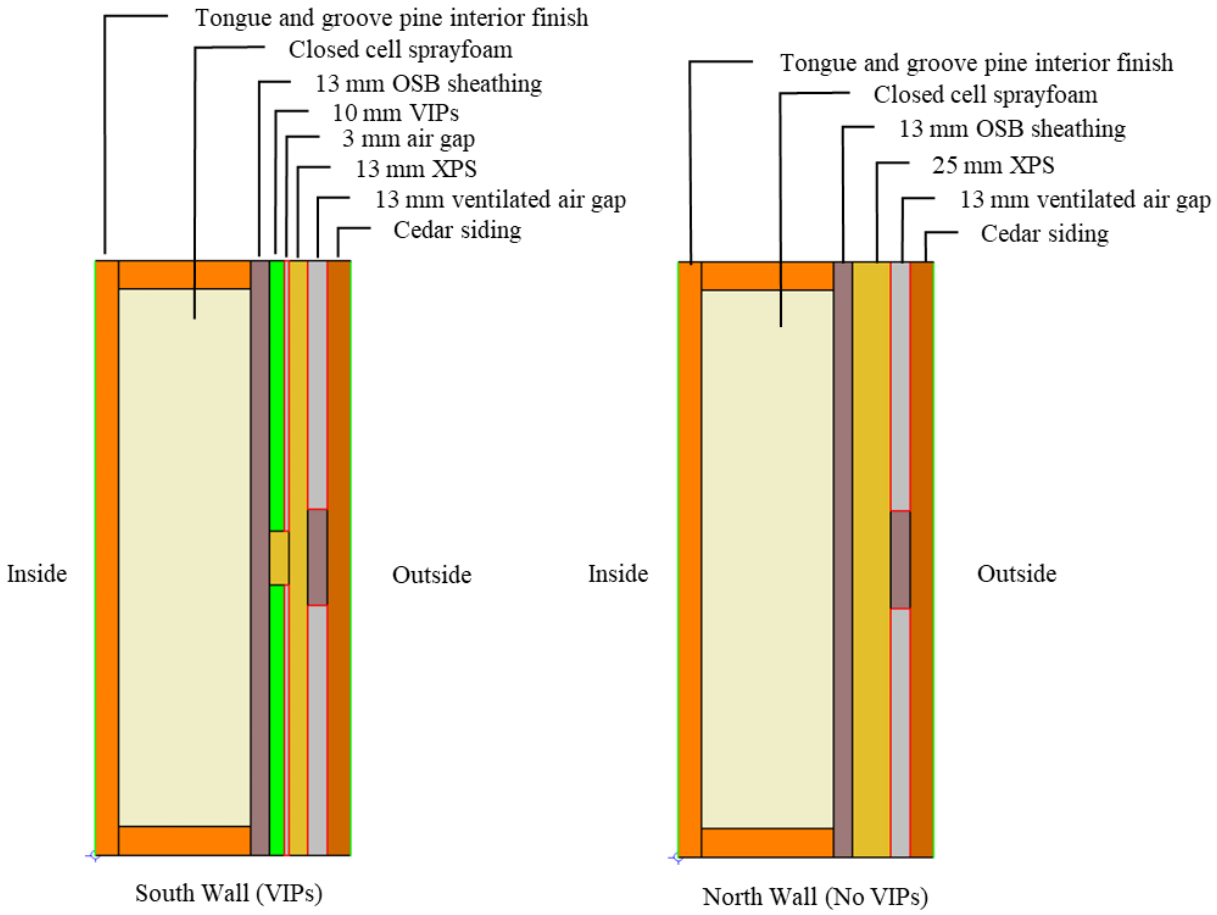


**Figure 4-1: 2D heat flow models of the south and north wall assemblies**

## 4.2 Air Leakage Characterization

Air exfiltration has been shown to be a significant factor affecting the risk of mold growth in wall assemblies in cold climates and is therefore an important part of this durability study. In the Northern Nomad, one of the areas of concern is the battery box as it contains significant air leakage pathways. These pathways could allow warm, humid indoor air to reach cold surfaces in the enclosure such as the sheathing where condensation could form. If the enclosure cannot absorb or dry the moisture adequately, condensation could persist and cause mold growth or other problems. Examining the air leakage at the battery box and the rest of the Northern Nomad will help characterize the durability of the house. Additionally, air leakage measurements can verify

the thermal efficiency of the Northern Nomad, as air infiltration is one of the main causes of heating and cooling loads. Blower door tests were conducted to measure the airtightness of the house. Additionally, infrared photos were captured to examine the locations of air leakage pathways and their relative sizes.

### 4.2.1 Blower Door Tests

Blower door tests were completed on two separate occasions; the first taking place near the end of the construction process, and the second was approximately one year after construction was completed. Between the two tests, electrical work was done in the battery box area including the drilling of holes in the enclosure to allow routing of conduit between interior and exterior components. A four-inch diameter vent was installed in the exterior wall at the battery box to allow gases to be exhausted in the event of a battery failure. Expanding foam was applied around the conduit and ducting to seal cracks at the inside and outside surfaces, but there remained cracks at locations in the wall that could not be sealed, allowing air movement between the wall cavity and the exterior air gap. The significant air leakage expected at the battery box could present a higher risk of moisture problems than the rest of the enclosure. By completing blower door tests before and after the battery box work, the airtightness of the building envelope could be measured and then the effect of the battery box leakage could be separately examined.

A blower door apparatus (Figure 4-2) with manual fan speed control was used to depressurize the house to a maximum vacuum of 50 Pa in 10 Pa increments. A Retrotec DM2 digital manometer was used to measure air pressure indoors, outdoors, and at the fan duct, as well as to calculate the flow rate in CFM. As the fan speed was increased to within 1 Pa of each desired pressure and as the flow rate settled, the pressure and flow rate were read from the digital display

and were recorded. During testing, the ERV ducts were blocked and water drains were plugged. Ambient temperature and wind speed were not recorded during the blower door tests.

**Figure 4-2: Blower door test apparatus, with the red manometer tube end sheltered from wind with a bucket**

### 4.2.2 Thermography

Infrared photos were taken on the afternoon of April 9th, 2019, several of which are presented in Section 5.2.2. The indoor temperature was 24°C and the outside temperature was -1°C with light snow and overcast conditions. Photos were captured both indoors and outdoors to observe any visible signs of thermal bridges, air leakage, or residual moisture. For each infrared photo, a regular photo was captured at the same time. Afterward, each photo was visually inspected to assess the severity of any observed deficiencies and to correlate observations with other data including blower door results and RSI measurements.

## 4.3 Ambient Conditions

For the duration of the study, the house was located on the Carleton University campus in Ottawa, Ontario, Canada. Figure 4-3 shows the position of the house, on a flat grassy space with nearby mid-rise buildings around the west, north, and north east sides, and the Rideau River to the south. The buildings were expected to contribute to radiant heat exchange at the house by reflecting solar irradiance onto the north side and emitting long wave radiation at night. The south side is much more exposed to wind and sunlight and in the winter, the snow-covered ground reflects substantial solar irradiance onto the south façade.

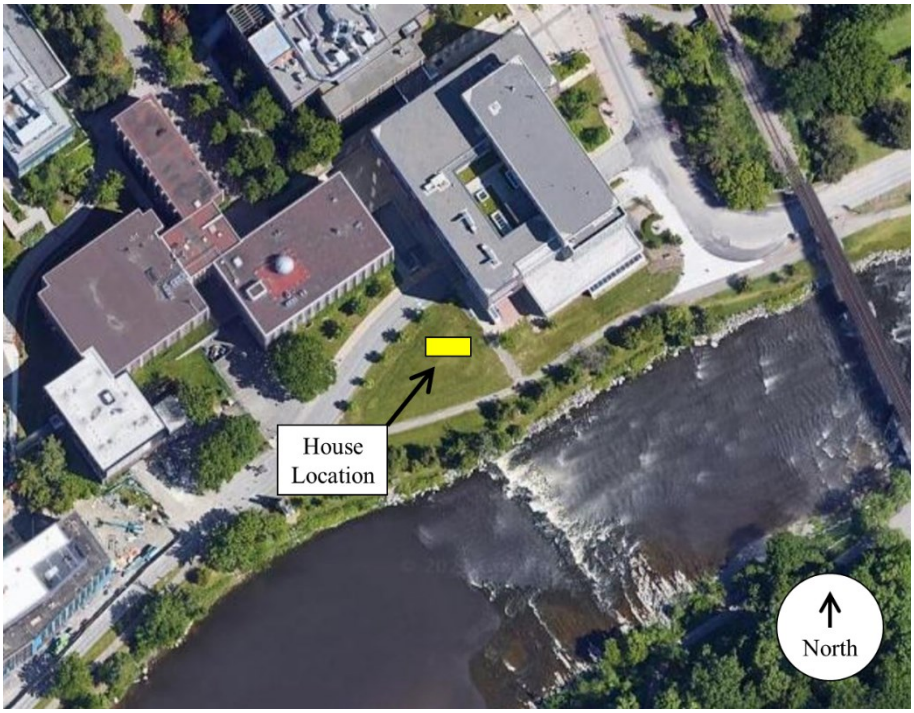


**Figure 4-3: Satellite image showing the location of the Northern Nomad, with buildings around the north side and the Rideau River to the south**

Ambient conditions were measured to provide boundary conditions for nearly all experimental activities. Indoor and outdoor temperatures and relative humidity were measured at

10-minute intervals using HTM2500 sensors positioned near the indoor and outdoor wall surfaces in consistently shaded areas, shown in Figure 4-4 and Figure 4-5.

**Figure 4-4: Outdoor RH&T sensor**

**Figure 4-5: Indoor RH&T sensor**

Wind driven rain was measured using an SMT driving rain gauge installed on the south facing exterior wall. The gauge works using a 929 $cm^2$ catchment area where wind driven rain is collected and funneled down into a tipping bucket with a volume of 5.44 $cm^3$ (Figure 4-6). Each movement of the tipping bucket registers a pulse that is counted by an A2 datalogger, representing 0.059 mm of wind driven rain. Pulses are added up and recorded for each 10-minute sampling interval. A pyranometer was installed on the south façade to measure incident solar radiation normal to the wall at 10-minute intervals.

**Figure 4-6: Wind driven rain gauge and pyranometer installed on the south façade**

## 4.4 ERV Performance Measurements

Ventilation characteristics are influential in the durability of a building against moisture problems and should be analyzed to fully understand the exposure conditions of the building enclosure. In the Northern Nomad, the ERV can have a significant effect on indoor humidity due to the small volume of the house, impacting occupant health and enclosure durability simultaneously. Experimental methods are used to measure the performance of the ERV installed in the Northern Nomad as well as its impact on indoor humidity. Performance metrics of interest include air flow rate, sensible and latent effectiveness, and defrost cycle characteristics. The rate of moisture addition to or removal from the indoor space is analyzed under different conditions. Measured performance is used to define model simulations to predict the impact of ERV operation

on indoor humidity under standardized moisture loads. This allows for results that are beyond the limitations of the experimental methods.

### 4.4.1 Garbage Bag Test

The airflow rate of an ERV is difficult to measure precisely, but an easy method of getting approximate results is the garbage bag test defined by CMHC [47]. To measure supply airflow, a standard sized garbage bag 79 cm wide and 119 cm long was crushed flat and held over the supply vent of the ERV while running, carefully sealing the opening of the bag to the edges of the vent. The bag was filled with air by the ERV and the fill time was recorded. The test was repeated 10 times consecutively and the mean fill time was calculated. This was done for the supply and exhaust vents on high and low speed settings, except for the high-speed exhaust stream as the exit port was not accessible at the time. The benefits of this test are that it required little time or cost, and it did not interfere with the normal performance of the ERV. The drawbacks are that it is not continuous and is presumably less accurate than other methods. To achieve more accurate results, this technique was used in conjunction with continuous air speed measurements.

### 4.4.2 Air Speed Measurements

It was expected that the ERV flowrates change over time due to ambient air pressure, wind, temperature, and filter cleanliness. To analyze the moisture-transfer rates of the ERV in different conditions, the air flow rate needs to be measured continuously. It was deemed infeasible to use airflow measuring equipment in this application so instead, air speed was measured using hot wire anemometers, or air speed probes, in the supply and exhaust air streams. These probes are small enough that they did not significantly disturb the flow and they integrated well with the data acquisition equipment. The measurement range of the probes was selected based on the expected

flow speed in the ERV ducts. The nominal flow rate of the ERV on the high flow setting is 68 $m^3/h$ and the ducts are 10 cm in diameter, so the highest average air velocity in the ducts was expected to be approximately 2.4 m/s. Air velocity probes with a measurement range of 0-5 m/s were used, accurate within 0.1 m/s. The probes were secured in the ducts by adding a short section of ducting to an existing joint and drilling holes for plastic cable glands that hold the probes. They were positioned such that the measurement point on the probe was in the center of the duct cross section. The installed sensors are shown in Figure 4-7. The sensors transmitted a voltage signal proportional to the air velocity between 0 and 5 V to an SMT A3 datalogger.

**Figure 4-7: Air velocity probes in the exhaust (left) and supply (right) ducts above the ERV**

To calculate flow rate from air speed, the average air speed and the duct diameters were used. It was assumed that the air velocity was not uniform across the cross section of the ducts, so the air speeds throughout the entire cross section of the ducts were measured. The probes were moved between specific positions in the duct and measurements were then mapped to a polar

coordinate system. The velocity of areas between measurement positions were approximated using centered differencing, achieving an approximate velocity field through most of the duct. Unfortunately, the probes had extra material at the tips that did not allow for measurements near the duct walls. As a result, average air speed could not be determined from the velocity field. Instead, the center-of-duct air speed was monitored during the garbage bag tests, and the flow rate was divided by the air speed to calculate an effective area (EA), representing the cross-sectional area of a theoretical duct with a uniform speed profile. EA was then used to calculate time-series flow rate based on air speed measurements. This was used in conjunction with psychrometric data to calculate ERV effectiveness, discussed in Section 4.4.3.

### 4.4.3 Psychrometric Monitoring

Continuous monitoring of the psychrometric conditions in the ERV supply and exhaust streams was used to gather data to determine the following:

- Sensible and latent heat exchange effectiveness under a range of conditions for modelling
- Rate of moisture addition or removal compared with moisture loads
- Effect of defrost cycles on cold weather performance

Temperature and relative humidity were measured at the inlets and outlets of the ERV using four SMT HTM2500 sensors (Figure 4-8) and one A3 datalogger. Measurements began in May 2019 and continued until April 2020 at a sampling interval of 10 minutes. Throughout this period, the ERV was switched between the high and low speed settings and was turned off for some time, providing comparison between different ERV operation modes.

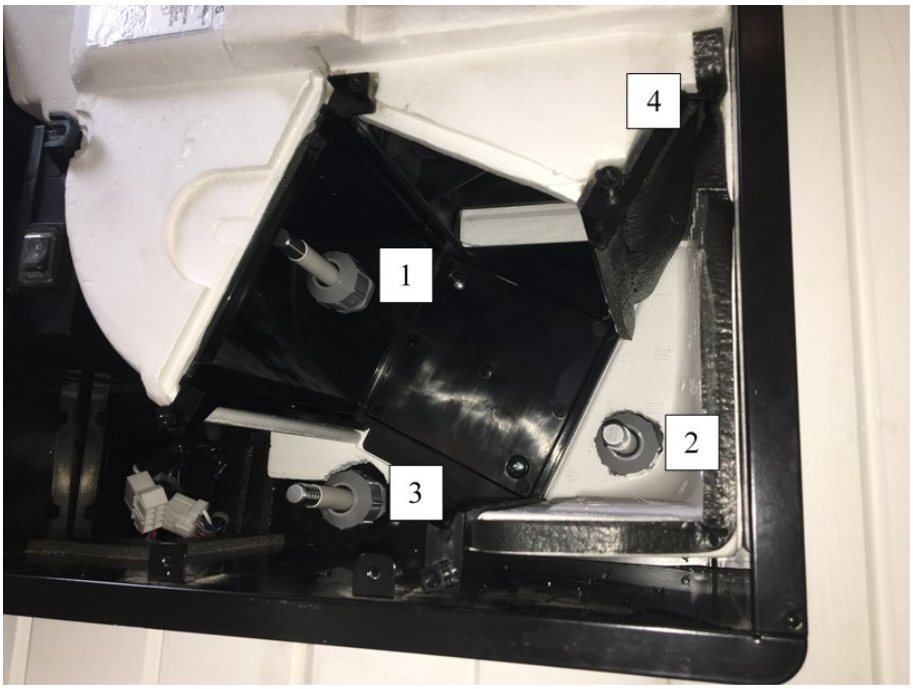


**Figure 4-8: RH&T sensors in the ERV measuring conditions at the supply inlet (1), supply outlet (2), exhaust inlet (3) and exhaust outlet (4). The core is removed for clarity.**

Measured flow rate, temperature, and relative humidity data were used to calculate sensible and latent effectiveness of the ERV under different conditions, according to Equation (**4.2**) defined by CSA-C439-18 [48]:

$$\varepsilon = \frac{M_s(X_1 - X_2)}{M_{\min}(X_1 - X_3)} \tag{4.2}$$

where $M_s$ is the supply mass flow rate, $M_{\min}$ is the lower of the supply and exhaust mass flow rates, and $X_1$, $X_2$, and $X_3$ are the temperature for sensible effectiveness ($\varepsilon_S$) and the humidity ratio for latent effectiveness ($\varepsilon_L$) at the supply inlet, supply outlet, and the exhaust inlet, respectively. According to the studies by Boardman and Glass [37] and Min and Su [38] discussed in Section 2.5, effectiveness was expected to vary with different operating temperatures and humidity levels. To check for variations, the effectiveness was evaluated hourly and inspected for correlations with the operating conditions. The flow rate was evaluated to check for balanced or

imbalanced ventilation which can have an impact on infiltration. Finally, the collective performance data of the ERV was used in calculating moisture addition and removal rates under different conditions.

## 4.5 Humidification

Short-term humidification of the house was done to simulate moisture loads and to study the response of the ERV to high indoor humidity. To specify the rate of humidification, the moisture loads associated with two adults were considered, as specified by ASHRAE [49]. Table 4-3 lists the different moisture sources, the amount of evaporated moisture each source generates, and the frequency of source. The total estimated moisture generation rate is 2.6 L per day.

**Table 4-3: Estimated moisture sources in a single-family dwelling with two adult occupants**

| Activity | Evaporated Moisture [L] | Frequency |
|---|---|---|
| Shower, 10 minutes | 0.5 | Daily |
| Breakfast, 2 Adults | 0.09 | Daily |
| Dinner, 2 Adults | 0.29 | Daily |
| Dishwashing: Breakfast | 0.05 | Daily |
| Dishwashing: Dinner | 0.16 | Daily |
| Lunch, 2 Adults | 0.13 | 2 per week |
| Dishwashing: Lunch | 0.04 | 2 per week |
| Daily Respiration/Perspiration, 2 Adults, 15 hours | 1.5 | Daily |
| **Daily Total** | **2.6** | |

To simulate this in the Northern Nomad, an ultrasonic humidifier with a 4 L tank and variable humidification rate was used. The humidifier could be controlled using either a relative

humidity setpoint up to 80% or a constant rate of humidification, marked as a level from one to three. Since the humidifier was designed for household use and not research applications, the humidity control was assumed to be inaccurate for setting actual humidity levels. Therefore, the constant rate settings were used instead. The humidification rate at each operating level was determined by measuring the volume of water required to refill the tank after each period of operation.

Moisture generation was implemented in the house during two periods: the first with the ERV off and then with the ERV on the high setting. Moisture balance equations were used to investigate the individual effects of ventilation, moisture generation, and air leakage during the two periods. With the ERV off, the moisture balance takes the form of Equation (4.3).

$$M_{gen} + M_{inf} - M_{exf} = \Delta M \tag{4.3}$$

With the ERV on, the moisture transported through the supply and exhaust streams are added to the moisture balance to give Equation (4.4).

$$M_{gen} + M_{inf} + M_{ERV,supply} - M_{exf} - M_{ERV,exhaust} = \Delta M \tag{4.4}$$

The moisture transfer rates can be defined by Equations (4.5)-(4.8):

$$M_{inf} = \overline{w}_{outdoor}\dot{m}_{air,inf}\Delta t \tag{4.5}$$

$$M_{exf} = \overline{w}_{indoor}\dot{m}_{air,exf}\Delta t \tag{4.6}$$

$$M_{ERV,supply} = \overline{w}_{supply}\dot{m}_{ERV,supply}\Delta t \tag{4.7}$$

$$M_{ERV,exhaust} = \overline{w}_{exhaust}\dot{m}_{ERV,exhaust}\Delta t \tag{4.8}$$

The mass flow rates of air through the ERV were calculated from the measured air flow rates and the humidity ratios were measured, leaving two unknown variables: $\dot{m}_{air,inf}$ and $\dot{m}_{air,exf}$. An air mass balance was used to eliminate one variable.

$$\dot{m}_{ERV,supply} + \dot{m}_{air,inf} = \dot{m}_{ERV,exhaust} + \dot{m}_{air,exf} \tag{4.9}$$

Combining Equations (4.4)-(4.9) gives the individual rates of air and moisture transport through air leakage and ventilation.

## 4.6 Envelope Monitoring

The greatest insights into the moisture characteristics of the Northern Nomad come from monitoring the building envelope itself under true climatic exposure. During the construction of the house, thermistors, moisture content sensors, and relative humidity sensors were installed in 12 different locations. The sensors were positioned in the floor, walls, and roof assemblies near VIPs to capture the surrounding psychrometric conditions. Additionally, sensors were installed at cavities or joints that were deemed 'high risk' for failure or to be used as a comparison for VIP sections. An explanation of each sensor location, type of sensor to be installed, and how they relate to the research objective is presented.

The roof assembly containing VIPs exhibits temperature and moisture conditions that are substantially different from the data that is currently available on above grade walls and roofs. The BIPV system introduces a significant source of heat and the VIPs block heat and moisture from dissipating into the roof cavity. A moisture content sensor and thermistor (MC&T) were installed on the inside face of the sheathing adjacent to the VIPs at symmetrical positions on the north and south facing roofs (Figure 4-9). A relative humidity sensor was also added to the interior face of

VIPs on the north and south facing roofs. This data is essential for determining the durability of the roof system and the aging of VIPs in different assemblies under different scenarios.

**Figure 4-9: Roof VIP with an RH sensor taped to the panel and an MC&T sensor in the sheathing adjacent to the panel**

A roof detail that is an area of concern is the joint between the dormer and the sloped roof. To confirm that this detail is suitable for future use, moisture content, temperature, and relative humidity were monitored at the junction.

As discussed, the south facing wall contains VIPs while the other three walls do not. To contrast the differences, sensors were installed in two locations on each of the north and south walls: the inside face of the sheathing centered in a stud cavity beneath a window, and just below the windowsill (Figure 4-10). Each location was instrumented with a thermistor, moisture content

sensor, and relative humidity sensor. Sensor locations are symmetrical between the north and south walls.

**Figure 4-10: RH, MC&T sensors installed in a wall cavity and below a windowsill**

The galvanized trailer frame and the VIPs in the floor are unique features of the floor assembly. To examine the moisture conditions in the floor, three different locations were instrumented. A thermistor, moisture content sensor, and relative humidity sensor were installed on the underside of the floor sheathing beneath the water storage tanks under the kitchen. Additionally, a thermistor and moisture content sensor were installed in the side of a floor joist. Lastly, a relative humidity sensor and thermistor were installed on the XPS insulation between the trailer frame and the wood frame.

A total of 11 thermistors, 10 moisture content sensors, and eight relative humidity sensors were installed and connected to SMT A3 data acquisition units. Data logging began in February 2019 and continued until March 2020, measuring at 10-minute intervals. The data loggers are typically setup with AA batteries that need replacing periodically, but to avoid this, dataloggers were powered using 5 V DC power supplies plugged into a power outlet in the house. The house was located at Carleton University during testing. SMT BiG software and the cloud-based analytics suite were used to save data and convert resistance and voltage measurements to engineering units, the equations for which are provided in Appendix A:. Several conversion equations for moisture content sensors were considered, discussed in Appendix B:, and the default conversion equation was selected. Indoor conditions were generally maintained between 19°C and 24°C with some variation over the measurement period due to different electrical work and media activities that took place in the house.

Data from the building envelope was examined to observe trends and instances describing the wetting and drying characteristics of the walls. Data from different locations in the house were compared. Data collected from ERV monitoring, RSI testing, air leakage testing, thermography, and ambient conditions were all considered when evaluating the building envelope data. Engineering judgement was used to relate datasets, estimate the physical phenomenon that caused the observed conditions, and evaluate the significance of them.

# Chapter 5: Results and Discussion

This section presents and discusses the results from the experimental and modelling work, following the same layout as the methodology. Insulation performance results from RSI measurements and heat flow modelling were discussed first, with a focus on the thermal characteristics of VIP integrated walls. Airtightness was discussed based on blower door test and thermography, with consideration for the risk of condensation. ERV performance was discussed, including flow rate, effectiveness, defrost characteristics, and the impact on indoor RH during moisture generation. Envelope monitoring results were analyzed with discussions regarding data collection challenges, moisture buffering capacity, wetting and drying characteristics, risk of mold growth, VIP aging, and the impacts of indoor humidity.

## 5.1 Insulation Performance

### 5.1.1 RSI Measurements

Results from the first attempts of RSI measurements indicated that the process needed improvement to conform to ISO 9869 [46]. The outdoor surface temperature sensor took at least one hour to reach the actual surface temperature due to the thermal capacity of the sensor that was moved from indoors to outdoors just before recording. This caused a large variation in RSI measurements and to achieve ISO conformity, the sensors needed to show less deviation at the beginning of the test. Additionally, the battery life of the dataloggers only lasted three days on the first few measurement attempts: the minimum length for an ISO conforming measurement. This limited the tolerance for non-conforming periods of data through the tests, including large deviations in the calculated average RSI over time. To improve measurements, the data loggers were installed and climatized prior to recording data and they were charged from nearby power

outlets as needed during the measurements. This allowed tests to run indefinitely and the first ISO conforming measurements were achieved. However, there were still problems with the results. Upon inspection, the interior surface temperature seemed too low due to nearby infiltration at the battery box, discussed in detail in Section 5.2.1. The lower surface temperature and increased heat flux at that location reduced the calculated RSI of the wall, so the sensor needed to be relocated for accurate measurements to be made. The sensors on the interior of the north wall also needed to be relocated because they were receiving sunlight through the opposing south facing window during the afternoon, causing an elevated surface temperature and reversed heat flux. While the measurement was ISO conforming, it did not accurately reflect the RSI of the wall. As with the exterior sensors, the indoor sensors needed to be sheltered from direct solar radiation. All the sensors were relocated to the kitchen area, as seen in Figure 5-1, and they were carefully positioned to be shaded from sunlight, away from significant sources of airflow, and not on studs or exterior battens. This is where final measurements were made.

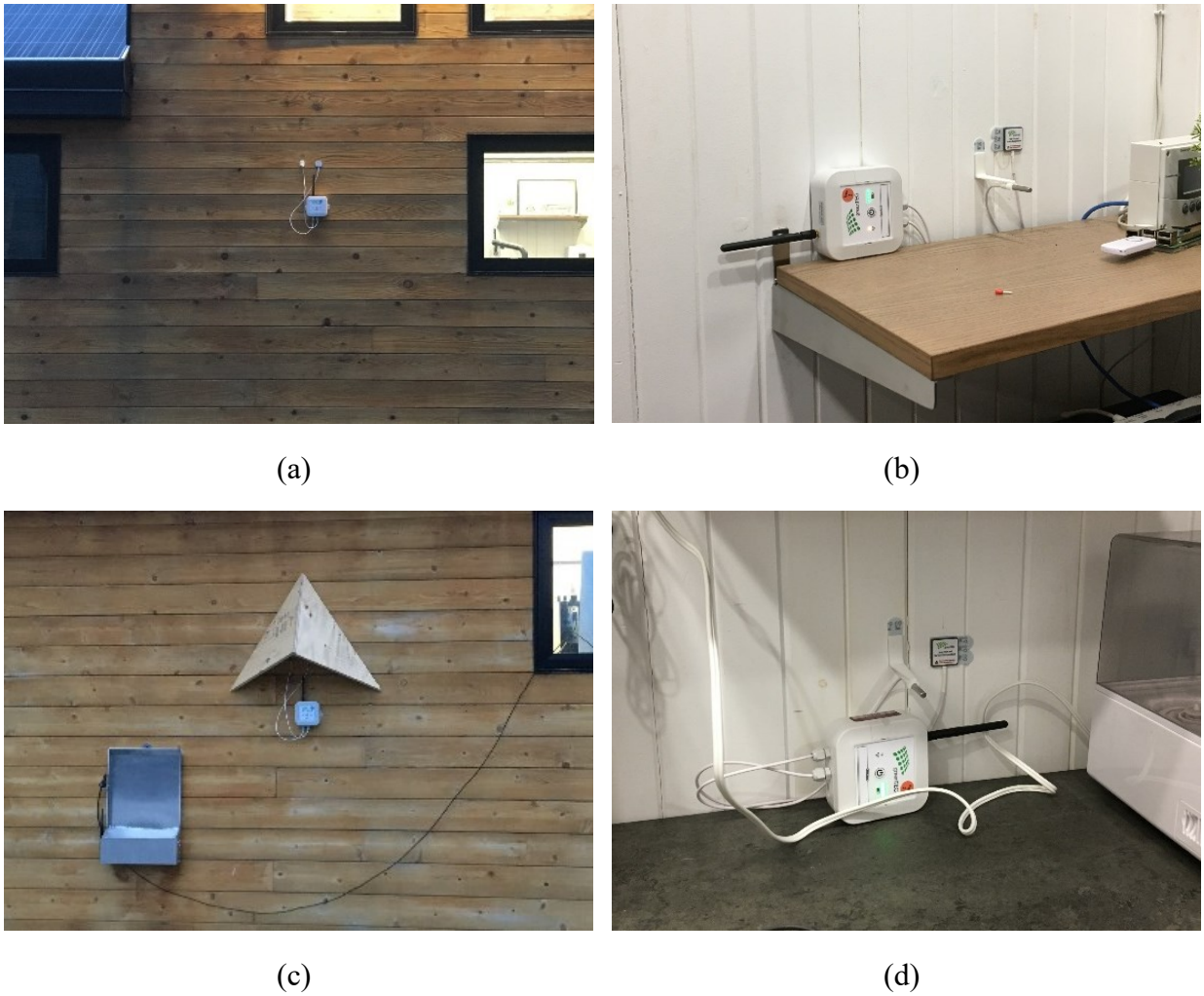

(a) (b)

(c) (d)

**Figure 5-1: Locations of the RSI monitoring equipment: (a) North wall exterior, (b) North wall interior, (c) South wall exterior, (d) South wall interior**

Measurements were recorded every 10 minutes for six days and 18 hours starting at 16:40 on November 21st, 2019. The indoor temperature was between 19.3°C and 23.3°C with an average of 20.9°C. Outdoor temperature was between -5.9°C and 15.7°C with an average 2.8°C. The measured temperatures and calculated RSI for the south wall over the measurement period are shown in Figure 5-2. Raw data for the north wall could not be accessed so it was not plotted. The results were ISO conforming and were comparable to nominal values. The estimated uncertainty of the RSI values is 0.14% based on a Gaussian error propagation of Equation (4.1) using sensor

error values listed in Section 4.1.1. The south wall achieved an average thermal resistance of 5.89 RSI (R-33.4) and the north wall achieved 4.59 RSI (R-26.0), both well above the minimum OBC requirement. It was concluded that the 10 mm thick VIPs improved the wall insulation by RSI-1.3, or 34%, making the south wall exceptional for a 2x4 stud, comparable with other highly insulated wall assemblies that are significantly thicker.

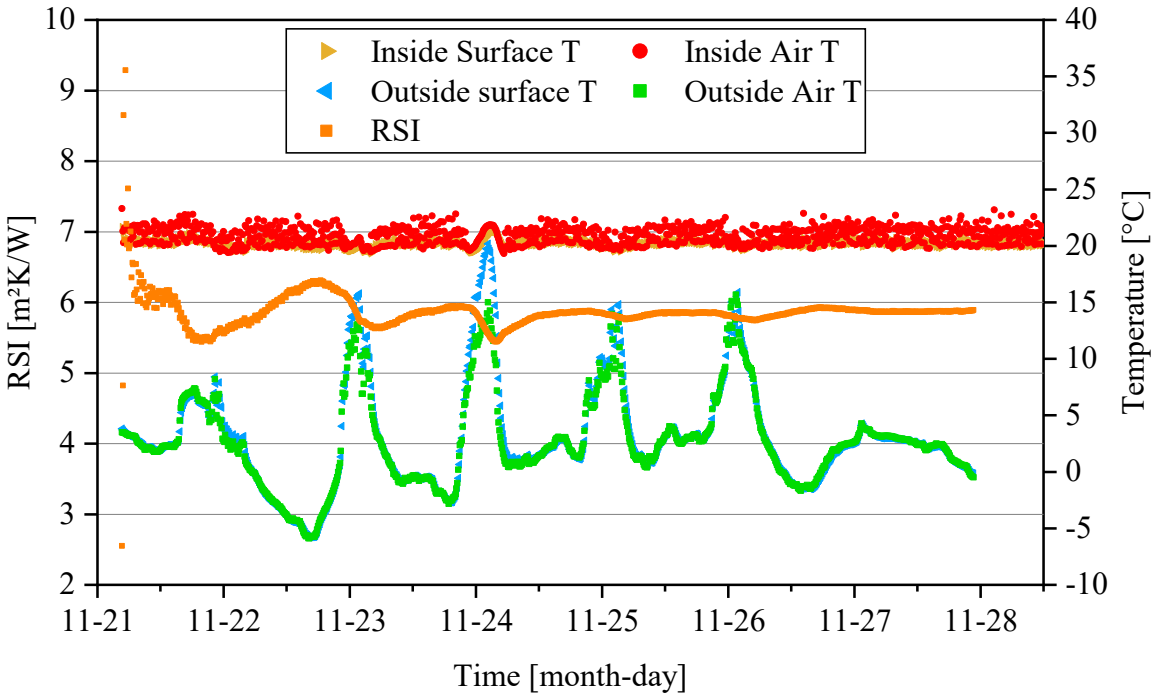


**Figure 5-2: R-value measurement data for the south wall**

### 5.1.2 Heat Flow Modelling

2D heat flow models of the south and north walls of the house were used to examine thermal bridging effects in the wall assemblies and to provide additional detail to expand on measured data. Calculated temperatures within the wall assemblies are shown in Figure 5-3 with infrared colour gradients, at 0°C outdoors and 20°C indoors.

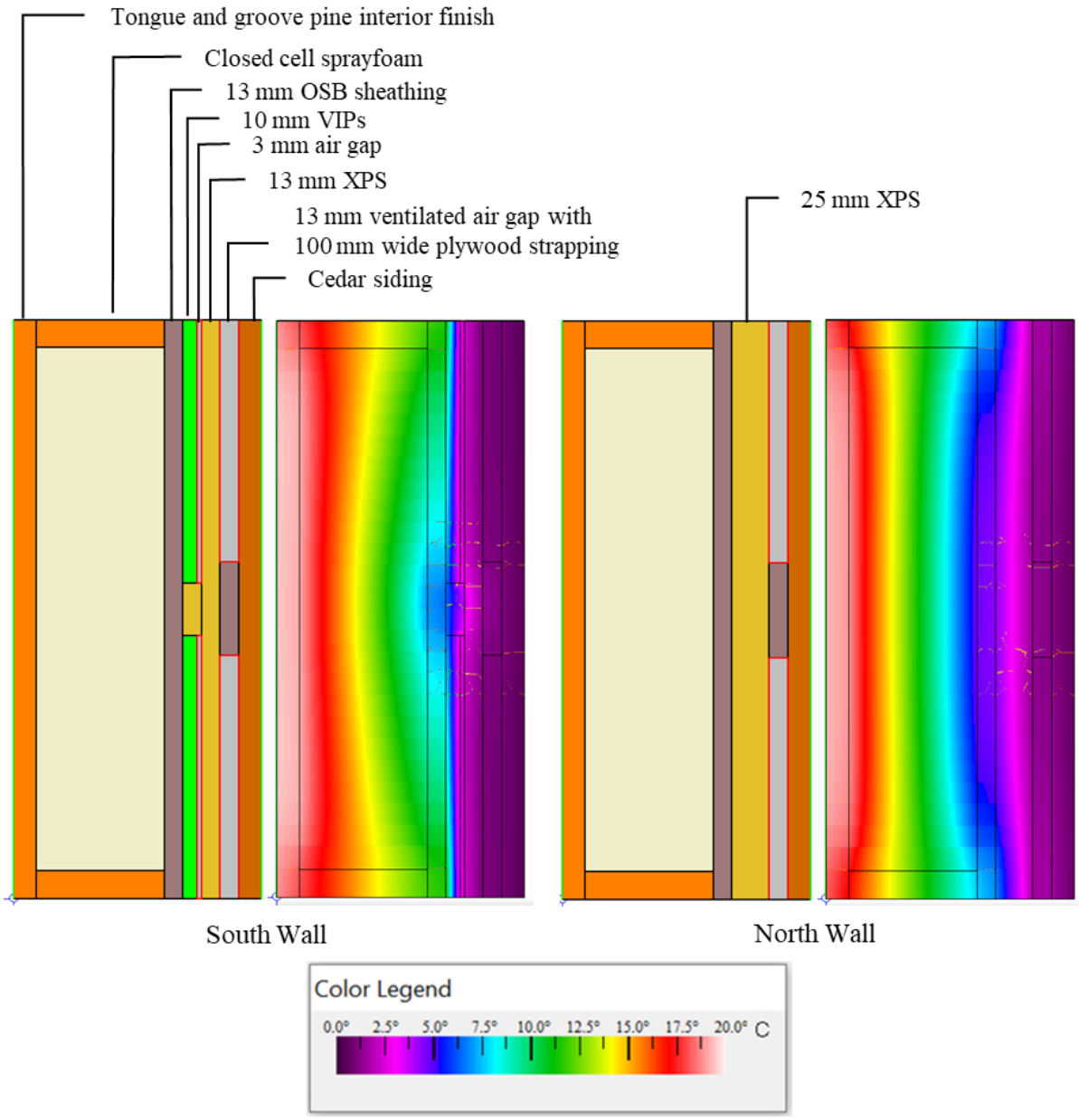


**Figure 5-3: Heat flow model results showing temperature gradients in the south wall (left) and north wall (right)**

From the heat flow models, the estimated thermal resistances were 5.90 RSI for the south wall and 4.23 RSI for the north wall. The models predicted that the wall containing VIPs performed 40% better than the wall without VIPs, with an increase of 1.67 RSI (R-9.5). Sheathing temperature was approximately 2°C warmer on average in the VIP wall, increasing the moisture

buffering capacity of the sheathing and potentially reducing the risk of condensation. Thermal bridging at VIP joints was very prominent, resulting in a total temperature variation of approximately 4°C at different locations of the sheathing. The wall without VIPs exhibited temperature variations of approximately 2°C due to thermal bridging through the studs. Results were compared with measured results from Section 5.1.1 in Table 5-1.

**Table 5-1: Measured and simulated thermal resistance of the south and north walls**

| Wall Assembly | Measured RSI [$m^2K/W$] | Simulated RSI [$m^2K/W$] | Difference [%] |
|---|---|---|---|
| North Wall (No VIPs) | 4.59 | 4.23 | -7.8 |
| South Wall (VIPs) | 5.89 | 5.90 | 0.1 |
| Improvement | 1.30 | 1.67 | |

When comparing between the measured and simulated results, several sources of uncertainty were considered and are discussed in additional detail in Appendix C:. In summary, the significant sources of uncertainty include VIP conductivity, air cavity effective conductivity, surface transfer coefficients, and radiant effects from the environment. The sensitivity to these uncertainties is unknown, but the close agreement between model estimates and RSI test results suggest that the total uncertainty is low enough that general conclusions can be made with reasonable truth. Without a thorough uncertainty analysis and validation, any further analysis that could propagate the unknown error of these results, such as annual heating energy calculations, should be avoided and a validated model should be used instead. The benefit of this unvalidated model is that it provides a fast, simple comparison for double-checking the results of the RSI testing. The estimated temperature profiles from the model can be considered when evaluating the

building envelope data in section 5.5, allowing for expanded discussions about how VIP arrangements may be modified to reduce mold growth risks and improve VIP service life.

The measured and simulated performance of the walls show that the thin VIP-integrated walls achieve high thermal performance in a thin assembly. VIP integration provided approximately 50% better insulation performance than code and a 34% increase over a baseline wall without VIPs, with no increase in thickness. The 5.9 RSI achieved by the 170 mm (6.75 inches) thick VIP wall is comparable to a 330 mm thick (13 inches) double-stud wall with blown cellulose insulation, at half the thickness. In the Northern Nomad, with 20 m of wall length, the thin walls preserve 3.2 $m^2$ of floor space compared to a double stud wall, which is 7% of the total floor space and is equivalent to the size of the bathroom. The space saving benefits of VIP integrated walls is evident, and their thermal performance is excellent for their thickness.

Having compared the wall model simulations with measured data, models of the floor and roof can be created similarly and evaluated with reasonable confidence. These models were not created in this work but were considered valuable for future work.

## 5.2 Air Leakage

### 5.2.1 Blower Door Tests

Before the battery box work, the blower door test (Test 1) indicated a normalized leakage (NL) of 0.32 L/s·$m^2$ @ 50 Pa. After the battery box work, the second blower door test (Test 2) showed 1.33 L/s·$m^2$ @ 50 Pa, confirming that the enclosure penetrations significantly reduced airtightness. Other airtightness units are listed in Table 5-2.

**Table 5-2: Measured airtightness from tests 1 and 2 expressed in different units**

| Airtightness Unit | | Test 1 | Test 2 |
|---|---|---|---|
| Air Changes per Hour | [ACH @ 50 Pa] | 2.5 | 10.3 |
| Normalized Leakage | [L/s·m$^2$ @ 50 Pa] | 0.32 | 1.33 |
| Normalized Leakage | [L/s·m$^2$ @ 75 Pa] | 0.46 | 1.74 |
| Equivalent Leakage Area | [cm$^2$/m$^2$ @ 10 Pa] | 0.32 | 1.85 |

Recall the high surface-to-volume ratio of the Northern Nomad house which inherently reduces the apparent airtightness performance, especially when considering air changes per hour. Instead, normalized leakage at 75 Pa is the metric used for comparing blower door results with different airtightness benchmarks, listed in

Table 5-3. The house performed well in the first test, exceeding the ASHRAE definition of a tight house by 9%, R-2000 by 30%, and UK best practices for homes by 57%. In the second test, the house was 14% leakier than an average home according to ASHRAE, and only 5% tighter than normal UK homes. In the first test, the house was comparable to a well-built new house in Canada, but in the second test, the house was more comparable to an average house from the 1950s in terms of $ACH_{50}$.

**Table 5-3: Comparison of blower door test results to various airtightness benchmarks**

| Standard | Normalized Leakage [L/s·m$^2$ @ 75 Pa] | Test 1 | Test 2 |
|---|---|---|---|
| ASHRAE 90.1, leaky | 3.05 | -85% | -43% |
| UK normal, offices and homes | 1.83 | -75% | -5% |
| Smoke control standards | 1.63 | -72% | 7% |
| ASHRAE 90.1, average | 1.52 | -70% | 14% |
| LEED | 1.52 | -70% | 14% |
| US Army Standard | 1.27 | -64% | 37% |
| IGCC 2012 | 1.25 | -63% | 39% |
| Energy Star Homes 12.6 | 1.21 | -62% | 44% |
| UK best practice, homes | 1.07 | -57% | 63% |
| UK best practice, offices | 0.71 | -35% | 145% |
| Canadian R-2000 | 0.66 | -30% | 163% |
| ASHRAE 90.1, tight | 0.51 | -9% | 243% |

The high air leakage of the Northern Nomad is estimated to have a considerable effect on energy consumption, indoor humidity levels, and potentially even durability. The primary concern is that warm, humid indoor air moving through the building envelope may reach cold surfaces near the exterior of the assembly and condense, which could lead to moisture buildup if there is not sufficient drying. Additionally, an interior surface cooled by infiltration to near or below the dewpoint of the indoor air could promote mold growth. Infiltration has combating effects: the air leakage areas may be the most likely areas for mold growth at high indoor humidity levels, but the increased air exchange tends to cause low indoor humidity that is beneficial for preventing mold growth. It is known, however, that leaky houses are more likely to develop mold, so the best

practice is to improve airtightness and control humidity properly. This is discussed more in the next section, where potential problem areas are investigated using infrared thermography.

### 5.2.2 Thermography

The infrared photos highlighted several cold surfaces inside the Northern Nomad. The air infiltration through the battery box is evident in Figure 5-4, showing surface temperatures as low as 15.6°C while the room temperature was 24°C. According to the infrared photos, the battery box appears to account for a significant portion of the heat loss in the house. This was a result of the vent holes added to the battery box to comply with regulatory standards on the safe usage and storage of lead-acid batteries. In the future, it would be beneficial to thoroughly seal the battery box from the interior space, or switch to lithium-ion batteries that do not require venting.


**Figure 5-4: Battery box photos: regular (left) and infrared (right) showing significant heat loss**

The window frames were around 18°C at their coldest parts, the door sill was around 12°C, the wall joint at north-east corner was around 16°C, and below the kitchen cabinets there was an unfinished section of flooring along the south wall that was around 13°C. These cold surfaces are the most likely areas to accumulate excess moisture if the indoor humidity is high enough, which

could lead to mold growth. If the indoor humidity were above 50% RH when the infrared photos were captured, the dew point would have been 13°C and there would have been condensation on the door sill and possibly under the cabinets. If the outdoor air were at -10°C, there may have been condensation at the battery box and on the walls in the corner of the bathroom. If the Northern Nomad were occupied by two or three occupants without ventilation, indoor conditions at 24°C and 50% RH in the winter may occur for short periods, for example, during cooking or showering activities. If these periods are frequent, there could be a risk of mold. Occupants may also desire to use a humidifier for health reasons which could elevate risks of mold. To avoid problems, there should be ventilation in place for those periods to moderate humidity. Alternatively, the cold areas could be improved with insulation or air sealing. The best solution would be a combination of ventilation, air sealing, and insulating.

In addition to locating potential condensation areas, thermography was used to investigate thermal bridging effects of VIPs and framing members. The ceiling of the house (Figure 5-5) exhibited some thermal bridges at the rafters, as expected, since the cavities contain VIPs and closed cell spray foam insulation. The ceiling surface was around 24°C between rafters and around 22°C on the rafters. Most of the interior of the envelope showed similar temperatures and minor thermal bridging. Thermal bridging around individual VIPs was not observed since they were too deep in the building envelope to be observed on the surface.


**Figure 5-5: Regular (left) and infrared (right) photos of the ceiling showing thermal bridging along rafters**

Exterior Infrared photos were taken during overcast conditions without significant sunshine earlier. Figure 5-6 and Figure 5-7 showed some heat loss at the window and door frames on the south façade, but thermal bridging around the VIPs was not observed due to the air cavity rainscreen. Some vertical variation in cladding temperature was observed which may indicate either the presence of buoyancy driven airflow in the cavity or higher wood moisture content in the lower part of the cladding. There was evidence of some snowmelt dripping down the cladding and accumulating above the trailer frame which may lead to stains or rot over time.

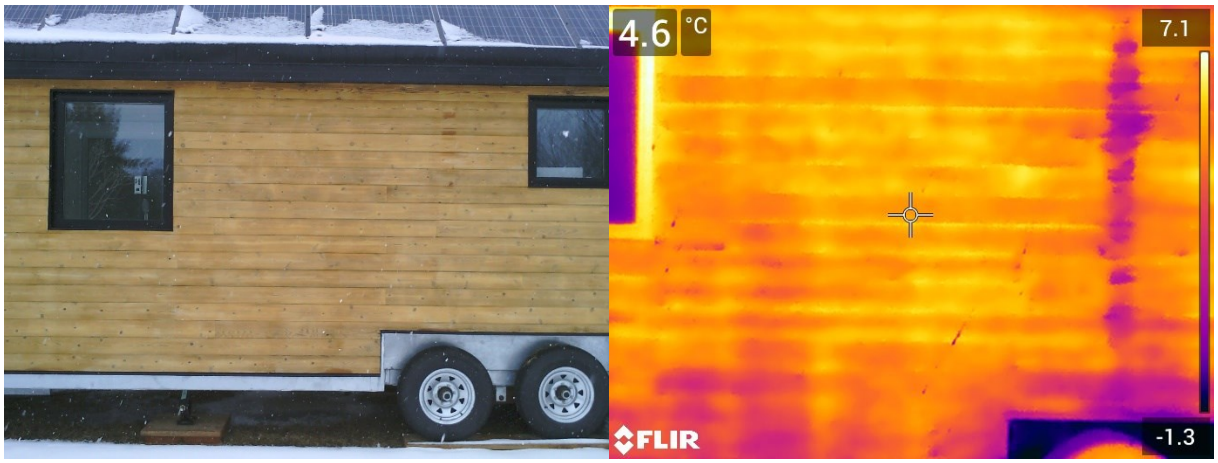


**Figure 5-6: Regular (left) and infrared (right) photos of the south façade showed some surface water (magenta), window frame thermal bridges, and some vertical variation in cladding temperature**

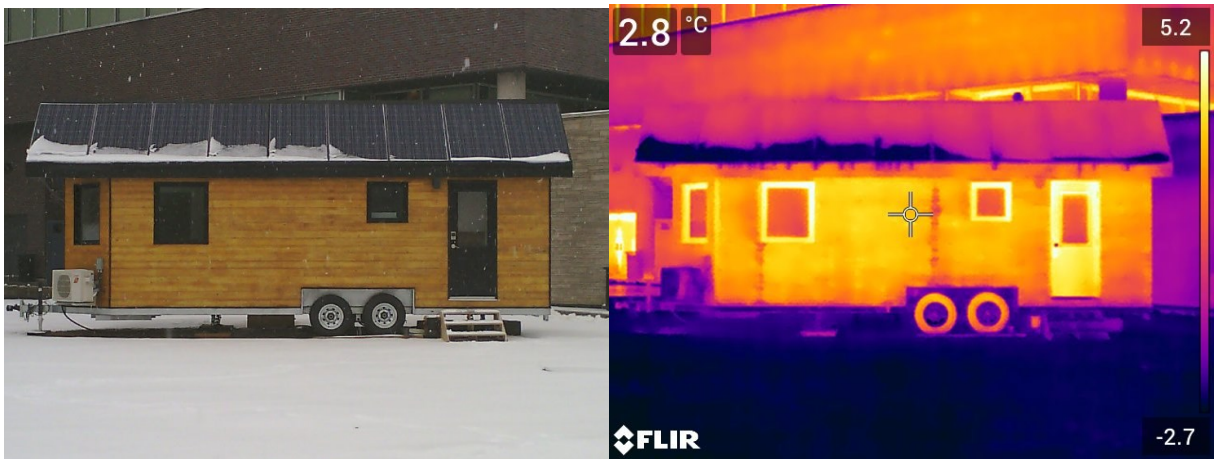


**Figure 5-7: South façade regular (left) and infrared (right) photos from a distance**

This concludes the evaluations of airtightness and insulation of the Northern Nomad which established that the house achieved high levels of insulation but poor airtightness due to the battery box penetrations. The findings from these evaluations were referred to as needed while discussing the remaining experimental results.

## 5.3 ERV

### 5.3.1 Airflow Measurements

Supply and exhaust air flow rates of the ERV in the Northern Nomad were measured using the garbage bag airflow test at high and low speed settings. Flow rate was measured on the low setting on June 6th, 2019 and the high setting on October 9th, 2019, although only the supply flow rate was measured on the high setting. When performing the tests, this method was refined such that the results were repeatable within 10% of the average result. Based on an analysis of the technique and apparatus used, there was little indication that the method would produce significant inaccuracy. By taking an average of 10 measurements, the results were deemed reasonably accurate for this study, which were estimated to be within 0.5 L/s of the true flow rate. The test results are listed in Table 5-4, showing that the ERV achieved a supply flow rate just below nominal with 8.5 L/s and it achieved a nominal exhaust flow rate of 9.5 L/s. The high speed supply flow rate was far below nominal (14.2 L/s) at 10.9 L/s. It was suspected that the ducting was too restrictive and the small blower in the ERV could not overcome the pressure loss along the ducts to maintain nominal airflow. It was also observed that the intake air filter can significantly reduce airflow if it is not cleaned regularly. A clogged filter resulted in a reduction of 3.1 L/s compared to a clean filter.

**Table 5-4: Measured and nominal flow rates of the ERV using the garbage bag method**

| | | Supply Low | Exhaust Low | Supply High Dirty Filter | Supply High Clean Filter |
|---|---|---|---|---|---|
| Average Fill Time | [s] | 10.9 | 9.9 | 12.1 | 8.7 |
| Measured Flow Rate | [L/s] | 8.6 | 9.5 | 7.8 | 10.9 |
| Nominal Flow Rate | [L/s] | 9.4 | 9.4 | 14.2 | 14.2 |

Air speed measurements were used to determine the time-series airflow rates in the ERV, with a goal of using an average duct velocity along with the duct area to calculate flow rate. Figure 5-8 and Figure 5-9 illustrate the air speed profiles in the supply and exhaust ducts on the low setting, approximated using centered differencing to estimate air speed between measurement locations. The air speed near the walls of the ducts could not be measured due to the geometry of the probes, leaving a large portion of the duct area uncharacterized. The air speed profiles were non-uniform, especially in the exhaust duct where the blower upstream appeared to contribute to highly variable air speeds at different measured locations. This variability made it difficult to extrapolate air speeds near the walls of the duct, so the average air speed could not be determined.

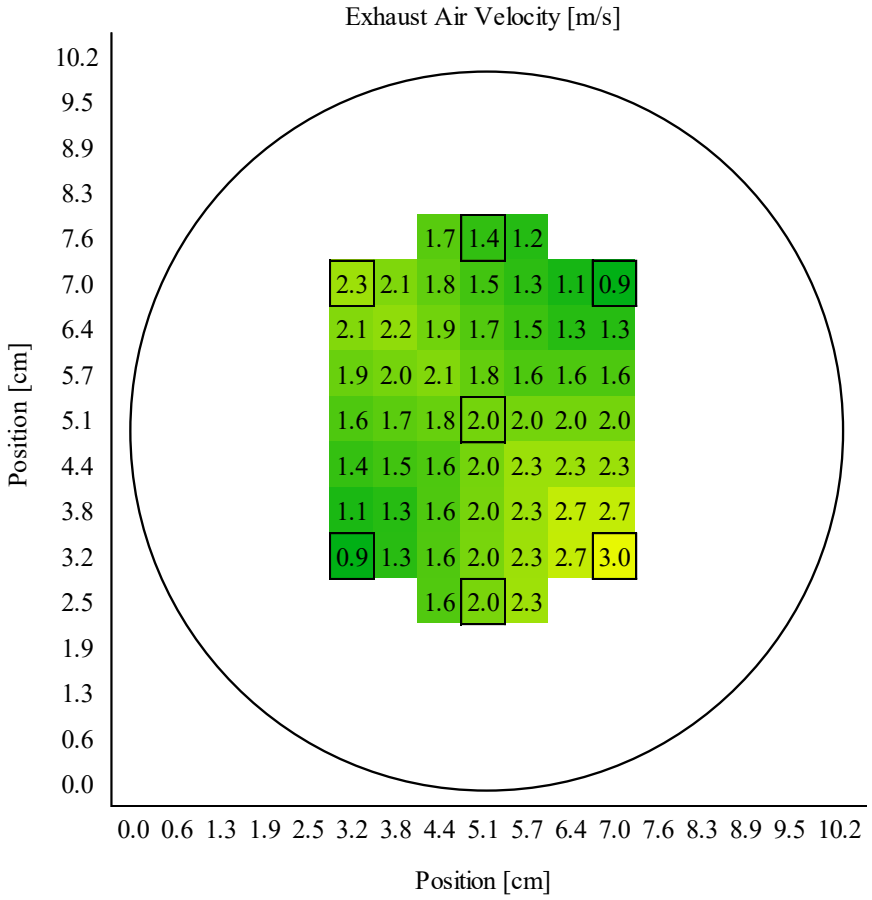


**Figure 5-8: Exhaust air velocity across the duct cross section, with measured points outlined**

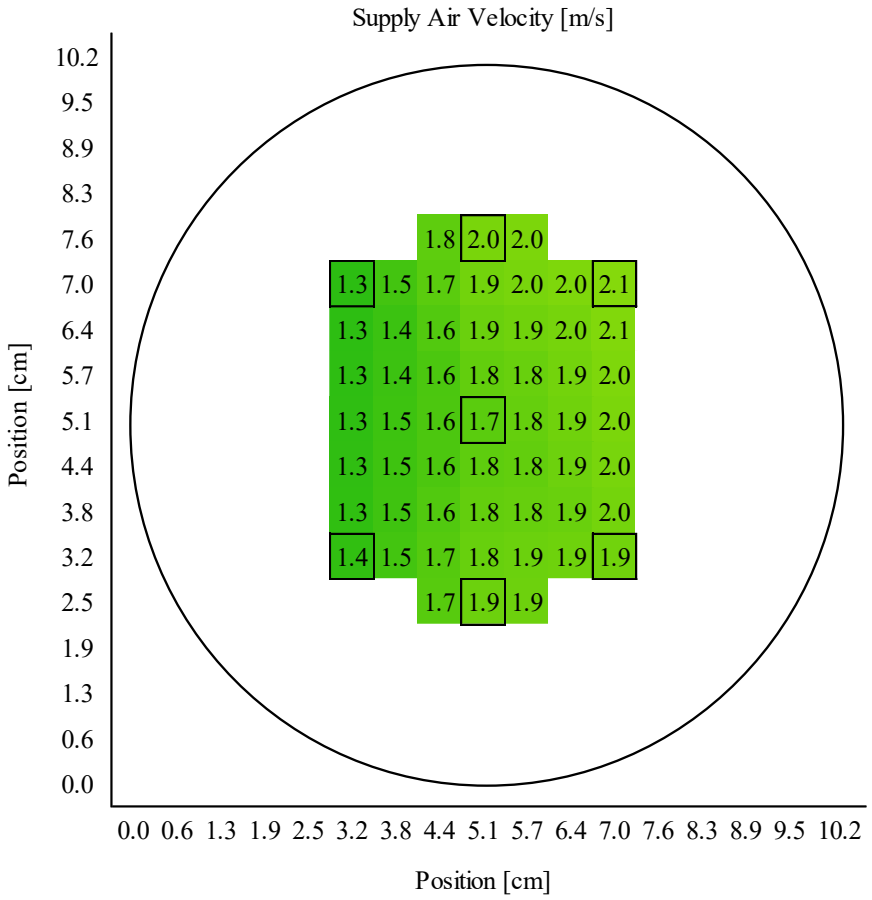


**Figure 5-9: Supply air velocity across the duct cross section, with measured points outlined**

Without air speed data near the walls of the ducts, average air speed could not be determined. An alternate method was used, described in Section 4.4.2, which used an effective area (EA) to convert center-of-duct air speed to flow rate. During the low-speed garbage bag test, where supply and exhaust flow rates were 8.6 L/s and 9.5 L/s, respectively, the center-of-duct air speeds were 1.75 m/s in the supply duct and 1.95 m/s in the exhaust duct. This resulted in an effective area of $4.9\times10^{-3} \pm 3.6\times10^{-4}$ m$^2$ for both airstreams. To verify, this was compared to the actual duct area which is $7.8\times10^{-3}$ m$^2$. Since the center-of-duct air speed is presumably higher than the true average air speed, the EA should be smaller than the actual duct area so this value of EA seems reasonable. This was used to convert the time series air speed data to flow rate shown in

Figure 5-10 for the period of May 23rd, 2019 to July 7th, 2019, where the ERV speed setting is indicated by the bars above the graph. The estimated error for this data is ± 0.61 L/s.

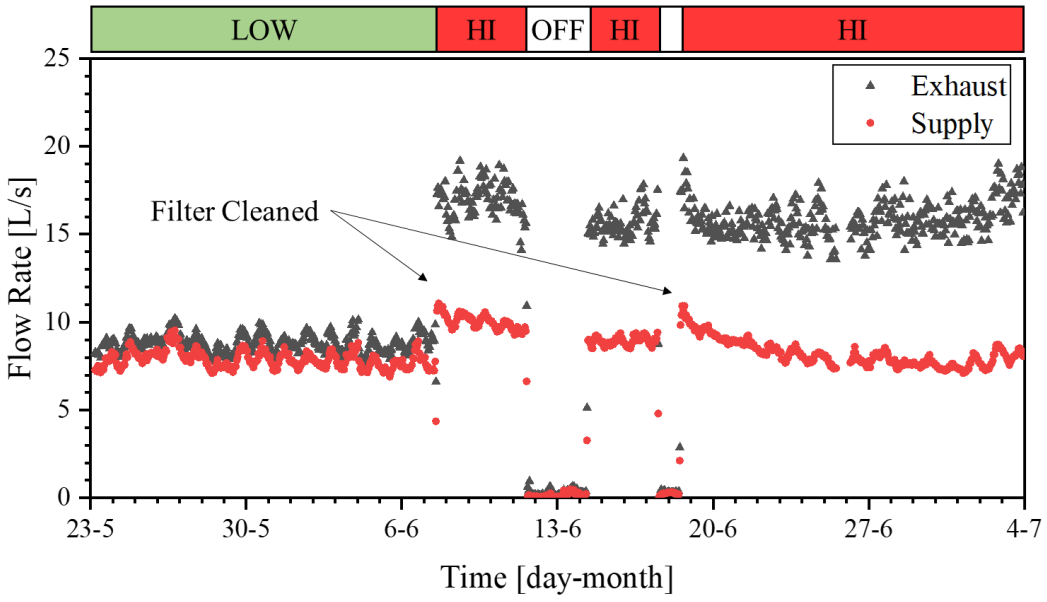


**Figure 5-10: Supply and exhaust flow rates from May 23rd, 2019 to July 7th, 2019 with the ERV speed setting (LOW, HI, OFF) and annotated dates when the filters were cleaned**

According to this data, the supply flow rate on the high setting with a clean filter was approximately 11 L/s, just 4% off from the garbage bag test. Assuming the results of the garbage bag test were reasonably accurate, this agreement suggests that this method is suitable for estimating flow rates in a ventilation system under different conditions using only air speed probes. It is noted, however, that the hot wire manometer readings fluctuate with temperature and no post-processing was applied to compensate for this which explains the daily fluctuations in flow rate. This error was acceptable for this study since average flow rates are all that is needed. More accuracy would require temperature compensation which can be found in the literature.

Figure 5-10 illustrates several insights about the ERV flow rates. Within one week after cleaning the supply air filter, the accumulation of contaminants restricted the supply flowrate by

around 20%. This caused a more drastic imbalance between exhaust and supply streams which increased air infiltration through the envelope, deminishing the heat recovery benefits of the ERV.

A summary of the flow rate data is shown in Table 5-5. On average, the low speed setting performed nominally, with a nearly balanced ratio of supply and exhaust flow. The high speed setting does not provide nearly as much ventilation as specified, perhaps because the manufacturer may be using ideal conditions for publishing specifications.

**Table 5-5: Nominal and average ERV air flow rates from air speed measurements**

| Speed Setting | | Low | | | High | | |
|---|---|---|---|---|---|---|---|
| **Flow** | | Supply | Exhaust | Imbalance | Supply | Exhaust | Imbalance |
| **Average** | **[L/s]** | 7.28 ±0.41 | 8.79 ±0.46 | 1.51 ±0.62 | 10.24 ±0.62 | 16.01 ±1.12 | 5.77 ±1.28 |
| **Nominal** | **[L/s]** | 9.4 | 9.4 | 0.0 | 14.2 | 18.9 | 4.7 |

The high speed setting was imbalanced by 5.77 L/s, exhausting air 56% more quickly than it supplied. This presumably depressurized the house and induced air infiltration, which is less energy efficient than if the ERV were balanced. This also created drier conditions in the winter and more humid conditions in the summer which can both reduce occupant comfort. This pressure-induced air leakage is detrimental to energy efficiency and occupant comfort, which are two of the main performance objectives of the Northern Nomad house. The ERV should be balanced so that it can contribute to the high performance of the house, not reduce it. Balancing can be done by damping the exhaust flow or enlarging the supply duct.

### 5.3.2 Psychrometrics

Temperature and relative humidity at each inlet and outlet of the ERV were recorded every 10 minutes from May 10th, 2019 to January 21st, 2020 allowing for a wide range of operating conditions to be observed. Hourly average temperatures at the two inlets of the ERV are plotted in Figure 5-11, for which the maximum estimated error is ±0.22°C according to Equation (A.7) found in Appendix A:. The ERV speed was set to low on May 10th, then switched to high on June 7th. The ERV was turned off on July 4th and turned back on to high mode on July 10th. It was turned off again on October 18th and turned on to high on November 5th. During November and December, the freezing outdoor temperatures made the ERV run in one of the two defrost cycles described in Section 3.2.

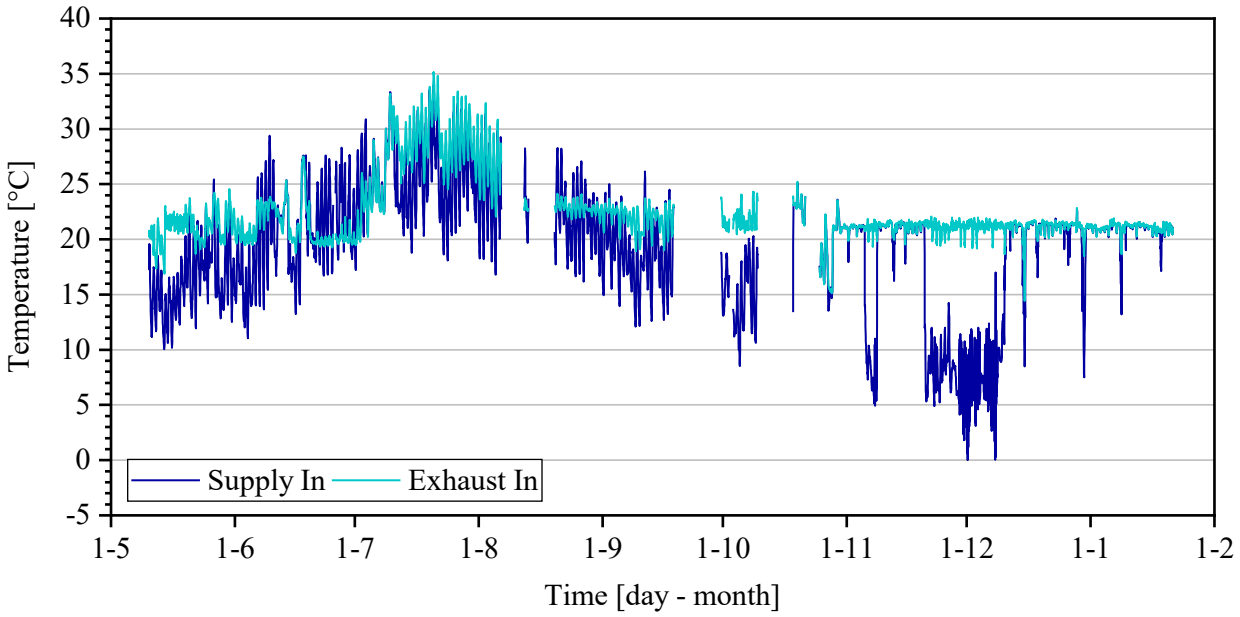


**Figure 5-11: Temperature of the air entering the supply and exhaust inlets of the ERV for the measurement period**

During ERV monitoring, the indoor temperature setpoints were 21°C for heating and 24°C for cooling. In early June 2019, the heat pump began losing cooling power and by July 8th, it had

stopped working completely. This means that the house had no cooling from July 8th until August 12th, when the heat pump was replaced. Due to the passive solar heating through the windows, low thermal mass, and no slab or foundation to conduct heat to the cool ground, the indoor air (28.9°C) was 4.5°C warmer than the outdoor air (24.3°C) on average during that period. Meanwhile, the ERV supplied 28°C air at around 8 L/s on average and it induced some infiltration due to the imbalanced exhaust (discussed in Section 5.3.1), so some cooling was provided. However, it could have been more effective if the ERV were balanced and if the supply air could bypass the enthalpy core.

### 5.3.3 ERV Effectiveness Characterization

Sensible and latent effectiveness were calculated hourly from 00:00 on May 10th, 2019 to 23:00 on December 31st, 2019. Some effectiveness values were above one or below zero due to transient effects, times when the ERV was off, and instances where indoor and outdoor conditions were too close in value. Consequently, it was decided to filter out these data points. Periods that would give the clearest results of effectiveness during heating and cooling were isolated and examined. This includes periods of constant ERV operation and suitable temperature or humidity differentials.

Calculating latent effectiveness required enough of a moisture differential between indoor and outdoor air to cause some moisture transfer between air streams. For the cooling season, the outdoor air contained more moisture than the indoor air so latent effectiveness was evaluated easily. The period from 00:00 June 22nd, 2019 to 00:00 July 14th, 2019 (22 days) provided appropriate conditions for determining latent effectiveness during cooling with the ERV on high mode, with mean air conditions of 21.2°C, 57% RH inside and 22.8°C, 66% RH outside. During

that time, the mean latent effectiveness was 0.35 and the mean sensible effectiveness was 0.64. Figure 5-12 illustrates the relatively symmetric and close packed distributions of sensible and latent effectiveness during this period, which suggests that the mean effectiveness values are reasonable for modelling or estimating the performance of the ERV during cooling.

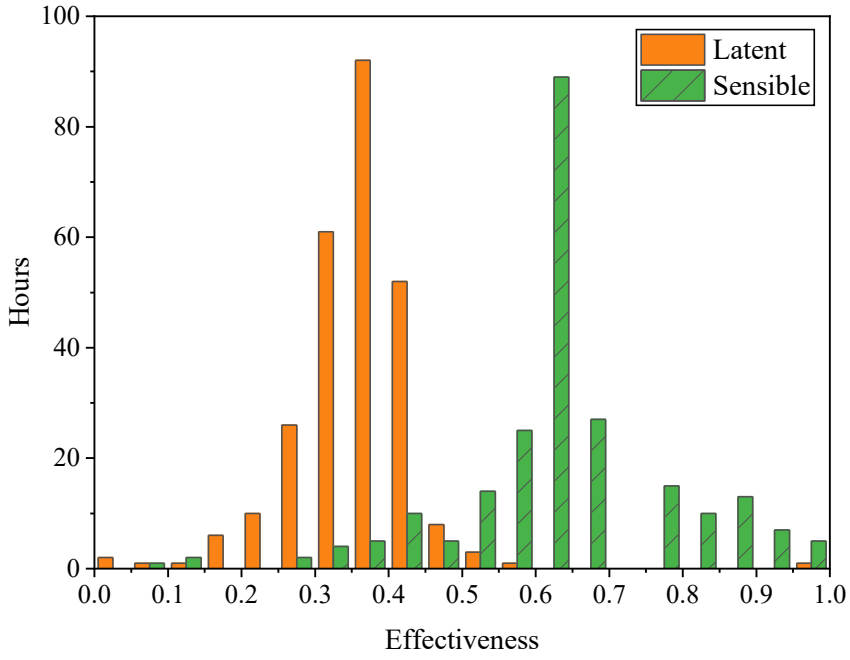


**Figure 5-12: ERV Effectiveness during cooling on high mode**

To determine latent effectiveness during heating, there must be indoor moisture loads to create a significant moisture differential, otherwise the indoor and outdoor humidity ratios are too similar and latent effectiveness is too variable. Furthermore, the outdoor air temperature should be above 0°C to avoid capturing defrost cycles in this analysis. A suitable period is between 13:00 on November 5$^{th}$, 2019 to 22:00 on November 7$^{th}$, 2019, when the house was humidified and the ERV was on the high setting. Average air conditions for this period were 21.1°C, 44% RH inside and 4.6°C, 73% RH outside. Effectiveness distributions are plotted in Figure 5-13 showing relatively

tightly packed datasets with a mean latent effectiveness of 0.26 and mean sensible effectiveness of 0.70.

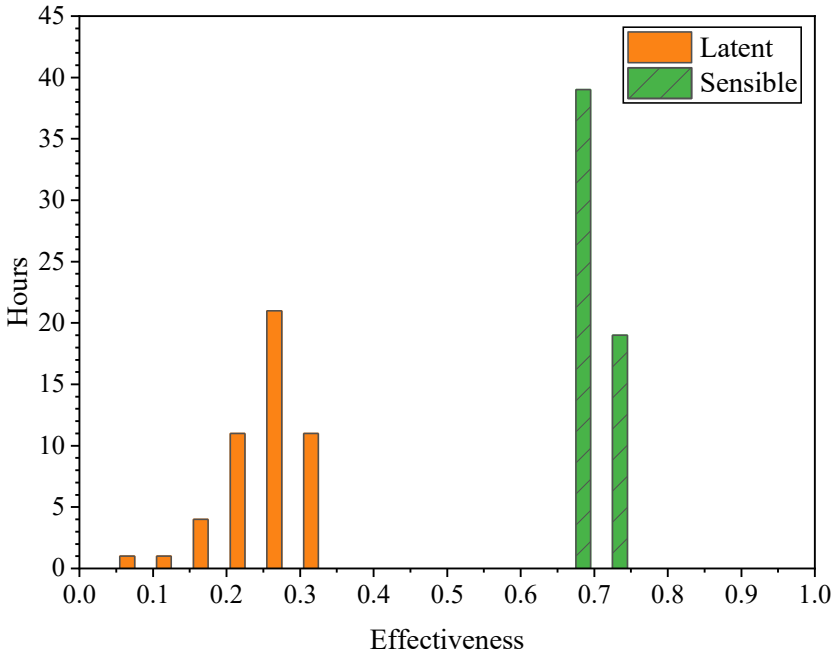


**Figure 5-13: ERV Effectiveness during heating on high mode**

For the low speed setting, the period from 00:00 on May 15th, 2019 to 00:00 on May 21st, 2019 (6 days) was evaluated, where average air conditions were 21.9°C, 37% RH inside and 13.7°C, 73% RH outside. For this period, the outdoor humidity ratio was usually higher than indoors except for some periods when the humidity differential was very small. The average sensible effectiveness was 0.77 and the average latent effectiveness was 0.55. However, the latent effectiveness was bimodal, as seen in Figure 5-14, with a collection of values around 0.45 when the humidity differential was high and around 0.70 when the humidity differential was very small. It can therefore be concluded that 0.45 is more appropriate for describing latent effectiveness during heating on low speed.

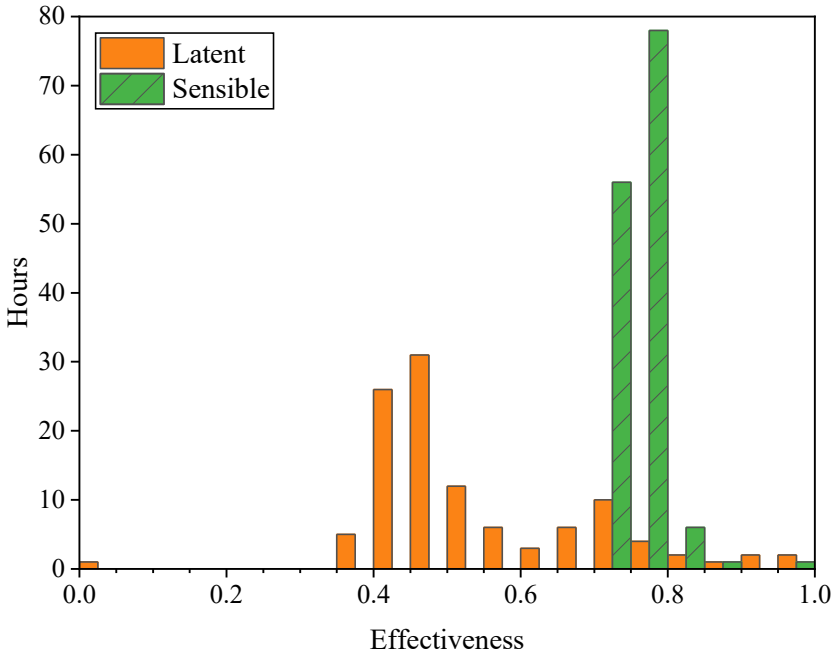


**Figure 5-14: ERV Effectiveness during heating on low mode**

The effectiveness data is summarized in

Table 5-6. This data can be used to provide accurate inputs to future energy models or hygrothermal models. Energy models could be used to predict energy loads based on different modes of ERV operation, which can determine ERV schedules for optimizing energy efficiency. Similarly, models can be used to predict indoor humidity in the Northern Nomad using different ERV schedules, which can be applied to hygrothermal models of the building enclosure to evaluate mold growth risk. This effectiveness data contributes to improving the accuracy of predictions regarding the impact of ERVs on moisture in buildings.

**Table 5-6: Summary of average ERV effectiveness data**

| | Heating | | Cooling | |
|---|---|---|---|---|
| Speed Setting | High | Low | High | Low |
| Indoor Air | 21.1°C<br>44% RH | 21.9°C<br>37% RH | 21.2°C<br>57% RH | Not Measured |
| Outdoor Air | 4.6°C<br>73% RH | 13.7°C<br>73% RH | 22.8°C<br>66% RH | Not Measured |
| Sensible Effectiveness | 0.70 ±0.02 | 0.77 ±0.02 | 0.64 ±0.02 | Not Measured |
| Latent Effectiveness | 0.26 ±0.05 | 0.45 ±0.05 | 0.35 ±0.05 | Not Measured |

### 5.3.4 Defrost Cycle

When the outdoor temperature dropped below freezing, the ERV entered the defrost cycle, closing the intake damper 30 minutes per 90-minute cycle. The defrost cycles were identified using the air temperatures in the ERV and a sample from December 6th is illustrated in Figure 5-15.

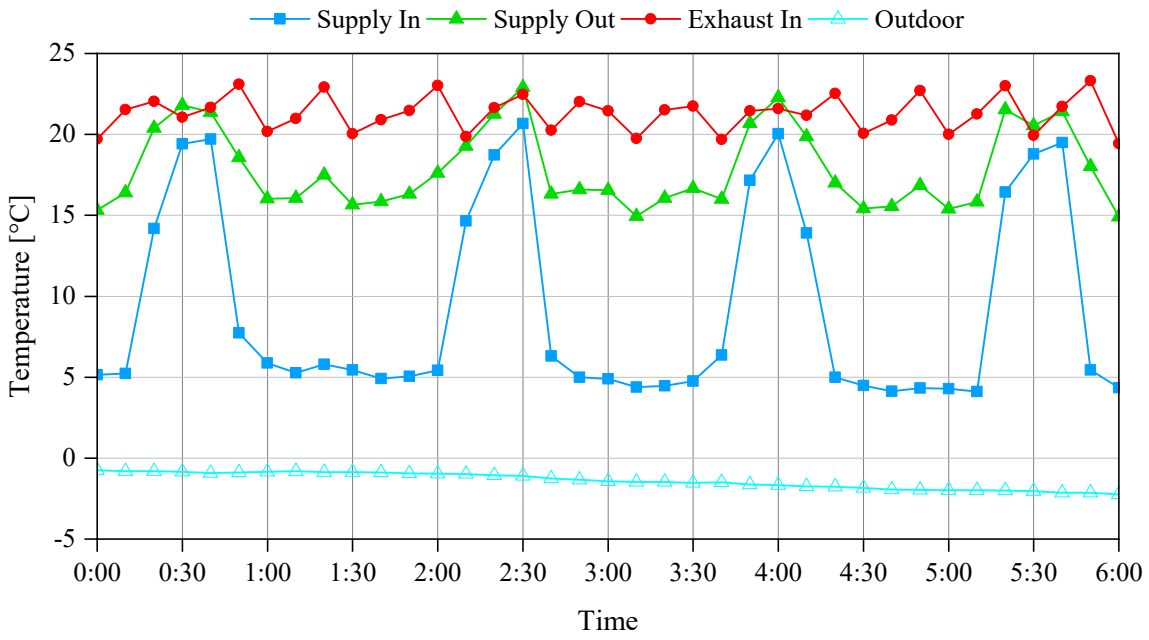


**Figure 5-15: Temperature data from December 6th, 2019, illustrating the 30/60 defrost cycle**

After several days, the outdoor temperature dropped further, activating the second defrost cycle where the intake damper was closed for 60 minutes per 80-minute cycle. The ERV operated in these two defrost modes for the entire winter. The overall exhaust and supply flow rates during defrost cycles are much more imbalanced than in normal operation which already demonstrated a substantial imbalance. This further increased air infiltration into the house during the winter which suggests that this ERV is not an energy efficient ventilation solution for this house in the Ottawa climate. An HRV may be a better choice for the winter since it does not require a defrost cycle. Alternatively, if the supply air could be preheated before entering the ERV, then the winter operation may be improved. On the Northern Nomad, the solar heat energy absorbed by the BIPV roof could be used to passively preheat supply air, improving winter ventilation, and potentially reducing heating energy demand. Evaluating energy efficiency is not the focus of this study, but the house was intended to be energy efficient, so any efficiency deficits that are found should be discussed.

In terms of the effect on moisture durability, the defrost cycle appears to be beneficial. During periods of high internal moisture generation, running in exhaust-only mode removes excessively humid air and replaces it with dry, infiltrated air, which ultimately keeps the enclosure dry. The ERV provides a path for air to leave the house instead of using air leakage paths within the enclosure, which could be problematic. As for occupant comfort, the low levels of indoor humidity that this system achieves would not be ideal, but with such high air leakage, it would be difficult to maintain a comfortable humidity anyway. It would be best to keep humidity levels between 40-60% RH which could be best achieved by keeping the ERV off when humidity levels are acceptable, and only running it when indoor humidity exceeds 60% RH.

## 5.4 Impact of ERV and Infiltration on Indoor Humidity

Short term humidification of the Northern Nomad revealed interesting details about how vapour moves between the indoors and outdoors through the ERV and through air leakage pathways. The house was humidified for several periods in October and November 2019, when the outdoor temperature ranged between -3°C and 19°C and the house was heated to a constant setpoint of 21°C. The amount of water consumed by the humidifier was measured each time it was refilled. Two separate periods of humidification can be examined: the first was with no ventilation, and the second was with the ERV set to the high speed setting.

### 5.4.1 Humidity Without Ventilation

The indoor RH and outdoor temperature during the humidification period without the ERV running are shown in Figure 5-15.

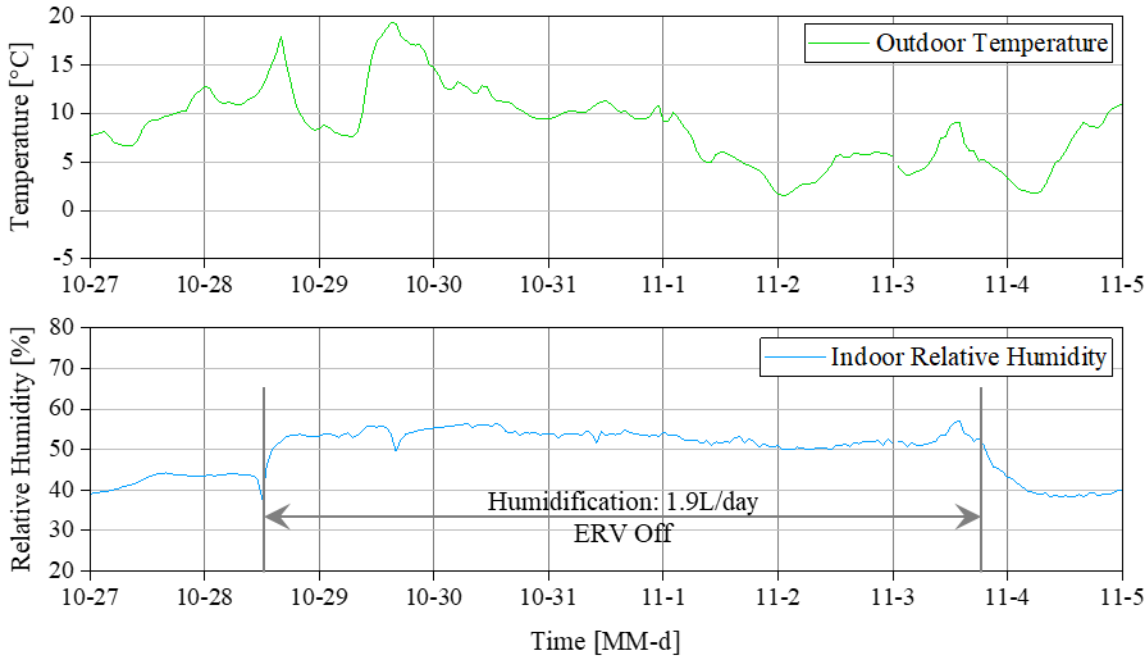


**Figure 5-16: Air conditions during a period of humidification with the ERV off**

With the ERV off, the house was humidified to an average of 53% RH at 21.5°C for six days with the average outdoor air at 7°C and 92% RH. Over this period, the average rate of moisture generation was 1.9L/day which was the closest setting on the humidifier for simulating the 2.6 L/day that was estimated for two occupants, as listed in Table 4-3. The resultant level of humidity was within the optimum range for human health according to Sterling et al [8], suggesting that in cool temperatures, no mechanical ventilation is needed to maintain a healthy humidity in the Northern Nomad when occupied. This is an indication that the Nomad exhibits a significant amount of air leakage, which was confirmed by blower door tests and thermography in Section 5.2. During testing, it was observed that more humidification was required during periods of colder outdoor temperatures, further confirming the presence of substantial air leakage.

The indoor temperature and RH from the humidification study were used to check if condensation is likely to form on cold surfaces that were identified with thermography in Section 5.2.2. The most likely instance of condensation during the humidification was when outside temperature was at its coldest, 1.7°C, at which time the indoor dewpoint temperature was 10.7°C. At a slightly lower outdoor temperature, thermography found no interior surfaces below 12°C, suggesting that condensation on indoor surfaces is not a concern under typical occupancy conditions where indoor humidity is estimated to stay below 55% RH most of the time. In a larger house, humidity levels caused by two occupants would be lower, so condensation is even less of a concern. The test data lacks information about humidity levels during humidification at outdoor temperatures below 1.7°C, which could lead to different conclusions about the risk of condensation without ventilation.

### 5.4.2 Humidity with ERV

The second period of humidification took place from 14:00 on November 6th, 2019 to 14:00 on November 8th, 2019, with the ERV on at the high flow setting and the humidifier on the highest output setting. The indoor RH and the outdoor temperature during this period are shown in Figure 5-16.

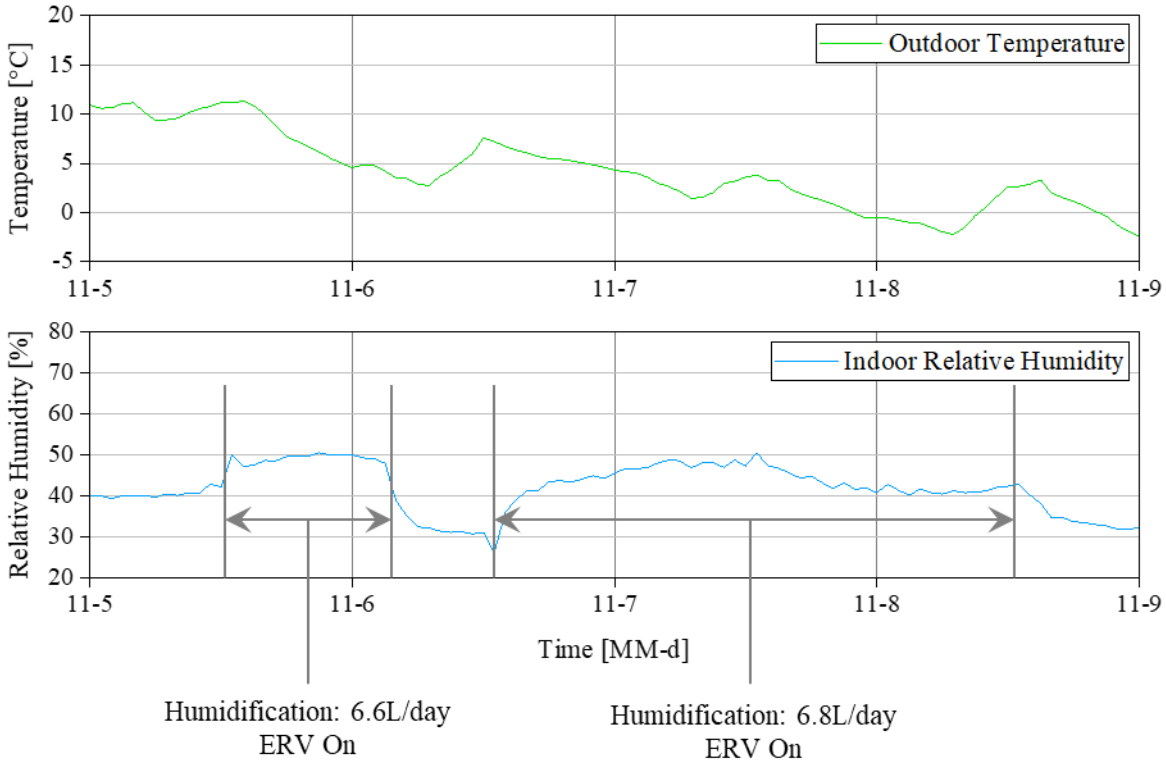


**Figure 5-17: Air conditions during a period of humidification with the ERV on**

The average outdoor conditions over these periods were 2°C and 73% RH. Excluding start-up periods, the indoor relative humidity varied between 40% and 50% RH, and the average moisture generation rate was 6.6 L/day for the first period and 6.8 L/day for another period. As expected, the ERV removed a substantial amount of moisture from the house, especially during colder and drier weather. Utilizing this ERV during periods of intense moisture generation would

sufficiently moderate indoor RH so that condensation and high surface RH on interior surfaces is avoided.

### 5.4.3 Moisture Balance Analysis

Moisture balance calculations, described in Section 4.5, were completed for the period from October 29th to November 3rd, 2019 where the ERV was off. In summary, the mass rate of moisture movement through the building envelope via air leakage was determined using a known moisture generation rate and the humidity ratios for indoor and outdoor air. The results estimated that the air leakage rate without the ERV was 0.67 ACH or 30 $m^3$/h. This can be compared with the blower door test results in Section 5.2.1 by dividing the measured air leakage rate at 50 Pa by 16 to estimate the equivalent air leakage rate at ambient pressure. Using this conversion, the blower door result of 10.3 ACH @ 50 Pa would give 0.65 ACH at ambient pressure, which agrees with the 0.67 ACH calculated from the moisture balance. This suggests that the air leakage estimates thus far are reasonable. 0.67 ACH is a very high air leakage rate that has a significant effect on conditioning loads and indoor humidity levels.

A moisture balance calculation was also completed for the period from November 6th to November 8th, 2019 when the ERV was on high. The calculation determined air flow rates and total moisture transported using known values for internally generated moisture, ERV flow rates, and humidity ratios indoors, outdoors and in the ERV ducts. The volumetric air flow rates of the infiltration, exfiltration, ERV exhaust, and ERV supply streams were found assuming air density at 20°C. The different air flow rates are listed in

Table 5-7, which shows that the total air exchange changes from 0.67 ACH with the ERV off to 1.7 ACH with the ERV on.

**Table 5-7: Ventilation and air leakage rates calculated from the air mass balance**

| Air Flow Path | ERV On (high) | | ERV Off | |
|---|---|---|---|---|
| | L/s | ACH | L/s | ACH |
| Infiltration | 12.39 | 1.0 | 8.33 | 0.67 |
| Exfiltration | 4.89 | 0.4 | | |
| ERV Supply | 8.63 | 0.7 | | |
| ERV Exhaust | 16.14 | 1.3 | | |

The moisture balance over the 48-hour period from 14:00 on November 6th, 2019 to 14:00 on November 8th, 2019 determined the individual moisture transfer rates listed in Table 5-8. Note that effectiveness was not required here because the relative humidity, temperature, and flow rate of the ERV inlets and outlets were measured. Other cases where these conditions are not measured would require effectiveness.

**Table 5-8: Summary of calculated moisture transfer rates from November 6 to 8**

| Variable | Value | Source |
|---|---|---|
| Internal moisture generated | 13,800 g | Measured volume of water when refilling the humidifier |
| Net change in water vapour | 0 g | Indoor RH at beginning and end of period were approximately equal |
| Water vapour added through ERV supply | 9,165 g | Calculated from measured RH, T, and air flow rate |
| Water vapour removed through ERV exhaust | 23,808 g | Calculated from measured RH, T, and air flow rate |
| Water vapour supplied through infiltration | 8,260 g | Calculated from measured RH and T, and air flow rate from mass balance equations |
| Water vapour removed through exfiltration | 7,417 g | Calculated from measured RH and T, and air flow rate from mass balance equations |

The greatest vapour transport path was the ERV exhaust stream, which removed all of the internally generated moisture from the house as well as additional moisture that entered the house through the ERV supply stream and infiltration. With 6.8 L of water evaporated indoors each day, the net moisture removal rate of the ERV was 7.3 L/day. This performance would be adequate for quickly reducing indoor humidity during extreme moisture generation events.

The flow rates and effectiveness results suggest that the ERV is not very effective at recovering heat and moisture in the Northern Nomad. While the latent effectiveness of the ERV is 0.35, it only accounts for 41% of the total supply air when infiltration is considered, so the "true" latent effectiveness is only 0.14. Similarly, the true sensible effectiveness is only 0.26. If the ERV were balanced, these values may be higher, but the biggest factor that reduces true effectiveness is airtightness. Therefore, it can be concluded that high effectiveness is not beneficial unless the ERV flow rates are balanced and the house is reasonably airtight. In other words, the benefits of an ERV or HRV are lost when flow rates are imbalanced and air leakage is high. The moisture exchange performance of an ERV is diminished in these conditions, and considering the defrost cycle of an ERV, an HRV would be more suitable for the Northern Nomad. If the airtightness were improved, the flows were balanced, and the supply air was preheated in cold weather, the ERV would be much more effective.

## 5.5 Envelope Monitoring Results

Long term monitoring of temperature, moisture content, and relative humidity in parts of the Northern Nomad building envelope began on February 1$^{st}$, 2019 and data was recorded at 10-minute intervals until March 11$^{th}$, 2020. 7330 hours of useful data were captured after filtering invalid or missing periods of data, as discussed in Section 5.5.2.

### 5.5.1 Ambient Conditions

Hourly indoor and outdoor temperatures during the envelope monitoring period are plotted in Figure 5-18 and Figure 5-19, with estimated errors of ±0.1°C and ±1.7% RH. Vapour pressure was calculated hourly and plotted in Figure 5-20, with estimated error of ±50 Pa, illustrating higher levels in the summer and lower in the winter. Daily total irradiance (±25 kWh/m$^2$) and wind driven rain on the south façade, plotted in Figure 5-21, indicate greater rain exposure in the summer, and less solar irradiance at the same time due to higher sun angles. These ambient conditions are used in discussing the moisture levels in the building enclosure in proceeding sections. No error specifications were provided for the wind driven rain sensor.

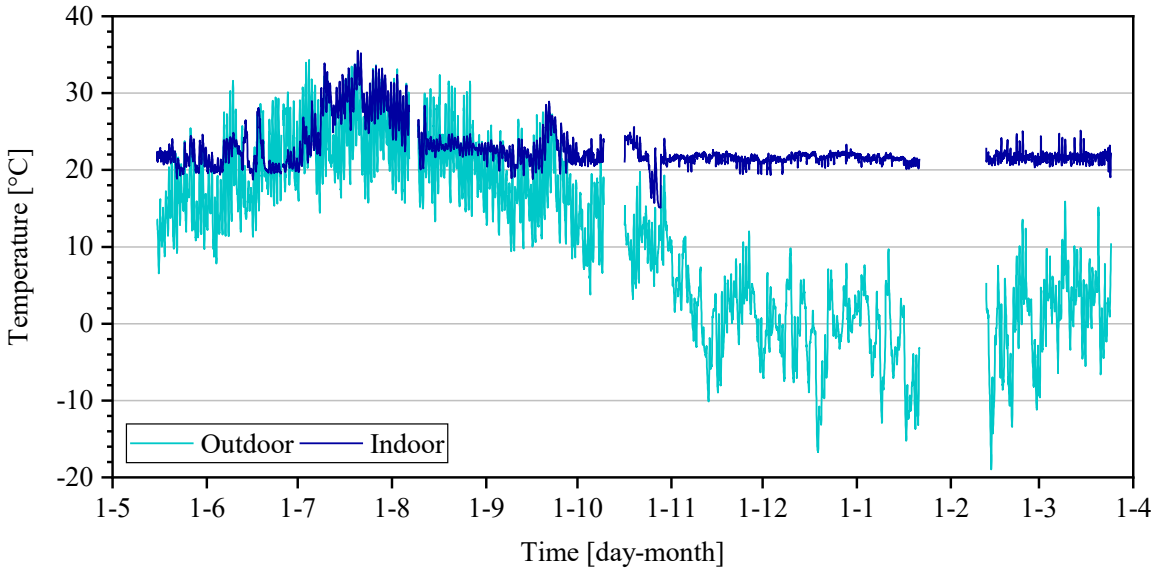


**Figure 5-18: Hourly indoor and outdoor air temperature during the monitoring period**

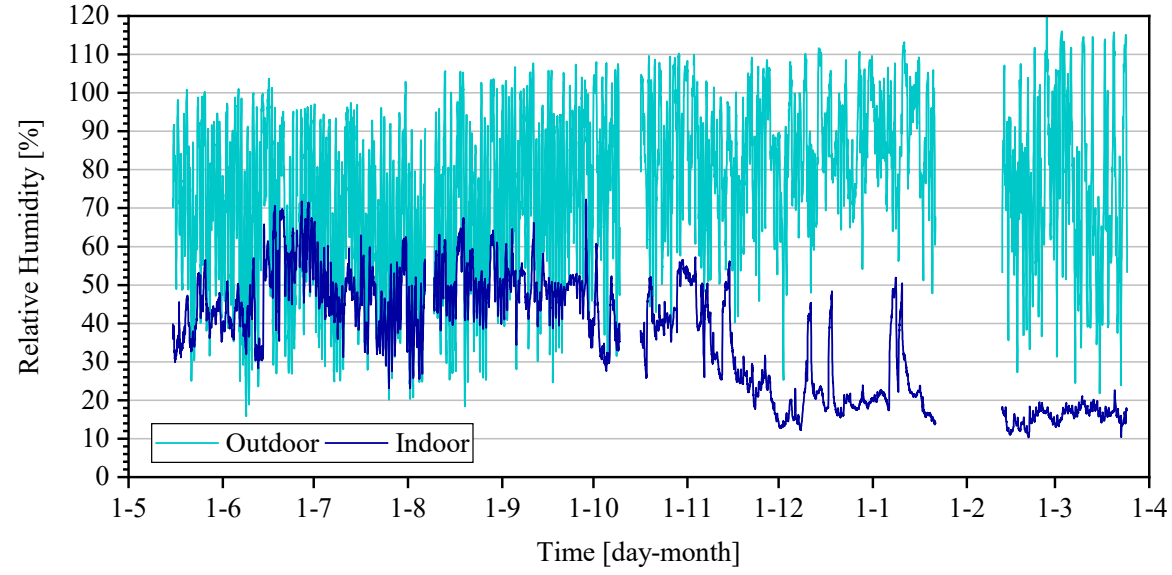


**Figure 5-19: Hourly indoor and outdoor relative humidity during the monitoring period**

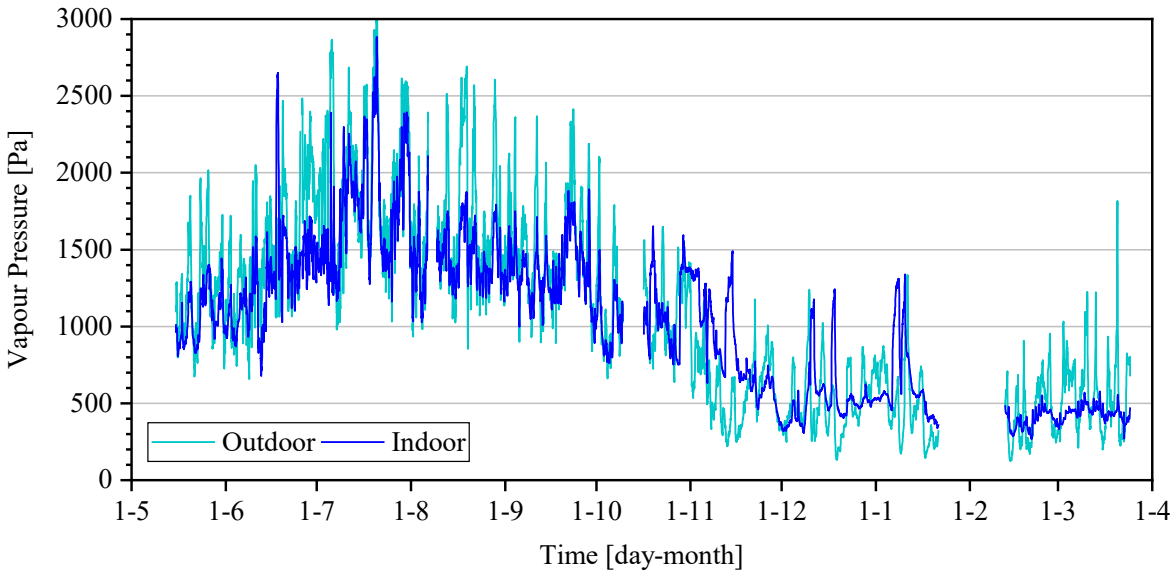


**Figure 5-20: Hourly indoor and outdoor vapour pressure during the monitoring period**

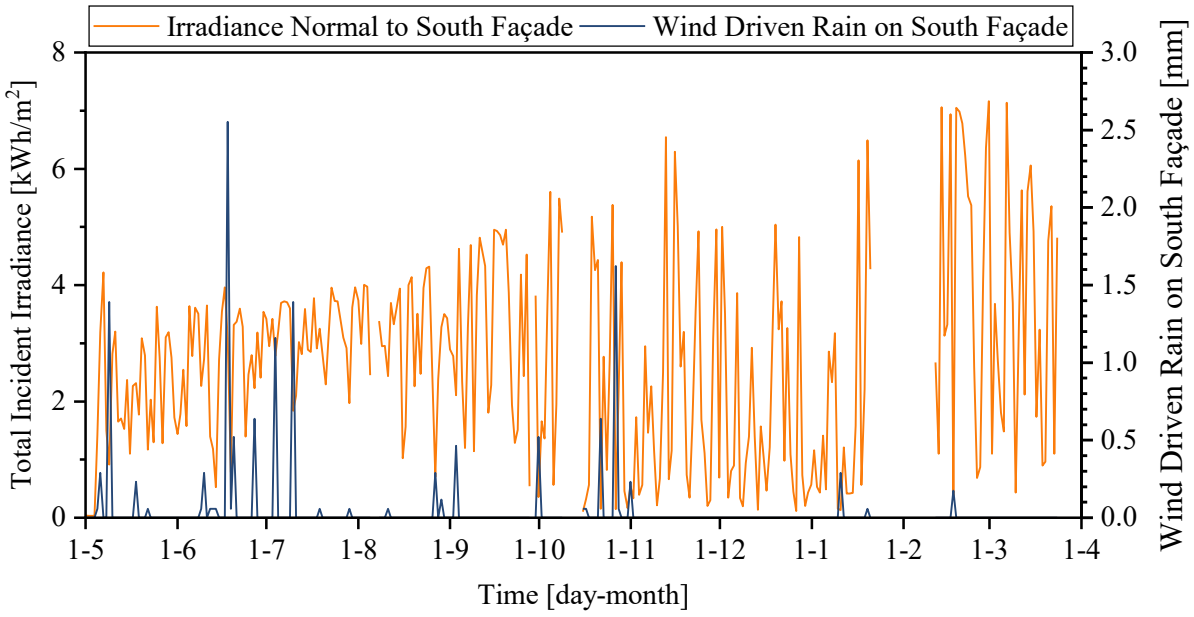


**Figure 5-21: Daily total irradiance and wind driven rain on the south façade**

### 5.5.2 Data Collection Challenges

#### *5.5.2.1 Relative Humidity Sensors*

It was observed early in the data collection process that some of the sensors installed in the building enclosure were not transmitting data and could not be included in the study. This includes every pair of relative humidity and temperature sensors, as well as the pair of sensors installed at the joint between the dormer and the sloped roof. This left seven locations with valid temperature and moisture content data: the south wall stud cavity, north wall study cavity, below the south window, below the north window, south roof sheathing adjacent to a VIP, north roof sheathing adjacent to a VIP, and the floor frame. The wires for the RH and temperature sensors were most likely damaged during construction, causing open circuit readings that were observed in the DAQ software. Since the sensors were embedded in the walls, floor, and roof assemblies, they could not be replaced without altering the thermal and hygric properties of the monitored areas. Future

studies should ensure that embedded instrumentation and wiring are protected by using conduit or marking wire and sensor locations so that they do not get cut or pinched.

Relative humidity data was important for drawing conclusions regarding the durability of the Northern Nomad, as MGI and VIP aging both require RH inputs. The MC data could still be analyzed using MC-based thresholds, but the study would be incomplete without some analysis regarding RH-based failure criteria, namely mold growth and VIP aging conditions. To adapt to this deficiency and estimate the RH at the measured locations, the EMC-RH relationship for OSB was employed extensively, discussed further in Section 5.6. Descriptions of mold growth analysis and VIP aging analysis are described in Sections 5.7 and 5.8, respectively.

#### *5.5.2.2 Gaps and Offset*

Throughout the study, an electrician was working on the off-grid electrical system and they needed to power cycle the house on several occasions. Since the data loggers were powered by the house, each power cycle erased any stored data that had not yet been synchronized to the DAQ system, causing several periods of missing data. To try and avoid this issue, the dataloggers were switched to internal AAA battery power on October 2$^{nd}$, 2019 and then switched back to household power on November 19$^{th}$, 2019, after electrical work was completed. During that period, all of the moisture content data shifted by approximately -1.6% MC. No cause for the shift could be determined. The power supply and battery packs were tested by measuring the resistance of a 10kΩ resistor with a datalogger powered by each source. There was no significant difference in the measured resistance using the battery pack compared to the power supply. Technical assistance from the manufacturer of the sensors and dataloggers gave no explanations. Since there was no determinable cause for the shift in data, it was uncertain whether the shifted data was more or less

accurate than the rest of the data. For a conservative analysis, it was assumed that the rest of the collected data was accurate, which was higher, and the period from October 2nd to November 19th was incorrect. For qualitative discussions, it was assumed that the actual moisture content during that period was consistent with the trends observed before and after it, which is a gradual increase with no major deviations. In future studies, there should be closer communication with contractors to avoid unwanted power cycles that cause loss of data. Alternatively, a power supply with backup battery capacity could be used to provide more reliable power.

### 5.5.3 Building Envelope Conditions

Temperature and moisture content data from the walls, roof, and floor of the Northern Nomad are plotted in Figure 5-22 to Figure 5-27. The gaps and offset in the data are annotated in Figure 5-23. The estimated error for hourly average temperature data is ±0.04°C based on sensor error. The error in moisture content data is an area of ongoing research and is currently unknown.

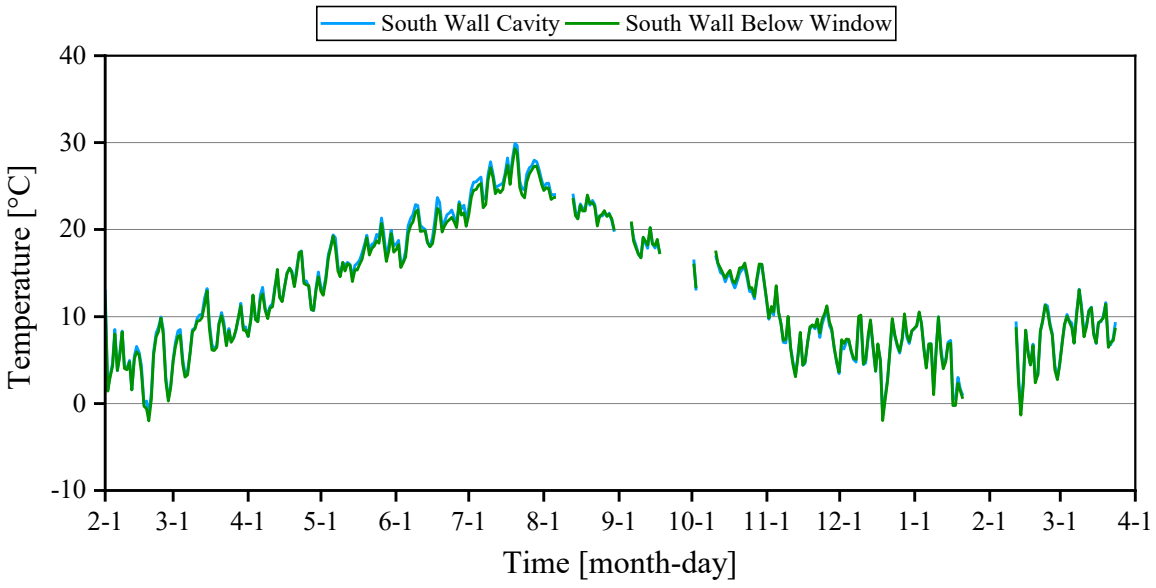


**Figure 5-22: Hourly averaged temperature at the south wall sheathing**

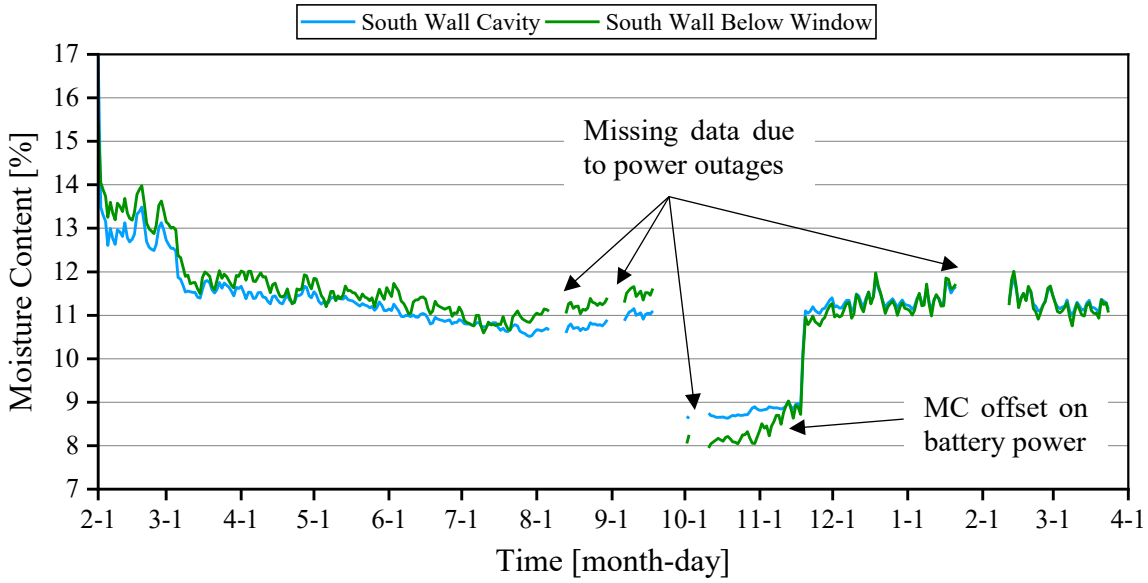


**Figure 5-23: Hourly averaged moisture content in the south wall sheathing**

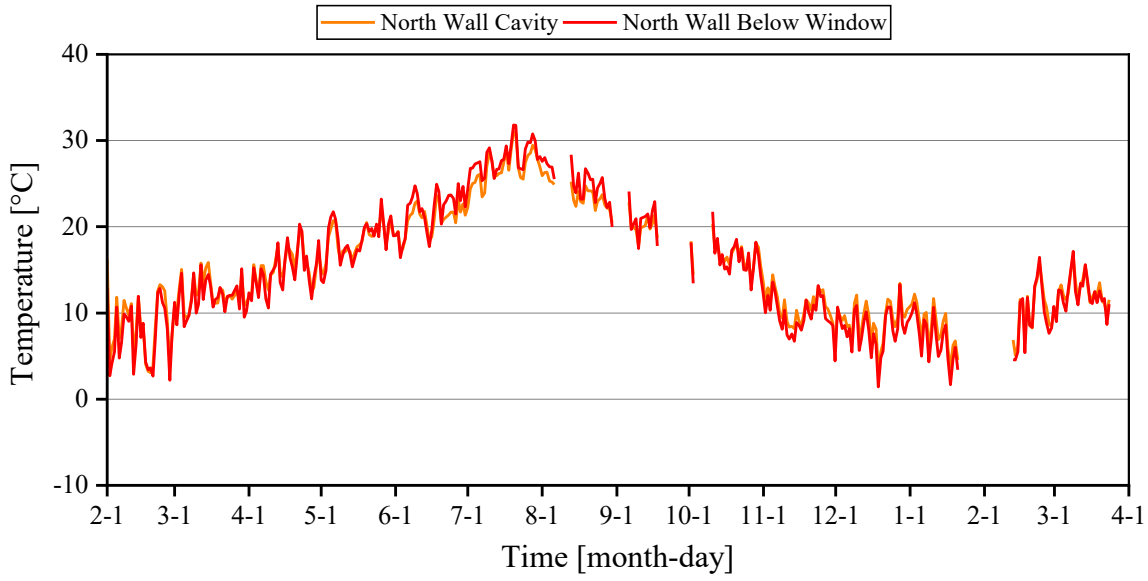


**Figure 5-24: Hourly averaged temperature at the north wall sheathing**

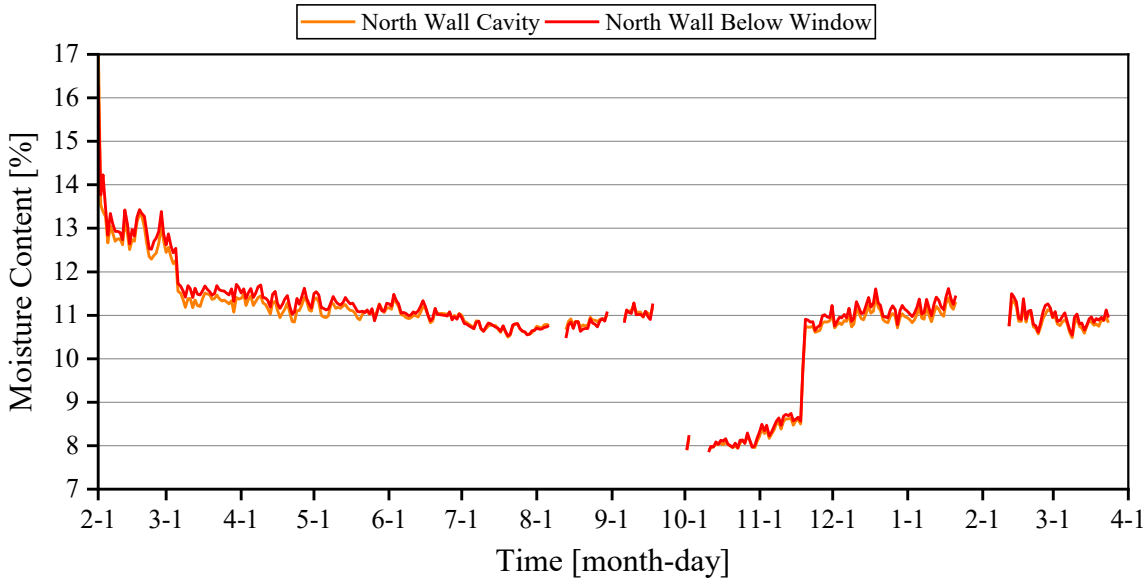


**Figure 5-25: Hourly averaged moisture content in the north wall sheathing**

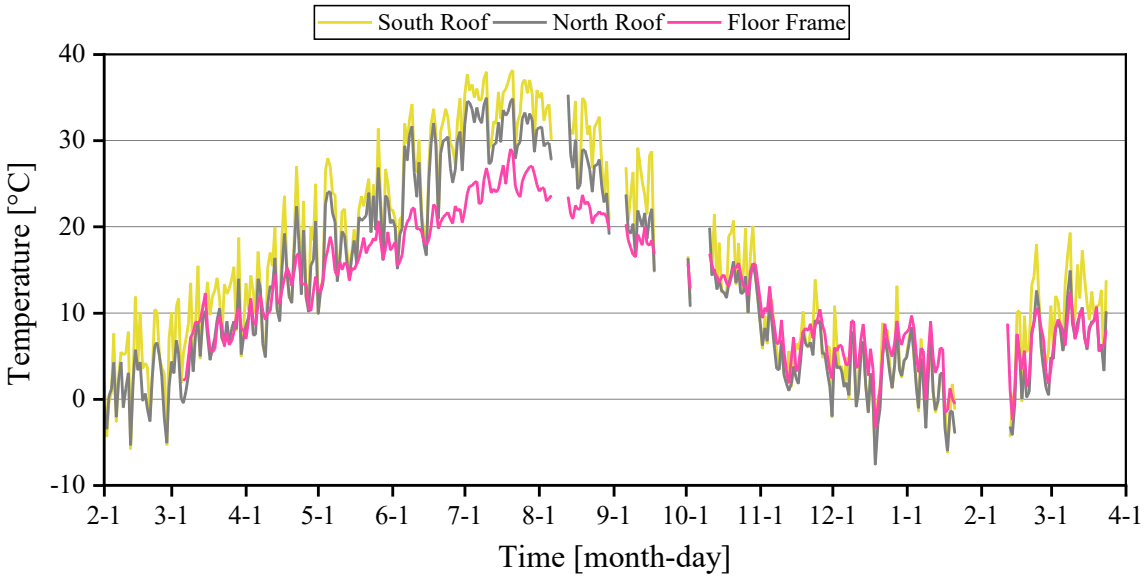


**Figure 5-26: Hourly averaged temperature at the roof sheathing and floor frame**

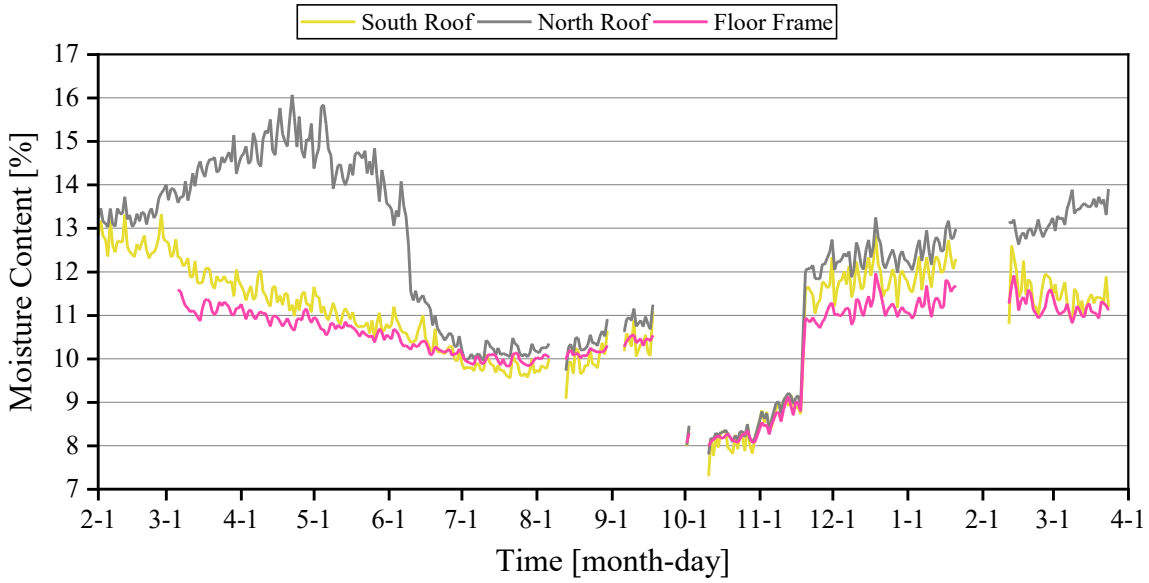


**Figure 5-27: Hourly averaged moisture content in the roof sheathing and floor frame**

The moisture content data showed cyclic seasonal variations in most monitored areas, decreasing from around 11-14% in February to 8-11% in July, and increasing to 10-13.5% in January, and decreasing again. This variation was closely matched with the opposite trend in temperature through the year, especially in the walls where the sensors were most protected from external moisture. Since the equilibrium moisture content in wood decreases at higher temperatures at the same relative humidity, it can be suggested that the walls of the house maintained steady relative humidity year-round with very little moisture addition or removal: an assumption used in many past studies regarding walls containing hygroscopic materials and adequate vapour barriers. The result was consistent year-round regardless of the high vapour pressure in the summer or the dryness of the winter which demonstrates how effective the walls are at blocking moisture loads.

The presence of VIPs showed no impact on the levels of moisture in the walls, demonstrated by the similarity between the north and south wall moisture content measurements.

The concern was that the VIPs would reduce the drying ability of the south wall and cause moisture accumulation after a period of wetting, but this was not observed. After periods with wind driven rain, there was no noticeable increase in moisture content of the sheathing which indicates that the roof and rainscreen were effective at managing rainwater. If the roof continues to provide adequate protection from rain and snow runoff, the walls should not exhibit moisture accumulation at the sheathing. It was noted that this is based on only two measurement locations so if moisture accumulated elsewhere, it would not have been observed.

The north roof showed different trends from the rest of the locations during the first half of the year. Instead of the moisture content decreasing gradually, it increased from 13-14% in February to 14.5-18% in mid-April and decreased quickly to 9-11% in July. This indicated that the north roof sheathing experienced less favourable conditions for drying through the spring. The probable causes of this are the presence of VIPs, the north-facing orientation, and the steep pitch of the roof that blocks low-angle solar radiation from the south. The VIPs against the sheathing limit the inward drying potential of the assembly, as they have very low vapour permeance. This could contribute to the elevated moisture content that was observed, but the main contributor is the lack of sunlight.

Solar radiation is important for drying the roof during the winter and spring since snow accumulates, melts, and can soak into the roof sheathing through imperfections in the waterproofing layer. Solar irradiance heats the PV panels which then heat the air gap, improving convection and drying. Without solar heating, the roof air gap is cooler, more humid, and does not circulate as quickly, providing less capacity to evaporate melted snow from the roof. The north facing roof exhibited this drying deficiency to an extent, allowing moisture content to temporarily

reach levels that could initiate moisture problems. However, the high moisture content did not persist, and moisture problems were avoided as the roof dried quickly once it began to receive more solar irradiance in May and June. The trend repeated during the second winter of monitoring.

Despite the higher MC levels in the north roof, it still did not reach the 20% MC threshold for wood decay. The highest "persistent" MC observed was 14%. Unless there is a detail somewhere on the house that creates a localized moisture problem, it is very unlikely that wood decay will occur in the north roof sheathing or anywhere else in the house under normal operation.

## 5.6 RH Estimation Using Isotherms

To analyze the measured MC data with respect to RH-related failure criteria, the failure criteria were converted to MC using a sorption isotherm with temperature adjustment. Three sorption isotherms for OSB near room temperature were found in the literature [50, 51, 52] and of the three, the one by Boardman et al. [50] was decided to be the most suitable isotherm for this work. Details about each study and the selection are provided in Appendix D:. The three OSB isotherms are plotted in Figure 5-28 along with the sorption isotherm for softwood lumber from the Wood Handbook [9].

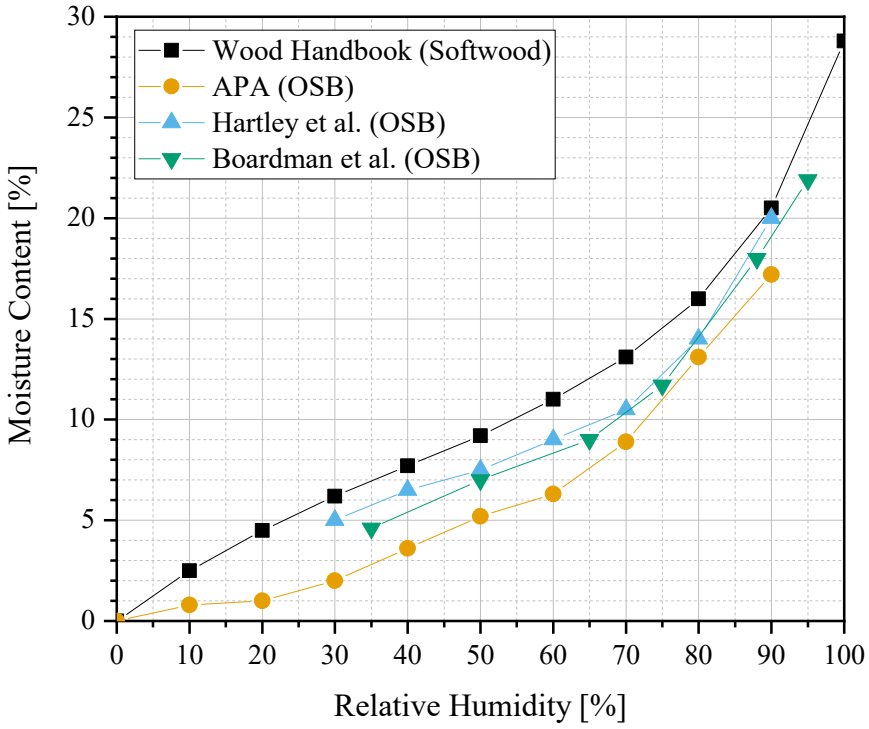


**Figure 5-28: Sorption isotherms for OSB and softwood lumber**

The EMC-RH relationship for OSB must be adjusted for conditions away from room temperature and it is reasonable to assume that the EMC-RH relations for OSB and other woods share the same temperature dependence. The best temperature adjustment available is that contained in the EMC-RH equation for spruce described in the wood handbook as follows:

$$EMC = \frac{1800}{W}\left(\frac{Kh}{1-Kh} + \frac{K_1Kh + 2K_1K_2K^2h^2}{1 + K_1Kh + K_1K_2K^2h^2}\right) \tag{5.1}$$

$$W = 349 + 1.29T + 0.0135T^2$$

$$K = 0.805 + 0.000736T - 0.00000273T^2$$

$$K_1 = 6.27 - 0.00938T - 0.000303T^2$$

$$K_2 = 1.91 + 0.0407T - 0.000293T^2$$

One way to visualize this relationship is using constant RH lines on an MC-T plot, as shown in Figure 5-29. The temperature effect on MC is subtle at lower RH levels and between -10°C and 20°C, but the effect is stronger at elevated RH and T.

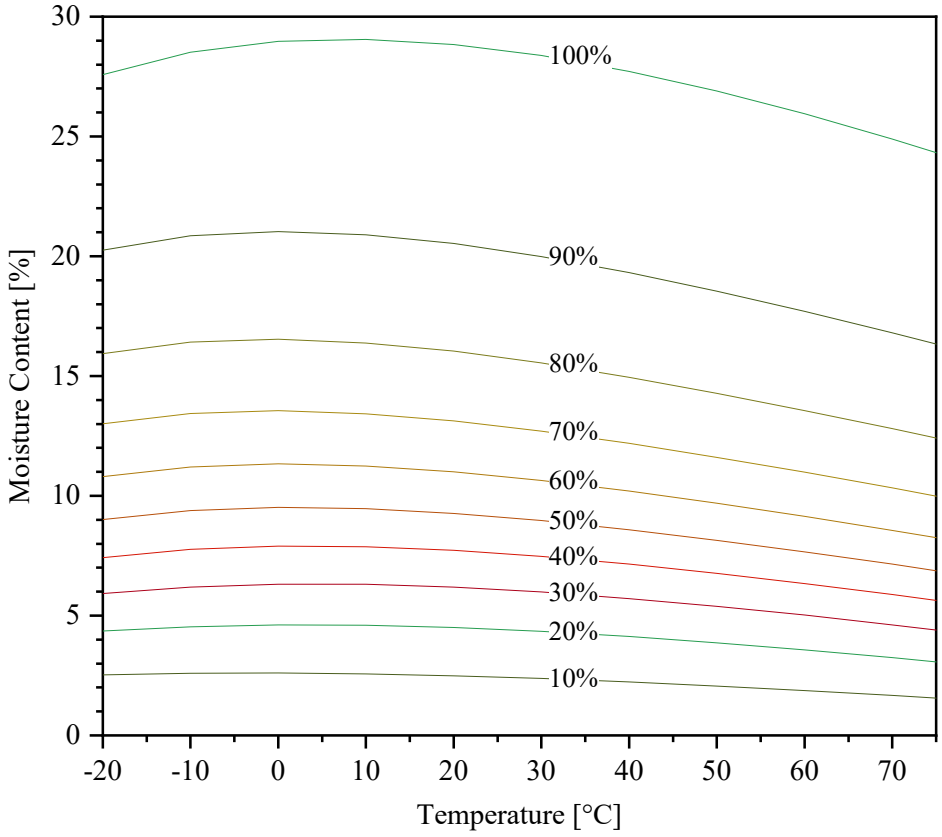


**Figure 5-29: Equilibrium relative humidity curves using Equation (5.1) for solid wood**

The procedure for applying Equation (5.1) to OSB is as follows. For equal MC, OSB requires a higher RH than spruce, so on an MC-T plot, a constant RH curve for OSB is the same as one for spruce that is a higher RH value. Key RH values for this study are 75, 80, 85, and 90 percent which, at room temperature, correspond to OSB MC of approximately 11.7%, 14%, 16.5%, and 20%. For spruce, these MC values correspond to 64% RH, 74% RH, 82% RH, and

89% RH (determined using Table 4-2 from the Wood Handbook [29]). Thus, on an MC-T plot, the constant RH lines for OSB at 75%, 80%, 85% and 90% RH are the same as the curves for spruce at 64%, 74%, 82% and 89% RH. These curves can be calculated easily using Equation (5.1) and can be added to plots of experimental MC&T data to assess the risk of mold growth and accelerated VIP aging. This method is deemed imperfect but reasonable for this study, considering the data available and the knowledge in the literature at this time. MC-T plots of each measured location are shown in Figure 5-30 to Figure 5-36. These plots are discussed in the following sections.

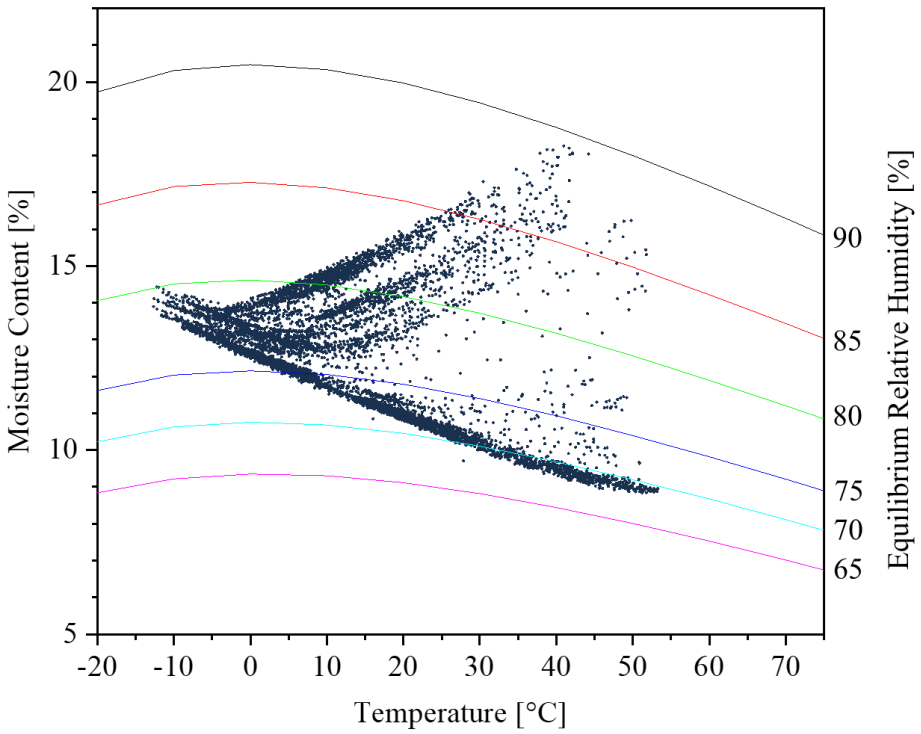


**Figure 5-30: MC-T of the north roof sheathing**

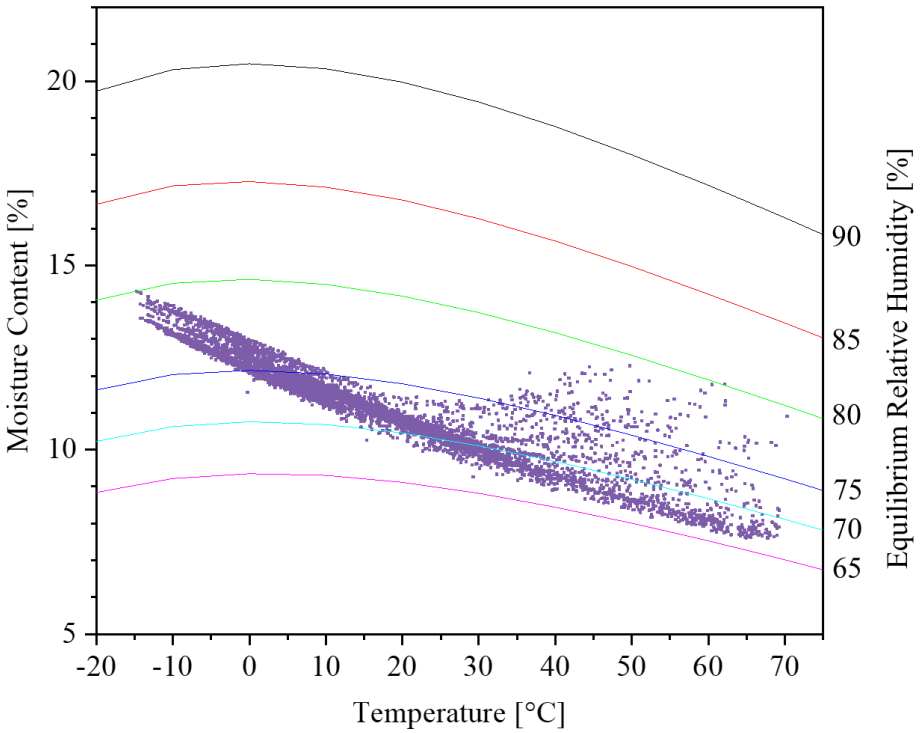


**Figure 5-31: MC-T of the south roof sheathing**

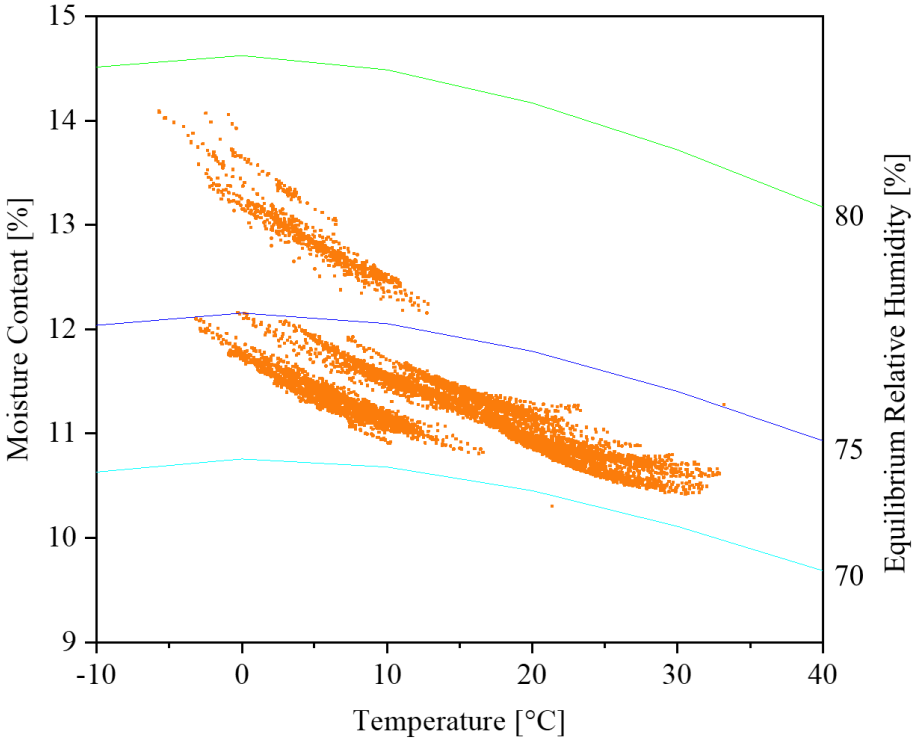


**Figure 5-32: MC-T of south wall sheathing in the stud cavity**

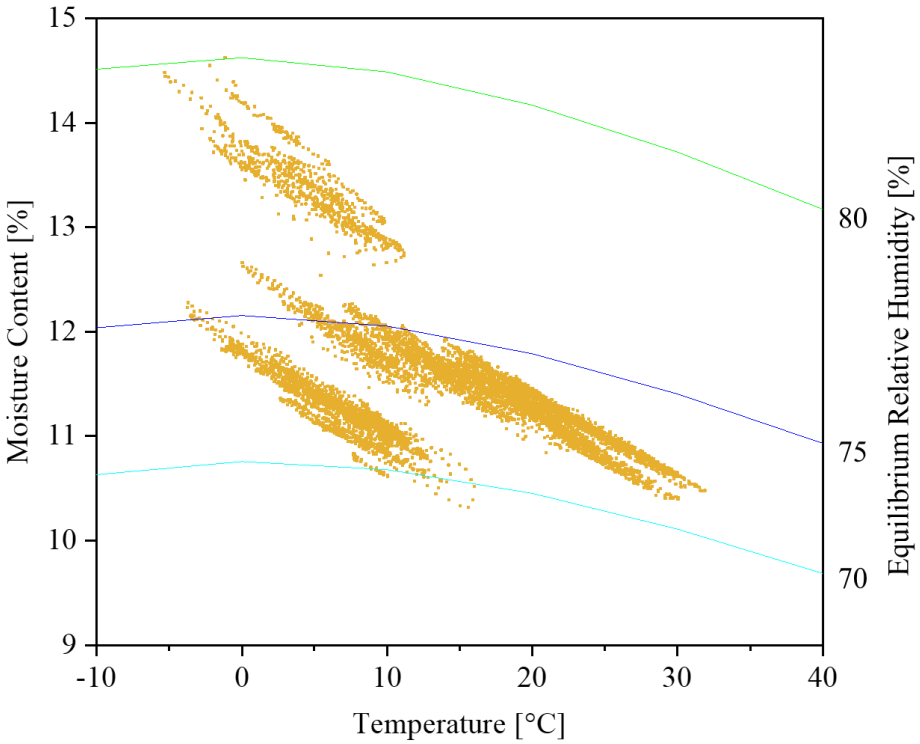


**Figure 5-33: MC-T of south wall sheathing below the windowsill**

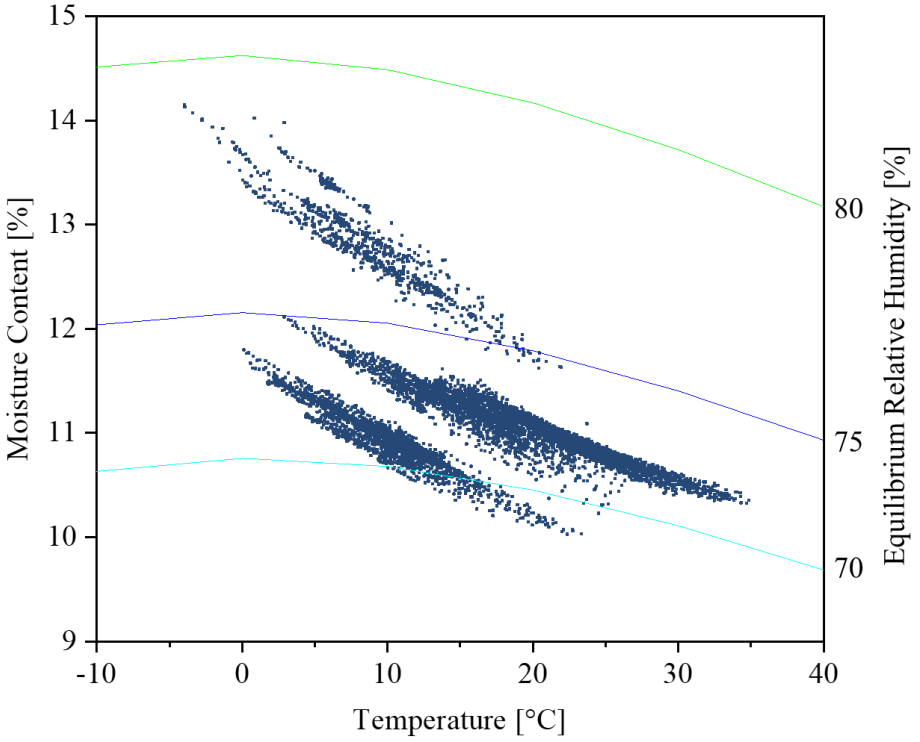


**Figure 5-34: MC-T of north wall sheathing in the stud cavity**

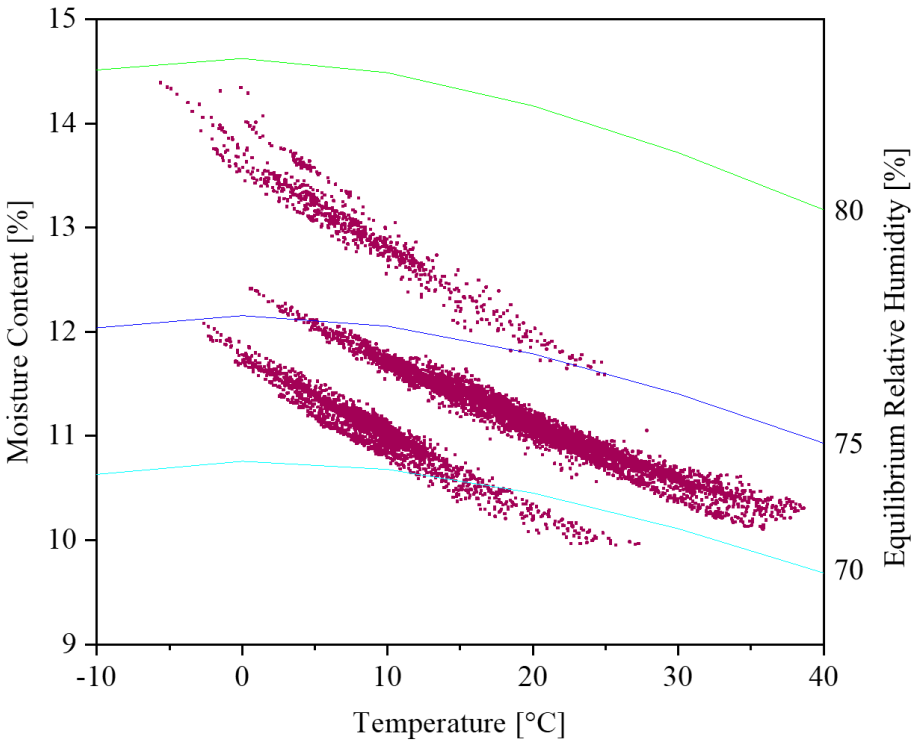


**Figure 5-35: MC-T of north wall sheathing below the windowsill**

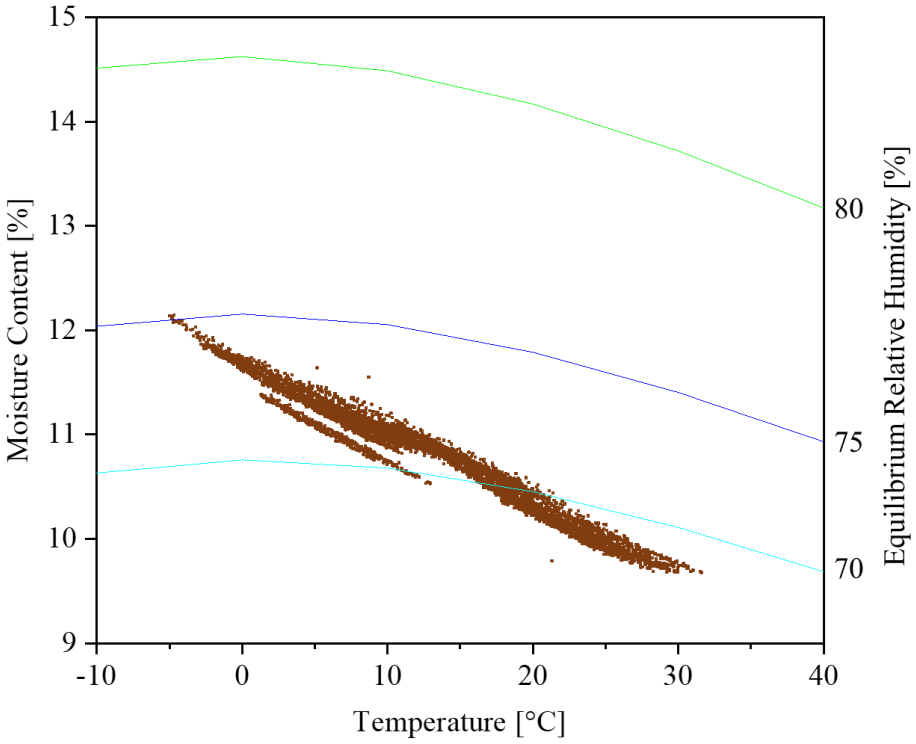


**Figure 5-36: MC-T of floor frame sheathing**

Evidently, the constant RH curves in Figure 5-30 to Figure 5-36 do not follow the data at lower temperatures. This may suggest that either the building materials do not stay at constant relative humidity or the curves are inaccurate. The curves were formed using well established trends from the literature combined with reasonable assumptions, but they mainly apply to equilibrium conditions. It cannot be assumed that the building envelope data is close to equilibrium, so it is possible that the shapes of the constant RH curves are inaccurate for lower temperatures. The alternative explanation would be that the building materials do not stay at a constant RH, which may be true since there is not a tremendous amount of moisture buffering capacity in the building envelope. This cannot be proven without measuring the relative humidity, so this claim is uncertain. Given the uncertainty with the constant RH curves, no firm conclusions will be drawn from their values. This is a limitation of this study that was a result of the damaged RH sensors. Suggestions for future work would be to ensure the integrity of sensors in the building envelope to prevent loss of data. This could involve adding extra sensors for redundancy, checking sensor functionality before closing the assemblies, and using conduit to protect wires.

### 5.6.1 Moisture Buffering Capacity

One concern regarding the walls in the Northern Nomad is that they may have a low moisture buffering capacity due to the use of closed cell foams and VIPs. Only the studs and OSB sheathing provide capacity to store moisture in the walls and roof, which may not be enough to regulate the relative humidity in the building envelope as ambient conditions fluctuate. When wood materials are heated, their capacity to hold water decreases, which is why moisture content was higher in the winter and lower in the summer. This property allows for moisture buffering capacity to be observed on an MC-T plot. Adequate moisture storage capacity can be characterized by a nearly straight, negatively sloped line on an MC-T plot, parallel to a constant RH curve. This

was demonstrated in the north wall, floor frame, and south wall windowsill. In these locations, there are nearby wood framing members that buffer moisture. Low storage capacity can be characterized on an MC-T plot by a curved downward trend that can change to an upward slope past a certain temperature, indicating an increase in RH. The north roof sheathing exhibited this most severely, where daytime moisture content increased in the spring as daytime roof temperatures increased above 0°C. The south roof demonstrated an upward curve at around 25°C, but both sides of the roof eventually dried so that the trends returned to a downward slope. The south wall cavity showed a very minor curve during daytime high temperatures around 25°C in the summer, but the moisture content did not increase. The presence of VIPs in these areas could be the cause of these elevated relative humidity levels, which aligns with the existing concerns about VIPs in buildings.

## 5.7 Mold Growth Risk Analysis

As discussed in Section 5.6, the thresholds of RH and T for mold growth were converted to limits of MC and T to allow the assessment of MC data regarding mold growth. Section 2.3 described the different conditions representing several risk levels of mold growth. These conditions were interpreted as thresholds for low, moderate, and high risk which were added to an MC-T plot of the north roof sheathing: the only location that showed any data points within the mold growth zone, as shown in Figure 5-37. All other locations were always below 80% RH, so mold risk was not a concern.

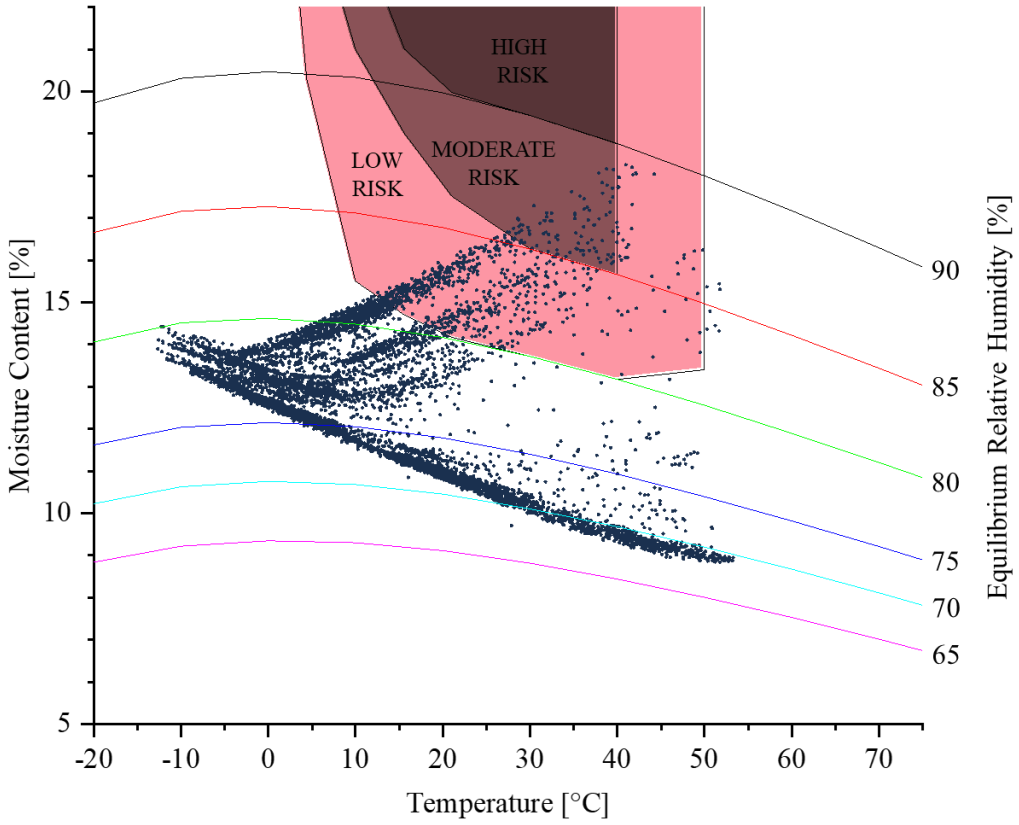


**Figure 5-37: Hourly MC-T in the north roof sheathing from February 1st, 2019 to March 11th, 2020. Risk zones represent conditions at low to high risk of mold growth when conditions are persistent.**

Recall that these thresholds apply to persistent conditions within each zone, with higher risk zones requiring less time for growth. Based on Figure 5-37, the north roof sheathing was within the low and moderate risk zones for just a portion of the total monitoring period. For more detail, data from February through June was plotted, and colour coded by month, shown in Figure 5-38. Only 2019 data was plotted since the 2020 data is similar. The only notable difference is that the average MC in February 2020 was approximately 0.5% lower than February 2019. Figure 5-39 shows the accompanying time series plots of MC and T of the north roof sheathing for this period.

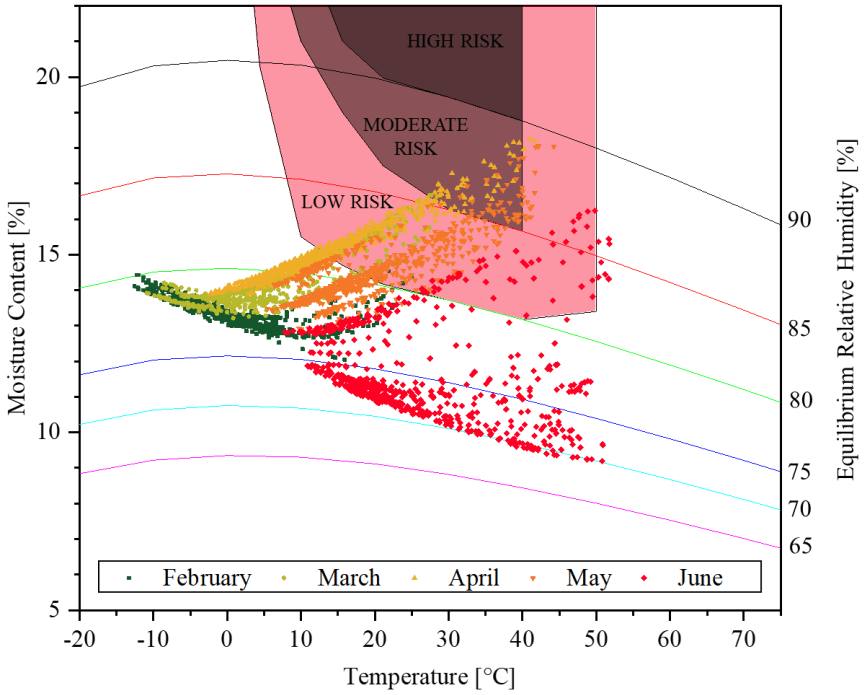


**Figure 5-38: Hourly MC-T in the north roof sheathing for February through June, 2019. Risk zones represent conditions at low to high risk of mold growth when conditions are persistent.**

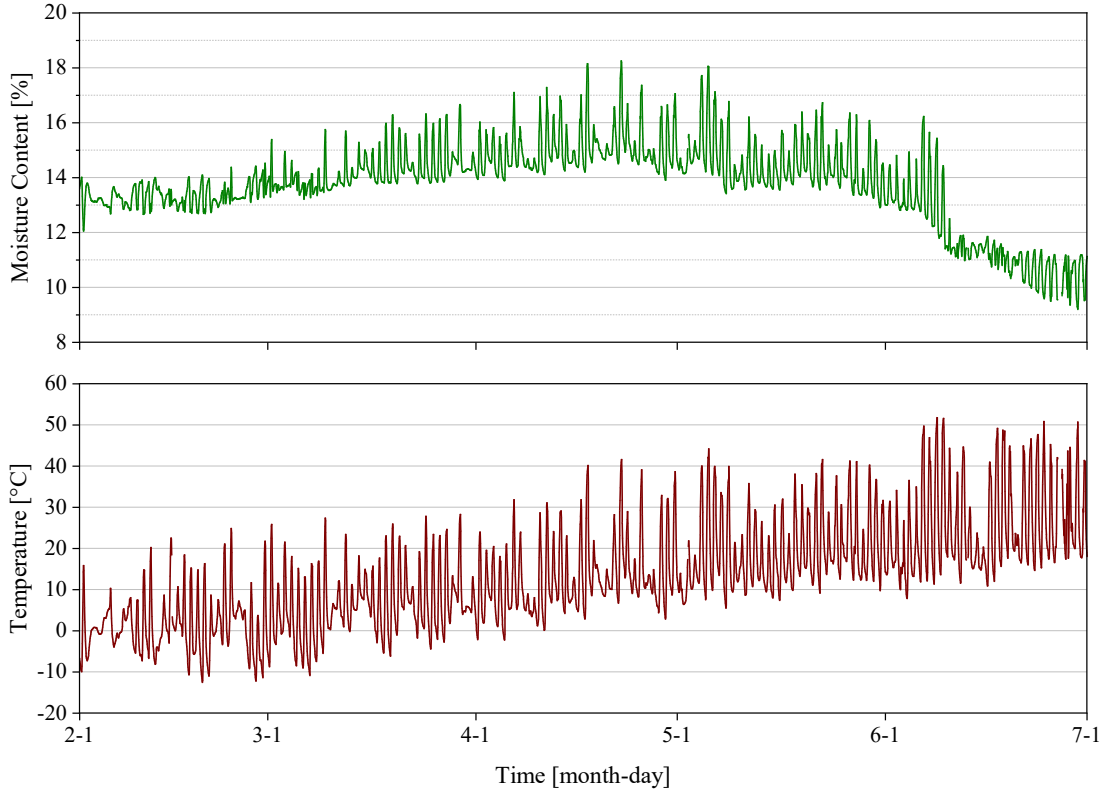


**Figure 5-39: Hourly moisture content and temperature in the north roof sheathing for February through June 2019**

The north roof sheathing only experienced conditions for mold growth between late February and early June 2019. During this period, MC and T fluctuated daily, and they only satisfied conditions for low and moderate risk of mold growth for part of the day. The worst month was May, when the monthly average conditions were 19.4°C and approximately 80-81% RH, which is just within the lower threshold for microscopic mold growth, but conditions fluctuated too much to cause problems. Similarly, the average conditions in April were 10.9°C and 80.5% RH: not humid enough or warm enough to facilitate any mold growth. The data shows that there was virtually no risk of mold growth during the measurement period. To extrapolate into the future, the slightly lower MC for February and March of 2020 compared to 2019 suggested that the mold growth risk is most likely to decrease.

Further analysis can be done using the MC guidelines. Comparing with the 18% MC rule presented by Tsongas & Riordan [24], the Northern Nomad passes with no risk of mold growth. Similarly, according to the 15% MC rule, which the north roof sheathing only briefly exceeds, the Northern Nomad does not appear to be at risk of future mold problems.

It was noted that the measured conditions do not necessarily represent the conditions throughout the rest of the house. The roof sensors may not represent the entire roof, so the highest MC may be in an unmeasured location and the variations would be a result of the variations in vapour permeability, thermal bridges, heat loss to the outdoors, and locations of moisture pathways. The MC was measured on the inside face of the roof sheathing in contact with the polyurethane spray foam, adjacent to a VIP. The spray foam is semi-vapour permeable, while the VIPs are vapour impermeable, so the highest MC may be at the middle of the VIP contact area where the moisture buffering capacity is lowest. It would be difficult to determine the location and

value of the highest MC, as well as the MC in the rest of the envelope from just the measured data. 2D hygrothermal model simulations with inputs from the experimental data may provide the best insights.

## 5.8 VIP Aging Analysis

Temperature and moisture content in proximity to VIPs in the Northern Nomad were analyzed to assess the relative appropriateness of VIP integration the roof, walls, and floor assemblies. Detailed service life calculations were not included in the scope of this work, but results were compared with existing knowledge to roughly estimate how the VIPs would age in each part of the house.

Recall from Section 2.2 that high vapour pressure and cyclic temperature are the most detrimental for VIP aging. Like the mold growth analysis, MC-T plots and constant RH lines derived in Section 5.6. were used to graphically estimate the RH of specific MC-T pairs, which was then converted to vapour pressures. Plots of the hourly average MC vs T of the south roof sheathing and south wall cavity, both in proximity to VIPs, are shown in Figure 5-40 with vapour pressure of various datapoints annotated. The time series version of the same data is shown in Figure 5-41 for reference.

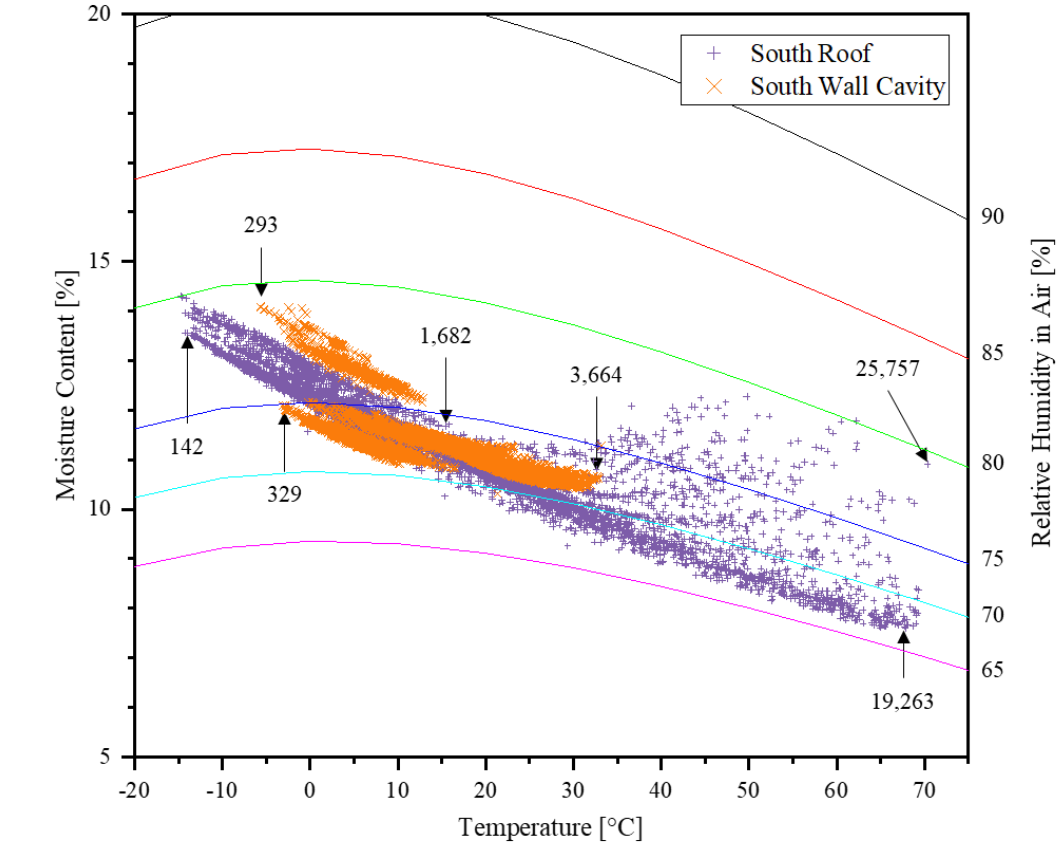


**Figure 5-40: MC-T plot of the south roof sheathing and the south wall cavity, with vapour pressure [Pa] of some points labelled**

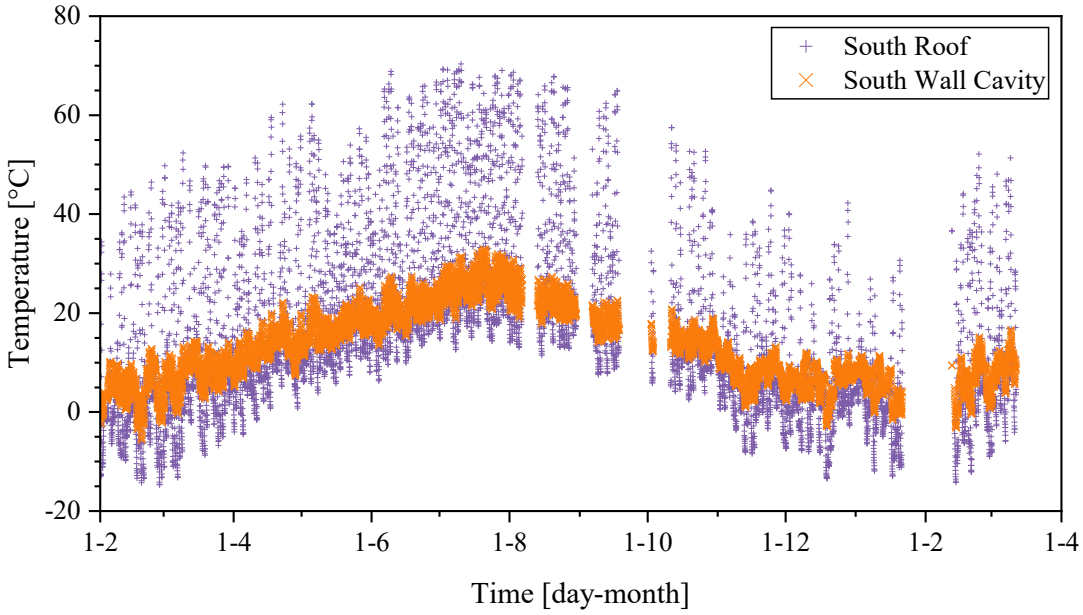


**Figure 5-41: Hourly temperature of the south roof sheathing and the south wall cavity**

The south roof sheathing showed uniquely high temperature oscillations through the monitoring period with very high peak temperatures and vapour pressures in the summer, as high as 70°C and 212 g/kg, respectively.

A simple analysis of the envelope data regarding VIP aging can be done using average and effective temperatures at each measured location. Effective temperatures were calculated using Equation (2.2) and are listed in Table 5-9 along with aggregate moisture content and temperature data statistics.

**Table 5-9: Summary of envelope data**

| Location | Average MC [%] | Average T [°C] | Effective T [°C] | Effective RH [%] | Maximum T [°C] | Minimum T [°C] |
|---|---|---|---|---|---|---|
| South Wall Cavity | 11.4 | 13.3 | 15.4 | 73 | 32.9 | -5.7 |
| South Wall Window Frame | 11.6 | 13.0 | 15.0 | 73 | 31.9 | -5.3 |
| North Wall Cavity | 11.2 | 15.6 | 17.2 | 73 | 34.9 | -4.0 |
| North Wall Window Frame | 11.3 | 15.5 | 17.8 | 73 | 38.6 | -5.6 |
| South Roof Sheathing Beside VIP | 11.2 | 16.1 | 27.2 | 73 | 70.3 | -14.7 |
| North Roof Sheathing Beside VIP | 12.7 | 13.7 | 20.4 | 77 | 53.3 | -12.6 |
| Floor Frame | 10.7 | 13.5 | 15.5 | 70 | 31.6 | -5.0 |

The south roof sheathing exhibited the highest effective temperature, 27.2°C, while the south wall window frame was the lowest at 15.0°C. The south roof effective temperature is 10.1°C higher than the average temperature, a significant difference due to the large daily temperature fluctuations.

Recall from Section 2.2 that VIP service life can be defined as the time required for thermal conductivity to increase by 100%, commonly from 0.004 W/mK to 0.008 W/mK. To estimate the service life of the VIPs in the different locations, the results can be compared with the findings from Simmler and Brunner [5], which used constant relative humidity and effective temperature from a building envelope simulation as inputs to a constant condition aging model. The model involves a series of mathematical steps to calculate the pressure increase rate, $\dot{p}$, equilibrium moisture content, $u_{eq}$, and moisture content increase rate, $\dot{u}$, as inputs to a final equation for the change in thermal conductivity over time, $\Delta\lambda(t)$ , in the form of Equation (5.2).

$$\Delta\lambda(t) = 0.035\dot{p}t + 0.5u_{eq}\left(1 - \exp\left(\frac{-\dot{u}t}{u_{eq}}\right)\right) \tag{5.2}$$

Following the same steps to determine $\dot{p}$, $u_{eq}$ , and $\dot{u}$ would be infeasible here, but the literature provides two solved temperature and humidity conditions, namely 21.5°C and 16.0°C at constant 80% RH, which is enough to estimate $\dot{p}$ and $\dot{u}$ using linear regression. A simplified, approximate model was then generated for temperatures in the range of 10-30°C and humidity between 70-80% RH. Changing the value of $u_{eq}$ has little effect so it was assumed constant. The simplified model takes the form of Equation (5.3):

$$\Delta\lambda(t) = 0.035\dot{p}t + 3.2\left(1 - \exp\left(\frac{-\dot{u}t}{6.4}\right)\right) \tag{5.3}$$

$$\dot{p} = 0.145T_{eff} - 40.2$$

$$\dot{u} = 0.0127T_{eff} - 3.53$$

According to Equation (5.3) and results from Table 5-9, the estimated service life of VIPs in the walls of the Northern Nomad is around 40 years. Estimated service life in the roof is around 27 years on the north facing side and 20 years on the south side. These estimates are suspected to be accurate within two years of the model used by Simmler and Brunner. Many building materials are intended to serve for 25 years, which sets a benchmark for VIP lifespans.

The VIP-integrated walls of the Northern Nomad appear to be suitable arrangements for achieving acceptable service life of VIPs. In this location, the VIPs were not exposed to harsh conditions and provided excellent thermal performance. The north facing roof also benefited from the thermal performance of the VIPs, but it is substantially worse for aging due to elevated thermal cycling, although still acceptable. The south facing roof exhibited poor conditions for VIP service life due to extreme temperatures which resulted in a lifespan estimate below the acceptable limit. Reducing the peak temperatures in the roof by increasing roof cavity ventilation may improve VIP service life. Alternatively, it may be advantageous to sandwich the VIPs in spray foam insulation midway through the roof cavity to reduce exposure to high temperatures and protect them from indoor humidity.

### 5.8.1 Impact of Indoor Humidity on Moisture Content

It was predicted that outdoor temperature and relative humidity would have strong effects on moisture content measurements and, consequently, the prevalence of moisture problems. One of the research goals was to see if indoor humidity would also have an effect and if that could be adjusted with the ERV, however it is difficult to isolate specific variables in an in-situ environment. To investigate the correlations between moisture content each variable, moisture content measurements from the south wall were plotted versus corresponding indoor relative humidity

(Figure 5-42), outdoor relative humidity (Figure 5-43), indoor temperature (Figure 5-44), and sheathing temperature (Figure 5-45) over eight days from 00:00 on July 16$^{th}$ to 00:00 on July 24$^{th}$, 2019. During this time, the air conditioning was off, so the indoor temperature and relative humidity were high and fluctuated with outdoor conditions. This should provide the best conditions for observing changes in envelope moisture content.

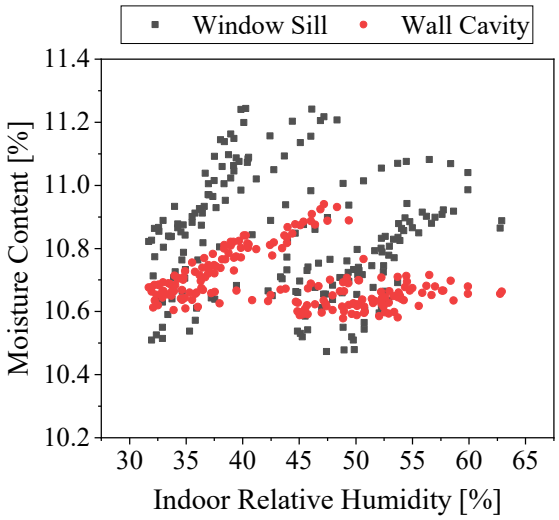


**Figure 5-42: MC versus indoor RH in the south wall sheathing from July 16 to 24**

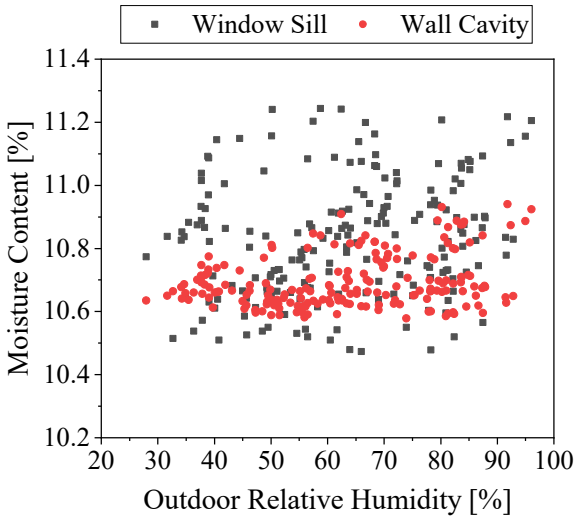


**Figure 5-43: MC versus outdoor RH in the south wall sheathing from July 16 to 24**

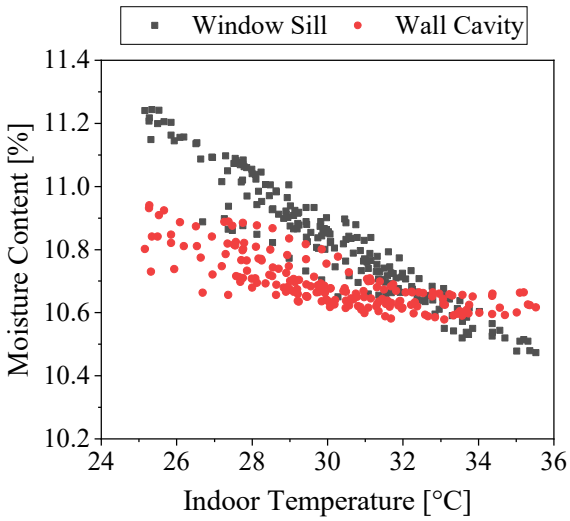


**Figure 5-44: MC versus indoor T in the south wall sheathing from July 16 to 24**

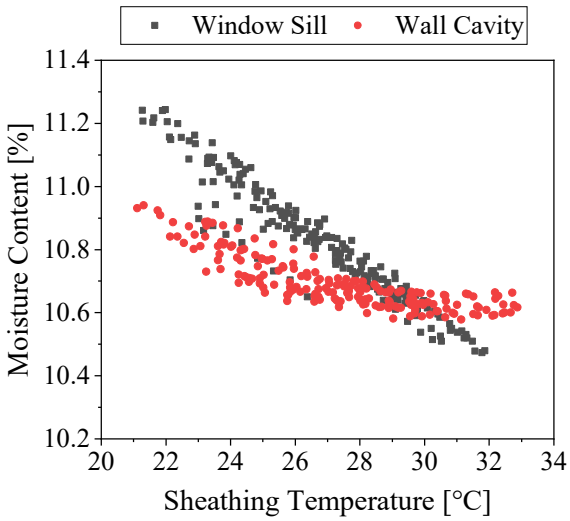


**Figure 5-45: MC versus sheathing T in the south wall sheathing from July 16 to 24**

Figure 5-42 shows a weak correlation between MC in the south wall and indoor RH, which was most likely the result of both variables changing with outdoor temperature. Without the ability to control ambient temperature in an in-situ setting, no certain conclusions could be made from this data regarding the relationship between indoor humidity and moisture in the walls. Figure 5-43 shows no significant correlation between moisture content in the south wall and outdoor relative humidity. Figure 5-44 shows a correlation with indoor temperature and Figure 5-45 confirms that

the moisture content measurements are correlated with temperature at the sheathing: a known property of wood. The roof and floor locations were evaluated in the same manner and the same results were observed. During the monitoring period, there was no total increase in moisture content anywhere, suggesting that vapour did not diffuse deeply into the wall. Figure 5-45 shows a steeper trend of moisture content versus local temperature in the windowsill than the wall cavity which is potentially due to the lower moisture buffering capacity in the cavity where there are no framing members nearby, as discussed in Section 5.6.1.

Figure 5-42 to Figure 5-45 suggest that the walls are nearly vapour tight in the monitored areas, and that a short period of elevated indoor humidity will not affect conditions in the wall sheathing. Longer periods of elevated indoor humidity, such as months of humidification through the winter, could allow enough time for vapour to diffuse into the envelope and result in some observable changes in the sheathing moisture content. Long term humidity testing and hygrothermal simulations may provide more details in this regard, so they are recommended for future work. The airtightness and ERV performance data presented in Sections 5.2 and 5.3 would be invaluable for such studies. It was also noted that the air leakage pathways discussed in Section 5.2.2, such as the battery box, were not monitored for moisture content. These areas are likely to have significantly different sensitivity to indoor and outdoor humidity than the locations that were monitored. Therefore, future work could involve closer monitoring of the problem areas identified in this study.

# Chapter 6: Contributions

The activities in this study provided several key contributions for advancing the knowledge of VIPs in buildings. Firstly, this is the first characterization study to be completed on a building envelope of this style. No other studies on VIP aging or moisture risks resulting from VIPs have included thin, newly built wall assemblies with closed cell sprayfoam, exterior VIPs, and a ventilated rainscreen. The roof assembly is also novel, with no previous findings on a roof with VIPs inside the sheathing, sprayfoam insulation, and integrated PV panels above a thin air cavity. Providing findings from this in-situ data contributes to the literature by broadening the knowledge about what types of assemblies are suitable for VIPs.

This work also contributed to future studies at Carleton University by providing instrumentation, data acquisition systems, and data analysis methods that shall be used to continue testing the house under different conditions. A significant amount of work was required to plan, set up, and troubleshoot the instrumentation and software tools used for collecting, organizing and analyzing data. With these tools in place, future studies can efficiently expand upon the findings of this work by monitoring the house with different moisture loads and ventilation schedules.

Further contributions include the performance characteristics about the house such as airtightness, insulation, and ERV performance, which can be used to validate future simulation studies such as hygrothermal modelling and energy modelling of the Northern Nomad. Additionally, these performance characteristics helped to provide recommendations about how the house could be improved, such as through air sealing and ERV balancing. Recommendations were also provided on how the next version of the Northern Nomad should be built to achieve better efficiency and longevity.

# Chapter 7: Conclusions

This work involved in-situ testing of the Northern Nomad house at Carleton University with the objective of characterizing the hygrothermal performance and durability of the thin, VIP-integrated building envelope. Various experimental techniques were used to characterize the moisture and temperature conditions in the building envelope as well as the insulation performance, airtightness, and ventilation performance. The data helped to understand the interactions between the VIPs, the building envelope, the indoor space, the ERV, and the outdoors. The results were evaluated based on efficiency, mold growth risk, VIP aging, and occupant comfort. Strengths and deficiencies were identified, and recommendations for the next iteration of the house were presented.

VIPs were found to provide excellent insulation performance in the Northern Nomad that was consistent with expectations. A thin layer of VIPs installed on the exterior of the wall sheathing improved performance by around 28-40%, compared to a wall without VIPs. The VIP-integrated walls achieved similar insulation performance to traditional high-performance walls but were around 50% thinner. In the case of the Northern Nomad, the savings in floor space were roughly equivalent to the size of the bathroom.

The VIPs certainly contributed to the goal of achieving net-zero energy consumption in the Northern Nomad, but poor airtightness and imbalanced ventilation kept the house from achieving its full performance potential. Vent holes that were required for electrical safety certification and insufficient seals in the battery box allowed excessive rates of air leakage, causing poor space conditioning efficiency. Warm, humid indoor air leaking outward in the winter could cause mold growth inside the walls or roof where the air is escaping, so periods of high indoor moisture loads

require ventilation to avoid problems. The ERV provided adequate ventilation for these cases, but it generally performed below optimal expectations. The measured sensible and latent effectiveness were modest, but the imbalanced flow rates caused significant air infiltration which nearly eliminated the energy recovery effect of the ERV. Operation during the winter created very dry indoor conditions, and in the summer, it increased cooling demand significantly. Despite its shortcomings, the ERV was effective at moderating indoor humidity during periods of high moisture loads, and additionally, it provided fresh air that improved air quality. Since the ERV was sometimes beneficial and sometimes not, intelligent control of the ERV using temperature and RH sensor inputs may help to effectively regulate moisture in the house in a wide range of weather conditions. The next version of this house would benefit from an HRV that will not defrost in the winter, with dampers for controlling the exhaust and supply streams to achieve balanced flow. Additionally, any potential air leakage pathways caused by electrical or plumbing work should be sealed before completing construction.

Moisture monitoring of the building envelope over one year identified some valuable details about the durability of the Northern Nomad. The water and vapour control layers were effective at protecting the building enclosure from excessive wetting. The exterior rainscreen walls kept rainwater from penetrating into the enclosure, and the closed cell spray foam provided a barrier to internal air and moisture. These features were important since the building envelope had a relatively low capacity for storing moisture due to the use of VIPs and closed cell spray foam. This caused elevated moisture content in the roof sheathing in the spring, especially on the north facing side where there was less sun exposure for drying. The south wall sheathing also showed indications of low moisture storage capacity, but the effect was minimal. Fortunately, the roof and walls demonstrated enough drying capacity to sufficiently dissipate excess moisture to avoid

moisture problems. Favorable periods of mold growth only occurred for a few hours at a time in the roof sheathing, which was not problematic. Therefore, the VIPs did not critically inhibit the ability of the Northern Nomad building envelope to maintain a balance of wetting and drying.

The VIP-integrated walls of the Northern Nomad appear to be suitable arrangements for achieving acceptable service life of VIPs. In this location, the VIPs were not exposed to harsh conditions and could have a service life of around 40 years. The north facing roof was substantially worse for aging due to elevated thermal cycling, although still acceptable at around 27 years. The south facing roof exhibited poor conditions for VIP service life due to extreme temperatures as high as 70°C, which resulted in a lifespan estimate of 20 years, which is below the acceptable limit. A better arrangement in the roof may be to sandwich the VIPs between XPS and spray foam insulation midway through the roof cavity, like the walls of the Harmony House [11], to reduce exposure to high temperatures and protect them from indoor humidity.

One feature that could be implemented in the Northern Nomad for the next iteration of the house is forced ventilation in the roof air cavity. The 50 mm air gap behind the PV panels was not enough to sufficiently cool the roof, causing very high temperatures. Forced ventilation using a blower ducted at the ridge could increase airflow through the roof cavity, cooling the roof on sunny days and, as a result, drastically improving the longevity of VIPs in the roof. During the heating season, the heat captured by this system could preheat the supply air entering the ERV, which could reduce heating loads and improve occupant comfort.

From this study, a great understanding of the moisture characteristics in the Northern Nomad was achieved. When integrated correctly, VIPs can be used to achieve thin, highly insulated enclosures that can withstand the harsh Ottawa climate without premature failure. Proper

ventilation and air sealing can support the longevity of the house and achieve energy efficiency and good occupant comfort. The knowledge gained from this work can be used to help advise research projects in the future.

# Chapter 8: Future Work

This study managed to achieve the research objectives with reasonable success, but several challenges and limitations left areas for improvement. The damaged relative humidity sensors necessitated the creative use of various equations from the literature to improvise a mold growth analysis using moisture content data instead. This was a long and difficult process that was certainly less accurate than if relative humidity data were available, so it is important that future work involves more care in protecting the instrumentation from damage during construction to achieve the best results.

The humidifier used for simulating internal moisture generation had a limited runtime before it needed to be refilled, making it difficult to simulate moisture loads for periods of weeks or months. Longer periods of humidification could provide clearer indications of the effect of indoor humidity on moisture in the building enclosure, which is a valuable insight. Future work should include the implementation of a more automated humidification system with a larger water capacity that can allow for long term humidity testing.

The experimental work in this study has produced useful performance data about the building envelope and ERV in the context of real-world conditions. The scope of this study did not include energy modelling or hygrothermal modelling, but these are excellent activities for future work. ERV effectiveness and flow rate data can be used to predict energy loads and indoor humidity based on different modes of ERV operation. Predicted indoor humidity can be applied to hygrothermal models to evaluate mold growth risk and the model may be validated using results from this work.

# References


[1] Natural Resources Canada, "Energy Use in the Residential Sector," Natural Resources Canada, Ottawa, 2016.

[2] Natural Resources Canada, "Survey of Household Energy Use," Natural Resources Canada, Ottawa, 2016.

[3] Natural Resources Canada, "Residential End-Use Model," Ottawa, 2019.

[4] Statistics Canada, "Report on Energy Supply and Demand in Canada, 1990-2017," Ottawa, 2019.

[5] H. Simmler and S. Brunner, "Vacuum insulation panels for building application Basic properties, aging mechanisms and service life," *Energy and Buildings,* vol. 37, pp. 1122-1131, 2005.

[6] H. Simmler, S. Brunner, U. Heinemann, H. Schwab, K. Kumaran, P. Mukhopadhyaya, D. Quenard, H. Sallee and K. Noller, "International Energy Agency Annex 39: Vacuum Insulation Panels - Study on VIP-components and Panels for Service Life Prediction of VIP in Building Applications," 2005.

[7] J. Straube, "Moisture in Buildings," *ASHRAE Journal,* no. January 2002, pp. 15-19, 2002.

[8] E. Sterling, A. Arundel and T. Sterling, "Criteria for Human Exposure to Humidity in Occupied Buildings," in *ASHRAE Transactions*, 1985.

[9] USDA Forest Products Laboratory, "Wood Handbook: Wood as an Engineering Material," US Department od Agriculture, Madison, WI, 2010.

[10] J. Lstiburek, "Moisture Control for Buildings," *ASHRAE Journal,* vol. 44, no. 2, pp. 36-40, 2002.

[11] C. Mattock, "Harmony House Equilibrium Project," Habitat Design + Consulting Ltd., Burnaby, 2011.

[12] E. Sveipe, B. P. Jelle, E. Wegger, S. Uvslokk, S. Grynning, J. V. Thue, B. Time and A. Gustavsen, "Improving thermal insulation of timber frame walls by retrofitting with vacuum insulation panels – experimental and theoretical investigations," *Building Physics,* vol. 35, no. 2, pp. 168-188, 2011.

[13] P. Johansson, S. Geving, C.-E. Hagentoft, B. P. Jelle, E. Rognvik, A. S. Kalagasidis and B. Time, "Interior insulation retrofit of a historical brick wall using vacuum insulation panels: Hygrothermal numerical simulations and laboratory investigations," *Building and Environment,* vol. 79, pp. 31-45, 2014.

[14] P. Johansson, C.-E. Hagentoft and A. S. Kalagasidis, "Retrofitting of a listed brick and wood building using vacuum insulation panels on the exterior of the facade: Measurements and simulations," *Energy and Buildings,* vol. 73, pp. 92-104, 2014.

[15] H. Schwab, U. Heinemann, A. Beck, H.-P. Ebert and J. Fricke, "Dependence of Thermal Conductivity on Water Content in Vacuum Insulation Panels with Fumed Silica Kernels," *Journal of Thermal Envelope and Building Science,* vol. 28, no. 4, pp. 319-326, 2005.

[16] H. Schwab, U. Heinemann, A. Beck, H.-P. Ebert and J. Fricke, " Prediction of Service Life for Vacuum Insulation Panels with Fumed Silica Kernel and Foil Cover," *Journal of Thermal Envelope and Building Science,* vol. 28, no. 4, pp. 357-374, 2005.

[17] S. Brunner and H. Simmler, "Monitoring of VIP in Building Applications," in *7th International Vacuum Insulation Symposium*, Zurich, Switzerland, 2005.

[18] H. Schwab, J. Wachtel, H. Scheuerpflug, C. Stark, U. Heinemann, H.-P. Ebert and J. Fricke, "Entwicklung und Anwendung von evakuierten höchsteffizienten Dämmungen für Gebäude (Vakuumdämmung für Gebäude)," ZAE Bayern, 2003.

[19] S. Pallin, D. E. Hun, R. K. Jackson and A. O. Desjarlais, "Moisture Durability Assessment of Selected Well-insulated Wall Assemblies," Oak Ridge National Laboratory, Oak Ridge, TN, 2015.

[20] A. Hukka and H. A. Viitanen, "A mathematical model of mould growth on wooden material," *Wood Science and Technology,* vol. 33, no. 6, pp. 475-485, 1999.

[21] H. Viitanen and T. Ojanen, "Improved Model to Predict Mold Growth in Building Materials," in *Buildings X*, Florida, 2007.

[22] H. Viitanen, T. Ojanen, M. Krus, V. Eitner, S. Bogl and D. Zirkelbach, "WUFI Mold Index VTT 2.1," Fraunhoffer Institute for Building Physics, 2019.

[23] H. R. Trechsel and M. T. Bomberg, Moisture Control in Buildings: The Key Factor in Mold Prevention, 2nd ed., ASTM International, 2010.

[24] G. A. Tsongas and F. Riordan, "Minimum Conditions for Visible Mold Growth," *ASHRAE Journal,* vol. 58, no. 9, pp. 32-43, 2016.

[25] E. Vereecken and S. Roels, "Review of mould prediction models and their influence on mould risk evaluation," *Building and Environment,* vol. 51, pp. 296-310, 2012.

[26] P. E. Laks, D. L. Richter and G. M. Larkin, "Fungal Susceptibility of Interior Commercial Building Panels," *Forest Products Journal,* vol. 52, no. 5, pp. 41-44, 2002.

[27] X. Ye, S. Wang, R. Ruan, J. Qi, A. R. Womac and J. C. Doona, "Water Mobility and Mold Susceptibility of Engineered Wood Products," *Transactions of the ASABE,* vol. 49, no. 4, pp. 1159-1165, 2006.

[28] S. Y. Harris, Building Pathology: Deterioration, Diagnostics, and Intervention, New York: John Wiley & Sons, Inc., 2001.

[29] S. V. Glass and S. L. Zelinka, "Moisture relations and physical properties of wood. Wood handbook : wood as an engineering material: chapter 4. Centennial ed. General technical report FPL," Forest Products Laboratory, Madison, WI, 2010.

[30] C. G. Carll and T. L. Highley, "Decay of Wood and Wood-Based Products Above Ground in Buildings," *Journal of Teesting and Evaluation,* vol. 27, no. 2, pp. 150-158, 1999.

[31] H. Ge, J. Straube, L. Wang and M. J. Fox, "Field study of hygrothermal performance of highly insulated wood-frame walls under simulated air leakage," *Building and Environment,* vol. 160, 2019.

[32] R. McClung, H. Ge, J. Straube and J. Wang, "Hygrothermal performance of cross-laminated timber wall assemblies with built-in moisture: field measurements and simulations," *Building and Environment,* no. 71, pp. 95-110, 2014.

[33] C. J. Simonson, T. Ojanen and M. Salonvaara, "Moisture Performance of an Airtight, Vapor-permeable Building Envelope in a Cold Climate," *Thermal Environment and Building Science,* vol. 28, no. 5, pp. 205-226, 2005.

[34] M. Said, W. Brown, C. Shirtliffe and A. Maurenbrecher, "Monitoring of the building envelope of a heritage house: a case study," *Energy and Buildings,* vol. 30, pp. 211-219, 1999.

[35] H. Orr, J. Wang, D. Fetsch and R. Dumont, "Technical Note: Airtightness of older-generation energy-efficient houses in Saskatoon," *Building Physics,* vol. 36, no. 3, pp. 294-307, 2012.

[36] A. Kirimtat and O. Krejcar, "A review of infrared thermography for the investigation of building envelopes: Advances and prospects," *Energy and Buildings,* vol. 176, pp. 390-406, 2018.

[37] C. R. Boardman and S. V. Glass, "Moisture transfer through the membrane of a cross-flow energy recovery ventilator: Measurement and simple data-driven modeling," *Journal of Building Physics,* vol. 38, no. 5, pp. 389-418, 2015.

[38] J. Min and M. Su, "Performance analysis of a membrane-based energy recovery ventilator: Effects of outdoor air state," *Applied Thermal Engineering,* pp. 4036-4043, 2011.

[39] "Highway Traffic Act, RSO 1990, Chapter H.8," 2020.

[40] Natural Resources Canada, "Residential Housing Stock and Floor Space," Natural Resources Canada, Ottawa, 2008.

[41] Point2, "Global Perspective: How Large are Canadian Homes?," Point2, Saskatoon, 2017.

[42] Panasonic Eco Solutions North America, "FV-04VE1 Specification Submittal Data," Panasonic Eco Solutions North America, Newark, NJ.

[43] J. Straube, "BSD-061: The Function of Form—Building Shape and Energy," Building Science Corporation, Westford, MA, 2012.

[44] AgiliCity, "How Can Using Form Factor Reduce Energy Consumption of Buildings?," Modelur, 2019.

[45] R. McLeod, K. Mead and M. Standen, "Passivhaus primer: Designer's guide," BRE, Watford, UK.

[46] A. Rasooli and L. Itard, "In-situ characterization of walls' thermal resistance: An extension to the ISO 9869 standard method," *Energy & Buildings,* vol. 179, pp. 374-383, 2018.

[47] Canada Mortgage and Housing Corporation, "CMHC Garbage Bag Airflow Test," CMHC, Ottawa, 2009.

[48] CSA Group, Laboratory methods of test for rating the performance of heat/energy-recovery ventilators, Toronto: CSA Group, 2018.

[49] ASHRAE, ASHRAE Handbook: Fundamentals, Atlanta, GA: ASHRAE, 2017.

[50] C. Boardman, S. Glass and P. Lebow, "Simple and Accurate Temperature Compensation for Moisture Pin Calibrations in Oriented Strand Board," *Building and Environment,* vol. 112, pp. 250-260, 2017.

[51] APA - The Engineered Wood Association, "Moisture Related Dimensional Stability," APA, Tacoma, WA, 2016.

[52] I. D. Hartley, S. Wang and Y. Zhang, "Water vapor sorption isotherm modeling of commercial oriented strand panel based on species groups and resin type," *Building and Environment,* vol. 42, no. 10, pp. 3655-3659, 2007.

[53] P. Garrahan, "Moisture Meter Correction Factors," in *In-grade testing of structural lumber*, Madison, WI, 1988.

[54] W. Maref, M. Lacasse and M. Booth, "Experimental Assessment of Hygrothermal Properties of Wood-Frame Wall Assemblies—Moisture Content Calibration Curve for OSB Using Moisture Pins," *Journal of ASTM International,* vol. 7, no. 1, pp. 1-12, 2010.

[55] A. J. Hailwood and S. Horrobin, "Absorption of Water by Polymers: Analysis in Terms of a Simple Model," *Transactions of the Faraday Society,* vol. 42, pp. 84-102, 1946.

[56] J. Lstiburek, "BSD-146: EIFS - Problems and Solutions," Building Science Corporation, 2007.

[57] ASHRAE, "Damp Buildings, Human Health, and HVAC Design," ASHRAE, Atlanta, GA, 2020.

[58] W. J. Fisk, E. A. Eliseeva and M. J. Mendell, "Association of residential dampness and mold with respiratory tract infections and bronchitis: a meta-analysis," *Environmental Health,* vol. 9, no. 72, pp. 1-11, 2010.

[59] C. Campbell, S. Bucking and C. A. Cruickshank, "In-Situ Temperature and Moisture Monitoring of a High-Performance Tiny House with Vacuum Insulation Panels," in *New Horizons in Green Civil Engineering*, Victoria, 2020.

[60] Natural Resources Canada, "Canada's GHG Emissions by Sector, End Use and Subsector," Natural Resources Canada, Ottawa, 2017.

[61] Statistics Canada, "Annual Demographic Estimates: Canada, Provinces and Territories, 2019," Statistics Canada, Ottawa, 2019.

[62] Y.-h. Choi, D. Song, D. Seo and J. Kim, "Analysis of the variable heat exchange efficiency of heat recovery ventilators and the associated heating energy demand," *Energy and Buildings,* vol. 172, pp. 152-158, 2018.

[63] M. J. Alonso, P. Liu, H. M. Mathisen, G. Ge and C. Simonson, "Review of heat/energy recovery exchangers for use in ZEBs in cold climate countries," *Building and Environment,* vol. 84, pp. 228-237, 2015.

[64] I. S. Cole, G. Trinidad and W. Chan, "Prediction of the Impact of the Environment on Timber Components : A GIS Based Approach," in *Durability of Building Materials and Components*, Ottawa, ON, 1999.

[65] W. T. Simpson, "Predicting Equilibrium Moisture Content of Wood by Mathematical Models," *Wood and Fiber,* vol. 5, no. 1, pp. 41-49, 1973.

[66] C. Carll and A. C. Wiedenhoeft, "Moisture-Related Properties of Wood and the Effects of Moisture on Wood and Wood Products," in *Moisture Control in Buildings - The Key Factor in Mold Prevention*, West Conshohocken, PA, ASTM International, 2009, pp. 54-79.

# Appendix A: Sensor Conversion Equations

Wood MC sensors measure the electrical resistance of wood, which changes with temperature, so the measured resistance values were converted to MC using a set of temperature-compensated conversion equations for OSB. The conversion equations (A.1) were derived by Garrahan [53] and Maref [54]:

$$MC = exp\left(b_0 - b_1 * ln\left(\frac{R}{1000}\right)\right) \tag{A.1}$$

$$MC_{\mathrm{T}} = \frac{MC + 0.567 - 0.026T + 0.000051T^2}{0.881 * 1.0056^{\mathrm{T}}} - b_2 \tag{A.2}$$

$$MC_{\mathrm{OSB}} = 100 * exp\left(b_3 * ln\left(\frac{MC_T}{100}\right) + 0.001187 * b_4\right) \tag{A.3}$$

$$b_0 = 4.095417, \qquad b_1 = 0.14006, \qquad b_2 = 0, \qquad b_3 = 1.055, \qquad b_4 = 1$$

where $R$ is the electrical resistance in ohms and $T$ is the compensation temperature in Celsius.

RH sensors used for measuring indoor, outdoor, and ERV inlet/outlet RH use the following temperature-compensated conversion equation from voltage measurements:

$$RH = \frac{-1.9206 \times 10^{-9} V_{\mathrm{out}}^3 + 1.437 \times 10^{-5} V_{\mathrm{out}}^2 + 3.421 \times 10^{-3} V_{\mathrm{out}} - 12.4}{1 + 2.4 \times 10^{-3}(T - 23)} \tag{A.4}$$

where $V_{\mathrm{out}}$ is the voltage measured at the sensor in volts and the DC supply voltage to the sensor is nominally 5 V. The RH sensors in the building envelope were a different model of sensor so they used a different temperature-compensated conversion equation:

$$RH = \frac{0.00636\left(\frac{V_{\text{out}}}{V_{\text{supply}}} - 0.1515\right)}{1.0546 - 0.00216T} \tag{A.5}$$

where $V_{\text{supply}}$ is the voltage supplied to the data acquisition unit in volts.

The resistance values (kOhms) measured by the thermistors were converted to temperature in degrees Celsius using Equation (A.6).

$$T = (0.0002277904328 \ln R + 0.0023050027)^{-1} - 273.15 \tag{A.6}$$

The estimated error associated with thermistor data was determined using a Gaussian error propagation with ±1% error in resistance measurements as per the sensor datasheet. The absolute error for each temperature measurement is expressed as:

$$error_T = \sqrt{\left(\frac{43.90}{(\ln R + 10.119)^2}\right)^2} \tag{A.7}$$

# Appendix B: Alternate Moisture Content Conversion Equations

The accuracy of MC data depends on the accuracy of the conversion equation used to convert resistance to MC. There exist several equations for this and the accuracy of the default equations (A.1)-(A.3) is unknown, so a sensitivity analysis was done to determine if the choice of conversion equation has a significant effect on the results. If the conclusions of the research are affected, the sensitivity is high, and the choice of conversion equations should be a careful one. If there is no effect on the conclusion, then the default equations are adequate.

Two alternate equations proposed by Boardman, Glass and Lebow [50] were considered. They measured the EMC of 130 OSB samples at different RH values from 35-95% RH using resistance and mass measurements to determine a new, more accurate, and simpler temperature-compensated conversion equation:

$$MC = b_0 + b_1\left(\frac{1000}{T+273.15}\right)^{b_4} + b_3\left(\frac{1000}{T+273.15}\right)^{b_4} log_{10}(log_{10}(R) - b_2) \qquad \text{(B.1)}$$

$$b_0 = -8.6810, \qquad b_1 = 3.7172, \qquad b_2 = 3.8974, \qquad b_3 = 2.9129, \qquad b_4 = 1.9000$$

The study found that Equation (B.1) had a RMSE of 0.726 for their dataset. The same study found that Equations (A.1)-(A.3) were not very accurate for their dataset, so they optimized the coefficients of Equations (A.1)-(A.3) to improve the RMSE from 1.7 to 0.927 using the following coefficients:

$$b_0 = 3.8786, \qquad b_1 = 0.0893, \qquad b_2 = 5.6819, \qquad b_3 = 1.0176, \qquad b_4 = 1.0667$$

These two alternative conversion methods were applied to the MC data. The result showed that all three methods converge at around 25°C. The two methods by Boardman, Glass and Lebow were

similar. They produced higher MC at low temperatures, up to 2% MC higher than the default equations at -10°C, and lower MC at higher temperatures, up to 1% MC lower at 53°C. When considering the MC data that was at the highest risk for mold growth, (north roof sheathing in the spring) the default equations used in this study produced higher, more conservative MC values which is ideal for this risk analysis. The overall difference is not significant enough to change the conclusion of this study, and therefore the default equation was used.

# Appendix C: Limitations of RSI Estimates

Presented here are some factors affecting the measured and simulated results from Section 5.1. The model assumed that the VIP thermal conductivity was the advertised center-of-panel conductivity of a new panel (0.004 W/mK), which does not consider aging or thermal bridging effects at the edges, corners, and joints between the VIPs. The panels in the house were already a few years old before installation, which could have aged the panels slightly, so the model may have over-predicted the south wall RSI value. The uncertainty in VIP thermal conductivity is one of the main reasons why measurements and simulations were used and compared.

Surface transfer coefficients are potential sources of uncertainty, so the measured results from Section 5.1.1 were used to calculate the coefficients. The RSI-measurements calculated surface transfer coefficients based on heat flux, surface temperature, and air temperature. The measured coefficients were 4.3 $W/m^2K$ for the inside surface and 8.6 $W/m^2K$ for the outside surface. The model assumed coefficients of 5 $W/m^2K$ inside and 8 $W/m^2K$ outside which are close to the measured values, so these assumptions were valid.

The rainscreen air cavity was treated as a radiant heat exchange cavity with convection, according to ISO 15099, with an effective conductivity of 0.775 W/mK under simulated temperatures. This treatment is not necessarily representative of the actual rainscreen due to the complexity of the dynamic heat transfer mechanisms behind the wall cladding. Solar irradiance, humidity, geometry, and surface roughness all affect the radiant and convective heat transfer, so it was difficult to model accurately. The RSI measurements also did not capture details about heat transfer in the rainscreen cavity, leaving some uncertainty in this area.

Radiant heat transfer on the exterior surfaces was ignored by the model, which may have caused discrepancies with the measured results. Radiant heat transfer varied between the north and south walls, with the south wall more exposed to solar irradiance and the night sky, and the north side usually receiving more exposure from the sun and nearby buildings that released thermal radiation at night. These factors were difficult to characterize so there may have been some uncertainty.

# Appendix D: OSB Sorption Isotherm Selection

A study by APA [51] determined an adsorption isotherm for OSB at 21°C from experimental measurements, but there was no information about the method used so its applicability is uncertain. Given the scarce number of studies though, the results were considered anyway.

Hartley at al. [52] modelled adsorption and desorption isotherms at 25°C for pine OSB (with a small amount of hardwood), aspen OSB, and poplar OSB, each with two different resin types. Only six samples were tested in total, giving just one sample for each combination of species and resin type, which is not a very large sample size for this test. Nonetheless, all samples in that study gave very similar isotherms, so results appear applicable for this work.

Boardman et al. [50] presented an adsorption isotherm based on mass and resistance measurements of 130 OSB samples, mostly from panels produced in Michigan and some from Texas and British Columbia. They found that regionality influenced isotherms, and since the OSB in the Northern Nomad is probably the same as the Michigan variety, the results are probably applicable here. Most measurements were at 23°C and some were at 26.6°C, but the effect of 3.6°C is negligible. This is the most trusted study of the three based on the sample size, method, and noteworthy researchers.

No studies were found to provide temperature correction for OSB isotherms specifically, but it is assumed that the EMC-RH relationships for OSB and plain lumber would have very similar temperature-dependence. The EMC-RH-T equation provided by Hailwood and Horrobin [55], which provides sorption isotherms midway between adsorption and desorption, demonstrates the temperature dependence of sorption isotherms for Sitka spruce. Figure D-1 shows the three OSB

adsorption isotherms as well as an isotherm produced by the Hailwood and Horrobin equation at 21°C [55].

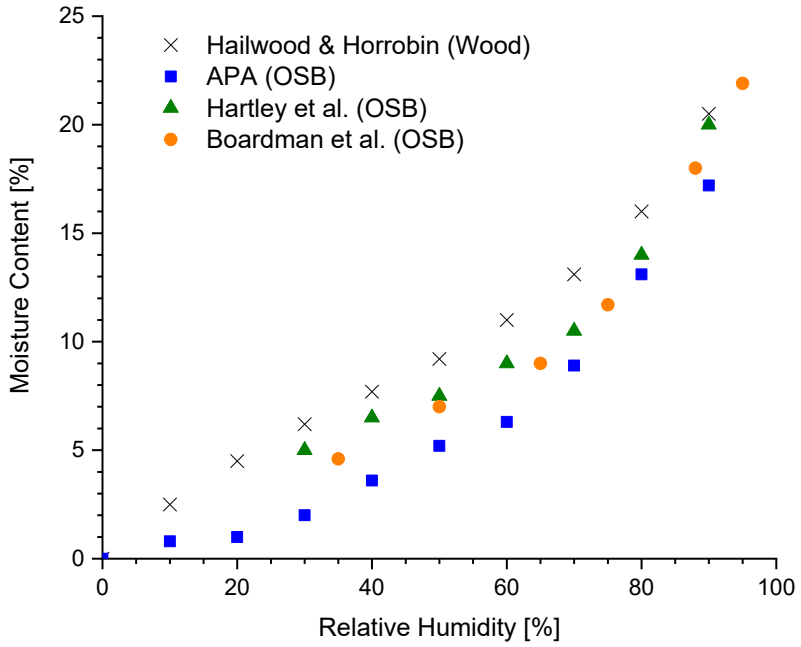


**Figure D-1: Comparison of three different sorption isotherms for OSB [50, 52, 51] and one for softwood [55]**

Figure D-1 shows close agreement between sorption isotherms by Hartley et al. and Boardman et al. over the range of MC values found in the measured data, with just 0.5% MC difference at 50% RH. The sorption isotherm by APA gives MC values approximately 3% MC lower than those by Hartley et al. between 30-60% RH, with closer agreement above 60% RH. All OSB isotherms are lower than the spruce isotherm, partially since OSB curves are for adsorption and the spruce curve is midway between adsorption and desorption, but also because of the material difference. At higher RH values (>70% RH), Boardman et al. is midway between the others. The best isotherm for analyzing Northern Nomad data was assumed to be that given by Boardman et al.

It was acknowledged that despite choosing what appears to be the most accurate adsorption isotherm, applying it to unsteady data introduced uncertainty since it is not in equilibrium. Much of the data oscillated daily by around 1% MC and 1°C which was acceptable, but some days changed by over 40°C and 4% MC. The amount of uncertainty in RH estimates from fluctuating MC was difficult to determine, but it was also not critical regarding mold growth analysis because mold growth does not initiate or spread significantly in just a few hours. Persistent high RH is the greater threat, in which case the conditions are closer to equilibrium and thus the uncertainty is lower.

Conversely, VIP aging has shown to be accelerated under cyclic heat and humidity [6], making the fluctuating periods more impactful. For this work, a detailed analysis of VIP aging was not in the scope and thus absolute certainty was not required. The more relevant comparison for this work was not with VIP aging rates, but among different locations in the house (roof, walls, north, south) to determine which areas are suitable for VIPs. For this comparison, a higher level of uncertainty in data values was acceptable. It was assumed that for analyzing RH data using EMC-RH relations, uncertainty was +/-5% RH.